RIGA TECHNICAL UNIVERSITY

Raimonds Bogdanovičs

PERFORMANCE EVALUATION OF SOLAR THERMAL AND HEAT PUMP TECHNOLOGY IN DISTRICT HEATING

Doctoral Thesis

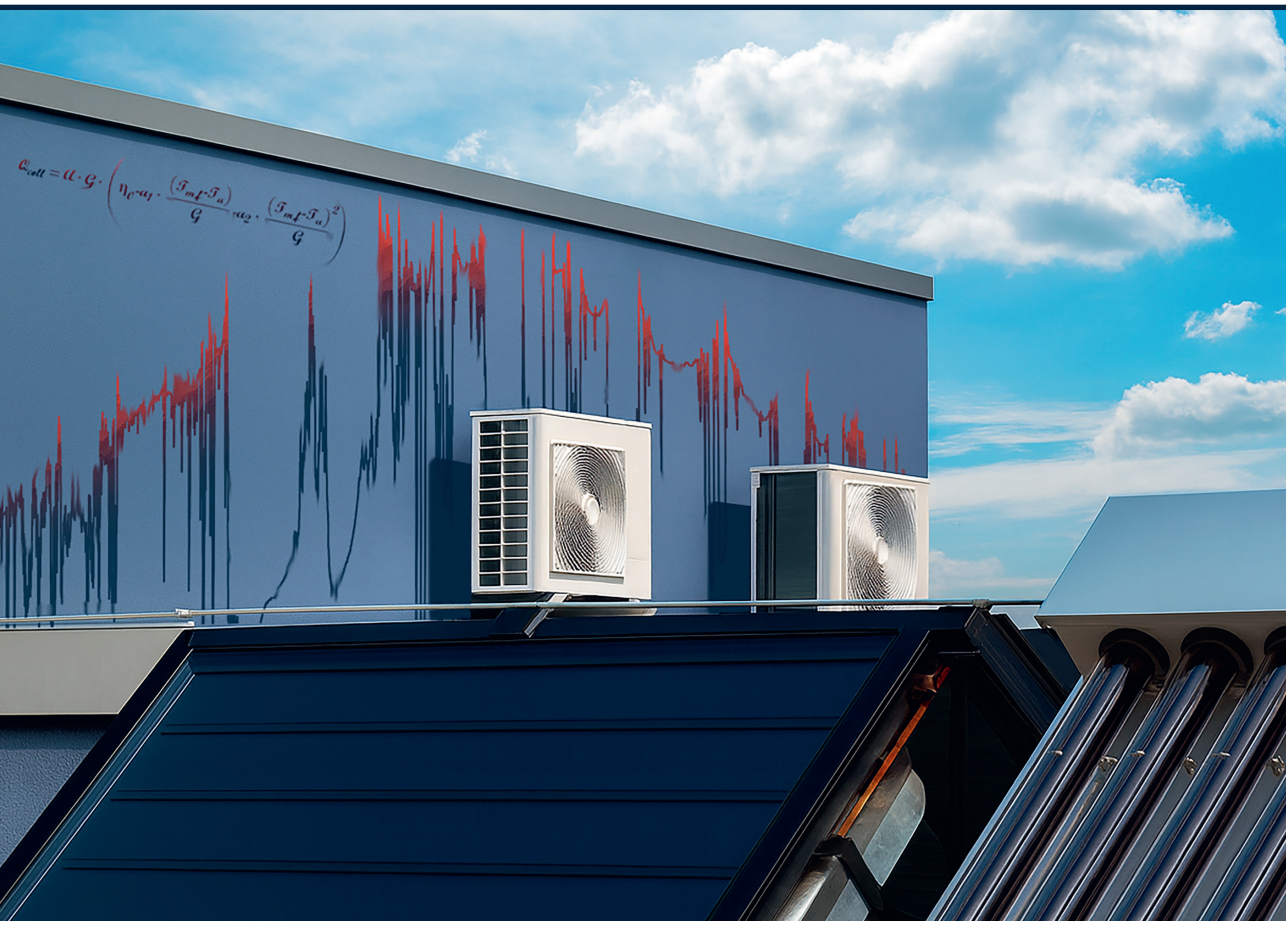

RTU Press
Riga 2025

RIGA TECHNICAL UNIVERSITY
Faculty of Civil and Mechanical Engineering
Institute of Sustainable Building Materials and Engineering Systems

Raimonds Bogdanovičs
Doctoral Student of the Study Programme "Heat, Gas and Water Technology"

PERFORMANCE EVALUATION OF SOLAR THERMAL AND HEAT PUMP TECHNOLOGY IN DISTRICT HEATING

Doctoral Thesis

Scientific supervisor
Associate Professor Dr. sc. ing.
JURĢIS ZEMĪTIS

Scientific co-supervisor
Associate Professor Dr. sc. ing.
ALEKSANDRS ZAJACS

Riga 2025

FOREWORDS

My journey into research began in 2017, when I started working at Riga Technical University as a research assistant during my Bachelor studies. I'm grateful to professor Dr. sc. ing. Anatolijs Borodiņecs who recognized my enthusiasm and believed in my potential, giving me the opportunity to dive into academia, contribute to scientific research, run computer simulations, analyze data, and plan and build experimental setups. That early trust laid the foundation for my academic path and ignited my interest in research and creative thinking.

I sincerely thank my supervisors Dr. sc. ing. Jurģis Zemītis and Dr. sc. ing. Aleksandrs Zajacs for their patience, support, valuable advice, timely consultations, and constructive criticism. Your guidance helped me navigate challenges and stay on track. Thank you for the mental support, for always being open to discussing problems, doubts, and ideas, and for the hands-on help during the building and setup of experimental facilities.

I could not have done this without my family. Your belief in me gave me strength when I needed it most. Through every late night, every setback, and every moment of doubt, you stood by me – not just with words, but with unwavering presence.

I also want to thank my colleagues from the Institute of Sustainable Building Materials and Engineering Systems for their support, teamwork, optimism, and for constantly challenging me to think critically and grow as a researcher.

My strong interest in the development of Latvia's and the Baltic region's energy sector – particularly in the context of climate change, decarbonization, and energy security – motivated me to pursue a Ph.D. Curiosity and a desire to learn and share knowledge have always driven me forward. While working in parallel as a heating, ventilation, and air-conditioning system designer, I consistently focus on precision, efficiency, and real-world impact. I aim for results that are both scientifically grounded and practically applicable, because I believe our field needs innovative, evidence-based solutions that can directly improve system performance and reduce environmental impact. I actively expand my technical skills through simulation tools and programming languages, and continuously seek improvement via seminars, workshops, and international conferences – staying up to date with the latest developments.

This dissertation reflects my commitment to bridging scientific research and engineering practice. I hope it contributes meaningfully to both.

ABSTRACT

Northern and Eastern Europe have relatively high district heating (DH) market penetration, but solar thermal energy remains underutilized. At the same time, heat pumps are widely used as environmentally friendly solutions for space heating and domestic hot water preparation. This research explores the potential of combining DH systems with solar thermal and heat pump technologies to maximize solar heat utilization in a more integrated and efficient way.

The solar energy is not stable and strongly influenced by cloudiness, which introduces temperature fluctuations that may affect heat pump performance within this complex system. Since heat pump manufacturers typically do not test performance under fluctuating temperature conditions, this study addresses a critical knowledge gap by developing and applying a novel methodology for measuring and evaluating these effects.

The research methodology integrates statistical analysis, experimental testing, field measurements, TRNSYS 18 dynamic simulations and energy performance calculations across various system configurations and temperature regimes. Results demonstrate that combining photovoltaic-thermal collectors with a brine-to-water heat pump in a low-temperature DH system can produce 1.8 to 4.6 times more thermal energy than solar thermal collectors directly connected to the DH grid and up to 7.6 times more than traditional systems with local storage, highlighting the importance of investigating such system operating parameters.

Statistical analysis of fluctuations caused by solar thermal collectors showed that the mean absolute deviation (MAD) of heat carrier temperature can reach up to 0.96 K at low temperatures (50 °C), and up to 2.20 K at high temperatures (80 °C). While sink-side fluctuations had minimal influence on heat pump performance, source-side fluctuations can reduce the coefficient of performance by 1 % per each 1 K increase in MAD, when the source temperature is low (up to 21 °C). If source temperature is higher, temperature fluctuations have no significant impact on COP. When MAD remains below 0.9 K, the impact falls within measurement uncertainty.

The results and findings can be used to support decision-making in the development of district heating systems. The developed research methodology is applicable to future studies aimed at evaluating heat carrier temperature fluctuations, calculating system thermal output and testing heat pump performance under varying conditions.

Key words: heat pump, solar thermal, district heating, temperature fluctuation.

ANOTĀCIJA

Ziemeļeiropā un Austrumeiropā centralizētās siltumapgādes (CSA) tirgus pārklājums ir salīdzinoši augsts, taču saules siltumenerģija joprojām tiek nepietiekami izmantota. Tajā pašā laikā siltumsūkņi tiek plaši izmantoti kā videi draudzīgs risinājums telpu apkurei un karstā ūdens sagatavošanai. Šajā pētījumā tiek pētīts potenciāls apvienot CSA sistēmas ar saules siltumenerģijas un siltumsūkņu tehnoloģijām, lai maksimāli izmantotu saules siltumu.

Saules enerģija nav stabila un to būtiski ietekmē mākoņainība, kas izraisa temperatūras svārstības un var ietekmēt siltumsūkņa darbību šajā sarežģītajā sistēmā. Tā kā siltumsūkņu ražotāji parasti nepārbauda darbību svārstīgos temperatūras apstākļos, šis pētījums risina būtisku zināšanu trūkumu, izstrādājot jaunu metodoloģiju šo efektu mērīšanai un novērtēšanai.

Pētījuma metodoloģijā ietilpst statistiskā analīze, eksperimentālie testi, lauka mērījumi, TRNSYS 18 dinamiskās simulācijas un enerģētiskās veiktspējas aprēķini dažādās sistēmu konfigurācijās un temperatūras režīmos. Rezultāti parāda, ka, apvienojot fotoelektrisko-termālos saules kolektorus ar ūdens-ūdens siltumsūkni zemas temperatūras CSA sistēmā, iespējams saražot 1,8 līdz 4,6 reizes vairāk siltumenerģijas nekā ar saules kolektoriem, kas tieši pieslēgti CSA tīklam, un līdz pat 7,6 reizes vairāk nekā tradicionālajām sistēmām ar vietējo uzkrāšanu, uzsverot šādu sistēmu darbības parametru izpētes nozīmi.

Statistiskā analīze par saules kolektoru izraisītajām svārstībām parādīja, ka siltumnesēja temperatūras vidējā absolūtā novirze (MAD) var sasniegt līdz pat 0,96 K zemās temperatūrās (50 °C) un līdz 2,20 K augstās temperatūrās (80 °C). Kamēr temperatūras svārstībām patērētāja pusē ir minimāla ietekme uz siltumsūkņa darbību, siltuma avota puses svārstības var samazināt veiktspējas koeficientu par 1 % katram 1 K MAD pieaugumam, kad siltuma avota temperatūra ir zema (līdz 21 °C). Ja siltumnesēja temperatūra ir augstāka, svārstībām nav būtiskas ietekmes uz siltumsūkņa veiktspēju (COP). Ja MAD ir zem 0,9 K, ietekme paliek mērījumu nenoteiktības robežās.

Šie rezultāti un atziņas var kalpot kā atbalsts lēmumu pieņemšanā centralizētās siltumapgādes sistēmu attīstībā. Izstrādātā pētniecības metodoloģija ir piemērojama nākotnes pētījumiem, kuru mērķis ir novērtēt siltumnesēja temperatūras svārstības, aprēķināt sistēmas siltumenerģijas ražošanas potenciālu un pārbaudīt siltumsūkņu darbību dažādos apstākļos.

Atslēgvārdi: siltumsūknis, saules kolektori, centralizētā siltumapgāde, temperatūru svārstības.

TABLE OF CONTENTS

NOMENCLATURE

3GDH	3rd generation district heating
4GDH	4th generation district heating
5GDH	5th generation district heating
AWHP	air-to-water heat pump
BWHP	brine-to-water heat pump
COP	coefficient of performance
DH	district heating
DHC	district heating and cooling
DHW	domestic hot water
ETC	evacuated tube collectors
EU	European Union
FPC	flat-plate collectors
LTDH	low-temperature district heating
MAD	mean absolute deviation
HP	heat pump
PV	photovoltaic
PVT	photovoltaic-thermal
RES	renewable energy sources
SD	standard deviation
ST	solar thermal
TRNSYS	the name of dynamic simulation software
ULTDH	ultra-low temperature district heating

INTRODUCTION

This Thesis started with a practical engineering challenge: how to maximize solar energy utilization in the district heating sector. This led to the concept of combining solar energy with brine-to-water heat pumps, raising a key technological question: Do variations in solar energy affect the performance of a solar-assisted heat pump? This, in turn, led to the scientific research question: How to measure and evaluate the influence of heat carrier temperature variations, caused by solar energy fluctuations, on brine-to-water heat pump performance.

Relevance of the study

In recent years, there has been a noticeable rise in scientific research on solar-assisted heat pumps – including thermal, photovoltaic and combined systems. However, limited attention has been given to the integration of these technologies with district heating networks, especially under Northern Europe's climatic conditions.

Achieving carbon neutrality by 2050, as outlined in the Paris Agreement, requires a fundamental shift away from fossil fuels for heat production. Integrating heat pumps and solar energy into low-temperature district heating systems presents a promising solution for producing and storing heat energy in a sustainable and efficient manner. The efficiency of heat pumps can be further improved by utilizing solar thermal heat, while photovoltaic panels can supply renewable electricity to power the heat pumps.

This combination not only enables the generation of heat energy without greenhouse gas emissions but also introduces the possibility of space cooling – an increasingly important consideration as Latvia experiences the impacts of a warming climate. The study's focus on maximizing solar heat utilization within district heating networks directly supports the broader goals of decarbonizing the heating sector and advancing renewable energy integration.

The aim of this Ph.D. Thesis is to investigate strategies for maximizing solar heat utilization in Northern Europe's climatic conditions within district heating systems by integrating solar thermal and heat pump technologies.

The main tasks:

1. Assess solar energy potential and variability in Latvia for integration with solar thermal and heat pump-based district heating.
2. Examine solar thermal collector performance under different heat carrier temperature regimes and analyze heat carrier temperature fluctuations under variable conditions.
3. Explore the integration of solar energy into district heating systems and evaluate the effectiveness of using district heating to store heat produced by solar collectors, in order to assess the feasibility of distributing the generated energy to nearby buildings.
4. Evaluate the combination of solar energy, heat pump and district heating system to identify strategies for maximizing solar heat utilization using limited building roof space.
5. Analyse the impact of heat carrier temperature fluctuations on the performance of the brine-to-water heat pump.
6. Examine the effect of solar thermal collector temperature and flow fluctuations on the operation of a brine-to-water heat pump.

Theses to be defended

- The integration of solar energy and heat pump technologies into low-temperature district heating networks is one of the most effective strategies for maximizing solar heat utilization.
- In systems with solar thermal collectors, heat carrier temperature fluctuations are primarily caused by solar irradiance variability and can be reduced by operating at lower temperatures.
- Source-side temperature fluctuations reduce the coefficient of performance of brine-to-water heat pumps, while fluctuations on the sink side have minimal impact.
- The coefficient of performance of brine-to-water heat pumps is particularly sensitive to source-side temperature fluctuations at temperatures below 20 °C. So the findings are specifically relevant when heat pumps are used as booster units in ultra-low-temperature district heating systems or when photovoltaic-thermal collectors serve as the heat source.

The scientific novelty of this Thesis lies in the development of an integrated methodology that combines experimental testing, simulation models and energy performance calculations to evaluate and maximize the performance of solar thermal and brine-to-water heat pump technology in a low-temperature district heating system under fluctuating heat carrier temperatures. Unlike conventional heat sources such as geothermal heat or groundwater, which maintain stable thermal conditions, this study specifically investigates the dynamic temperature variations introduced by solar energy fluctuations, an aspect rarely explored in existing research.

This research examines the dynamic interaction between solar thermal collectors, district heating systems and heat pumps, focusing on how solar-induced temperature variations affect the heat pump's coefficient of performance (COP) at different heat carrier temperatures. Since heat pump manufacturers do not typically test for these conditions, this study fills a critical gap by providing an experimental assessment and a novel methodology for measuring and evaluating their impact under real operating conditions. **It hypothesizes** that temperature fluctuations driven by solar energy integration significantly influence the COP of the brine-to-water heat pump, requiring advanced evaluation techniques beyond standard testing procedures.

The proposed methodology integrates multiple methods, including statistical analysis, literature reviews, field measurements, the development of two experimental test facilities and numerous computer simulations using the TRNSYS 18 dynamic simulation software. By conducting energy performance calculations for different system configurations and temperature regimes, this research demonstrates how the proposed system can maximize solar energy utilization, thereby providing evidence of its feasibility for real-world applications.

The practical implementation lies in supporting the development of the district heating sector by providing valuable insights into the integration of renewable energy sources, particularly solar energy and heat pumps. The results, including statistical analysis, experimental data and simulation outcomes, can inform strategic decision-making processes for modernizing district heating networks, optimizing solar heat generation and improving system efficiency. While the research focuses on Northern Europe and especially Latvian climatic conditions, the proposed methods and findings are adaptable to other regions, offering a broader application for advancing sustainable and resilient district heating systems.

Research methodology

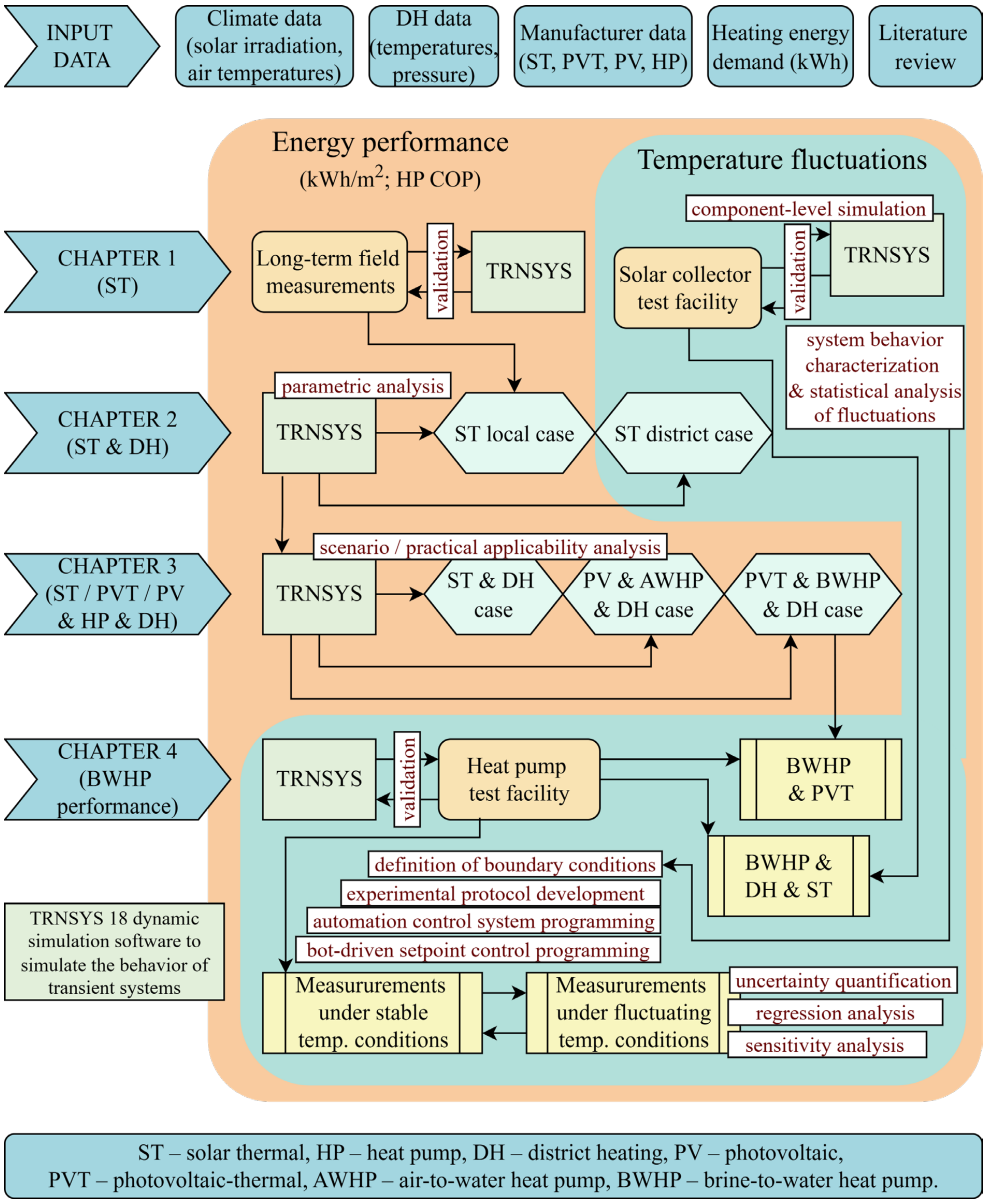

Fig. 0.1. Research methodology.

The study contributes to the United Nations Sustainable Development Goals (SDGs), particularly Goal 7, “Affordable and clean energy”, Goal 11, “Sustainable cities and communities”, and Goal 13, “Climate action”.

List of publications related to this study

Article (SCOPUS):

1. **Bogdanovics, R.**, Zemitis, J., Zajacs, A., Borodinecs, A., 2024. Small-Scale District Heating System as Heat Storage for Decentralized Solar Thermal Collectors during Non-Heating Period. *Energy*. Vol. 298.
2. Zajacs, A., Lebedeva, K., **Bogdanovics, R.**, 2023. Evaluation of Heat Pump Operation in a Single-Family House. *Latvian Journal of Physics and Technical Sciences*. Vol.60.
3. Zajacs, A., **Bogdanovics, R**., Zeiza-Seleznova, A., Valancius, R., Zemitis, J., 2022. Integration of decentralized solar collectors into a district heating system. *Sustainable Cities and Society*, Vol.83.
4. Zajacs, A., **Bogdanovics, R**., Borodinecs, A., 2020. Analysis of low temperature lift heat pump application in a district heating system for flue gas condenser efficiency improvement. *Sustainable Cities and Society*. Vol. 57.

Conference papers indexed in SCOPUS:

1. **Bogdanovics, R.**, Zemitis, J., Zajacs, A., Borodinecs, A. (2025). Optimizing the Integration of Booster Heat Pump with Solar Thermal Collectors and Low-Temperature District Heating System in the Baltic Region: Laboratory Measurements. *2025 ASHRAE Winter Conference*. February 8–12, 2025, Orlando, Florida, USA.
2. **Bogdanovics, R.**, Zemitis, J., Zajacs, A. (2023). TRNSYS model of district heating system used as heat storage for decentralized solar thermal collectors. *18th IBPSA Conference on Building Simulation, BS 2023*, Building Simulation Conference Proceedings. September 4–6, 2023, Shanghai, China.
3. **Bogdanovics, R.**, Zajacs, A. (2022). Supply Temperature Stabilization of Decentralized Solar Thermal Collectors for Integration into District Heating System. *2022 ASHRAE Virtual Winter Conference*. ASHRAE Transactions. January 29–February 2, 2022, online.
4. Zajacs, A., Borodinecs, A., **Bogdanovics, R**. (2020). Assessment of the efficiency and reliability of the district heating systems within different development scenarios. *11th International Conference on Sustainability and Energy in Buildings, SEB 2019. July 4–5, 2019, Budapest, Hungary.*

Conference papers (not indexed):

1. Ļebedeva, K., **Bogdanovičs, R.**, Zajecs, D. (2023). Use of Existing Water Tanks for Improvement of Building Heating/Cooling System Using Heat Pumps and Solar Collectors, *International Conference on Innovative Engineering Technologies*, Proceedings of the IRES International Conference. May 23–24, 2023, Barselona, Spain.
2. **Bogdanovics, R.**, Zeiza-Seleznova, A., Zemitis, J., Zajacs, A. (2022). TRNSYS model with 3-way valve for heat carrier temperature control of solar thermal collectors integrated into district heating system, *BuildSim Nordic 2022 Technical papers*. August 22–23, 2022, Copenhagen, Denmark.
3. **Bogdanovics, R.**, Zemitis, J., Zubovics, A. (2022). Energy balance of solar collector assisted heat pump in 5th generation DHC system in Northern Europe, 2nd International Sustainable Energy Conference (ISEC 2022) Conference Proceedings. April 4–7, 2022, Graz, Austria.

1. Solar energy applications

The photovoltaic (PV) system is designed to convert sunlight into electricity through the photovoltaic process. It is often the first concept associated with solar energy and has seen widespread application in Latvia in recent years. However, a significant portion of energy demand comes from heating – including building heating and domestic hot water preparation. This study specifically focuses on the solar energy usage in the heating sector.

Electricity generated by PV systems can power electric boilers or heat pumps to produce heating energy. Alternatively, heating energy can be absorbed directly from the sun using solar thermal (ST) collectors – devices that convert solar irradiation into heat. ST collectors are rarely used in the Baltic countries. When implemented, they are mainly combined with storage tanks for hot tap water and are seldom utilized for space heating or pool water heating. This limited adoption presents a challenge which is addressed in this study – how to make solar heating a more technically and economically viable and attractive solution for consumers.

There are many types of ST collectors (Weiss & Spörk-Dür, 2024): flat-plate collectors (FPC), evacuated tube collectors (ETC), unglazed solar collectors. Additionally, photovoltaic thermal (PVT) collectors integrate both solar heat and solar electricity generation within a single device, offering higher energy yields per unit area. This dual functionality is particularly beneficial when roof space is limited, supporting integrated solar energy solutions essential for achieving a climate-neutral energy supply in residential and commercial buildings.

1.1. Solar energy availability

According to the United Nations geoscheme, Latvia is classified as part of Northern Europe. While this study primarily focuses on Latvia's statistical data, the results are largely applicable to other Northern European countries due to their similar climates, regulatory frameworks and shared emphasis on promoting renewable energy sources.

According to (Central Statistical Bureau of Latvia, n.d.), the share of renewable energy sources (RES) in Latvia's gross final energy consumption has shown slight fluctuations but maintained a steady upward trend, rising from 32.8 % in 2004 to 43.2 % in 2023. This increase was observed in both the electricity and heating sectors, reaching a 54.3 % share of RES in electricity and 61.4 % share of RES in heating and cooling by 2023 (statistics table: ENA020). The share of electricity generated from renewables in Latvia grew from 49.6 % (3191.4 GWh) in 2019 to 77.3 % (4846.6 GWh) in 2023. The amount of electricity produced by solar micro-generators and power plants increased significantly – from 2.4 GWh in 2019 to 122.6 GWh in 2023 (statistics tables: ENB210 and ENA050). However, this accounted for only about 2.5 % of the total renewable electricity generated in 2023. In 2024, the total gross electricity production in Latvia was 6083 GWh, with 3209 GWh (52.8 %) generated by hydro power plants, 2196 GWh (36.1 %) by combined heat and power plants, 275 GWh (4.5 %) by wind turbines and 403 GWh (6.6 %) by solar power plants (statistics table: ENB010m).

Latvia is facing a rapid increase in the number of installed solar power plants and aims to further boost the share of RES in electricity production by expanding the installed capacities of

wind turbines and PV panels in combination with energy storage systems and bidirectional electric vehicle charging stations (Cabinet of Ministers Republic of Latvia, 2024) but according to the chairman of the board of the distribution system operator JSC "Sadales tīkls" (Delfi.lv news portal, 2024), solar generation capacity had already reached 660 MW by the end of 2024 and is expected to grow to 900 MW by 2025, exceeding the Latvia's electricity demand during the summer season and potentially causing low or even negative electricity prices during sunny weather. The key challenge, therefore, is managing this surplus solar electricity. One solution is to promote electrification, including the use of cheap solar energy in the heating sector.

Latvia plans to increase the share of RES in heating and cooling by modernizing the installed biomass utilization equipment, increasing the installed capacities of heat pumps and solar collectors, promoting the transition to high-capacity heat pumps or electricity use in district heating and cooling (DHC) systems, and encouraging the combination of various technologies for heat energy production (Cabinet of Ministers Republic of Latvia, 2024).

According to (Weiss & Spörk-Dür, 2024), the global aggregate installed capacity of solar thermal collectors at the end of 2023 amounted to 560 GW_{th} (800 million m^2) with an aggregate annual heat production of 456 TWh which increased by 3 % in 2023 compared to 2022. The total installed photovoltaic thermal (PVT) collectors at the end of 2023 amounted to 1.6 million m^2 with the 822 MW_{th} thermal capacity and 292 MW_{peak} electric capacity. In Latvia, the total solar thermal collector's capacity was 30 MW_{th} in 2022 but half of it (15 MW_{th} or 21,672 m^2 flat plate solar collector farm) was installed in 2019 in Salaspils and was connected to the existing city district heating system, this system is one of twenty largest solar district systems in the world. 92 % of all installed solar thermal collectors in Latvia are flat-plate collectors and remained are evacuated tube collectors.

According to (Central Statistical Bureau of Latvia, n.d.), the heat produced from renewable energy sources in Latvia had minor changes – after increasing by 15.8 % from 4265.3 GWh in 2019 to 4937.3 GWh in 2022, it reduced by 7.2 % in 2023, reaching 4582.8 GWh (statistics table: ENA060). With total number of heat plants of 630 with 2372.4 MW installed capacity and 3342.4 GWh produced heat in 2023, 367 heat plants (1014 MW) operate by using biomass (including firewood, wood chips, pelleted wood, fuelwood etc.), 231 heat plants (643 MW) operate on natural gas, liquefied petroleum gases or fuel oils and only 32 heat plants (716 MW) combine two or more energy sources, one of which is fuelwood or other biomass. Comparing with 2007 year, in 2023 the number of heat plants decreases by 10.6 % and the total installed heat capacity decrease by 37.4 % but the share of renewables increased – in 2007 about 72 % of installed heat plant capacity was based only on fossil fuel but in 2023 only about 27 % of capacity is based only on fossil fuels (statistics tables: ENB100 and ENB090).

It can be concluded that the heating sector is gradually shifting towards the increased use of renewable energy sources, primarily biomass, which is a positive trend. However, the use of solar energy for heating purposes remains minimal. Further analysis clearly shows that relying solely on solar energy as a stable and primary heating source is not feasible, as solar availability is significantly limited during the heating season. However, there are promising opportunities to integrate solar energy efficiently by combining it with other energy sources, especially during the non-heating period, where solar energy can be utilized for domestic hot water preparation.

The economic viability and payback period of integrating solar energy into the heating sector remain key concerns for the industry, along with identifying the most suitable and effective technologies. While the financial aspects are undoubtedly important, they are often variable and influenced by market conditions, so this study primarily focuses on evaluating technological solutions, aiming to explore how to maximize solar heating output while minimizing space requirements, providing a foundation for informed decision-making.

Solar thermal collector output

The power of the solar thermal collector can be found by the equation (Frank et al., 2015):

$$Q_{\text{coll}} = A \cdot G \cdot \left(\eta_0 - a_1 \cdot \frac{\left(T_{\text{m,f}} - T_{\text{a}}\right)}{G} - a_2 \cdot \frac{\left(T_{\text{m,f}} - T_{\text{a}}\right)^2}{G} \right), \tag{1.1}$$

where

Q_{coll} – thermal output of the collector, W;
A – solar collector area, m^2;
G – hemispheric solar irradiance on collector plane, W/m^2;
η_0 – maximum efficiency of the solar collector, dimensionless;
a_1 – heat transfer coefficient at $(T_{\text{m,f}} - T_{\text{a}}) = 0$, $W/(m^2K)$;
a_2 – temperature-dependent heat transfer coefficient, $W/(m^2K^2)$;
$T_{\text{m,f}}$– mean fluid temperature in the collector, °C;
T_{a} – ambient air temperature, °C.

From the European market available solar collector databases (SPF Institute for Solar Technology, n.d.) some solar thermal (ST) collectors – 3 flat-plate (FPC) and 3 evacuated tube (ETC) – have been selected and their technical parameters are shown in Table 1.1.

Table 1.1

Technical characteristics of ST collectors (SPF Institute for Solar Technology, n.d.).

ST collector	η_0	a_1	a_2
FPC Nr.1	0.831	3.08	0.0100
FPC Nr.2	0.773	2.27	0.0181
FPC Nr.3	0.613	5.45	0.0109
ETC Nr.1	0.608	1.14	0.0012
ETC Nr.2	0.568	1.04	0.0024
ETC Nr.3	0.368	0.61	0.0046

Technical characteristics are presented for the gross area and the theoretical thermal outputs of collectors from Table 1.1 are calculated according to eq. (1.1) and presented in Fig. 1.1.

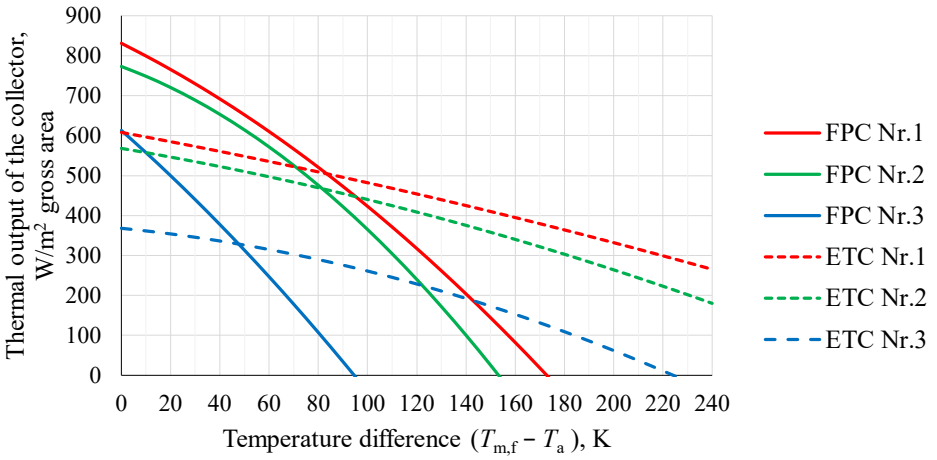

Fig. 1.1. The dependence of the thermal output of solar collectors on the temperature difference at the intensity of solar irradiation of 1000 W/m^2 according to the formula (1.1).

Climate analysis: solar irradiation

According to data from PVGIS-SARAH3 database (European Commission, 2024b), in Riga, the average solar irradiation intensity at the optimal slope (42°) for solar collectors from 2005 to 2023 was 1218 kWh/m^2 (Table 1.2), which is only 6.4 % less than in Copenhagen, similar to Stockholm and 1.4 % greater than in Dublin. In all 3 mentioned location the number of installed capacity of glazes water collectors per 1000 inhabitants is bigger than in Latvia. As the specific solar yield of solar thermal systems for domestic hot water heating in multi-family houses in Latvia is almost the same as in Denmark (414 kWh/(m^2·a) compared to 413 kWh/(m^2·a)) – one of the leading European countries in the solar thermal field (Weiss & Spörk-Dür, 2024), it seems promising to develop this field in Latvia.

Table 1.2

Capacity of glazed water collectors in operation in 2022 and statistics of global irradiation data at the optimum surface for different locations.

(Weiss & Spörk-Dür, 2024): capacity of glazed water collectors in operation,		According to (European Commission, 2024b) monthly global irradiation data (PVGIS-SARAH3), 2005-2023 years, at the optimum slope (42° - 44°), kWh/m^2			
Place	kW$_{th}$ per 1000 inhabitants in 2022	Yearly average	Standard deviation	Average 6-month (April – September)	Standard deviation
Riga	16.36	1218	56	921	46
Stockholm	22.27	1225	48	931	46
Dublin	56.99	1201	45	806	36
Copenhagen	212.10	1301	48	966	47

Placing a solar collector at an optimal angle (42°) increases the annual solar irradiation on the surface by 19 %, compared to horizontal surface. If the goal is to maximize energy during the summer, solar collectors should be installed at an angle of about 30° to the ground, while a 45° angle allows to get more thermal energy from September to April. The fluctuations in solar irradiation throughout the year are relatively stable (Fig. 1.2). In Riga, over a 19-year period, the lowest monthly solar energy amount on a flat surface at a 42° angle to the ground was 10.2 kWh/m², the highest was 224.0 kWh/m². Approximately 76 % of the irradiation was from April to September (data analysis based on PVGIS-SARAH3 (European Commission, 2024b)).

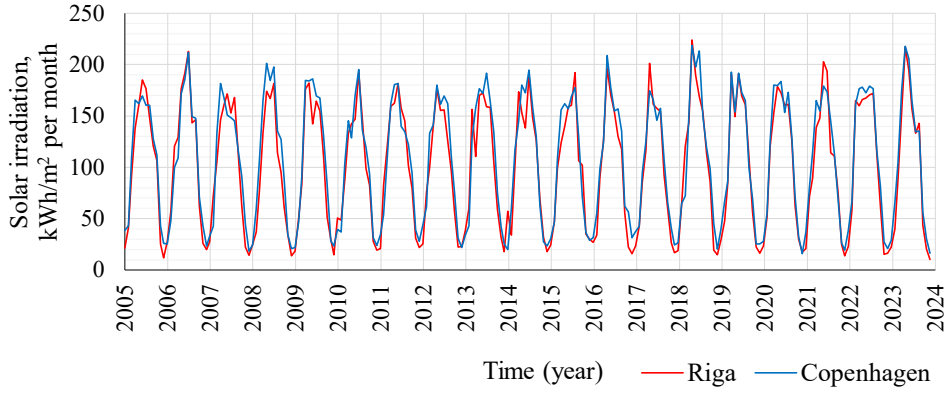

Fig. 1.2. Monthly total solar irradiation intensity in kWh per 1 m^2 of flat surface at an angle of 42° to the earth's surface in Riga and Copenhagen (European Commission, 2024b).

Cloudiness has a big influence on the output from solar collectors. It can significantly reduce solar irradiation and cause variations in thermal output. Fig. 1.3 shows the measurements of solar irradiation changes during the summer on sunny and cloudy days. It is interesting that during the cloudy day the intensity in short periods was higher (>1000 W/m^2) than in the sunny day, which can be explained by the cloud enhancement phenomenon. It occurs when sunlight is scattered and focused by the edges of clouds, briefly increasing solar irradiation intensity beyond clear-sky levels, affecting the maximum solar energy output (Järvelä et al., 2020).

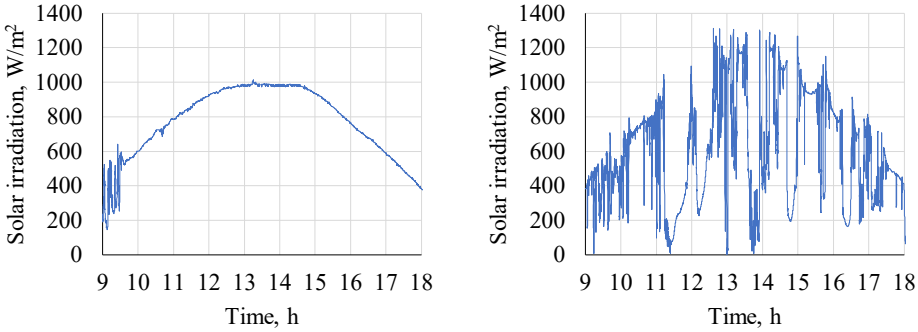

Fig. 1.3. Measured solar irradiation intensity on a sunny (left) and cloudy (right) day from 9:00 till 18:00 in Riga on 45° surface facing south. Step: 2 sec. (Bogdanovičs, 2021).

Cloud coverage or cloudiness is the portion of the sky covered by clouds at a given location and time. Cloud coverage is typically measured in oktas. Usually, 0 oktas mean a clear sky, and 8 oktas indicate overcast – when the entire sky is covered with clouds. However, the Latvian meteorology agency uses a 13-oktas system, where 0 oktas still mean a clear sky, but overcast is represented by 9 and 12 oktas. 10 oktas indicate overcast conditions with thick, dark, rain clouds. 13 oktas are used when the sky is not visible due to fog or snowfall. The climate analysis in the context of solar energy would be incomplete without the data about cloudiness, so the analysis was done based on (Latvian Environment Geology and Meteorology Centre, n.d.) data.

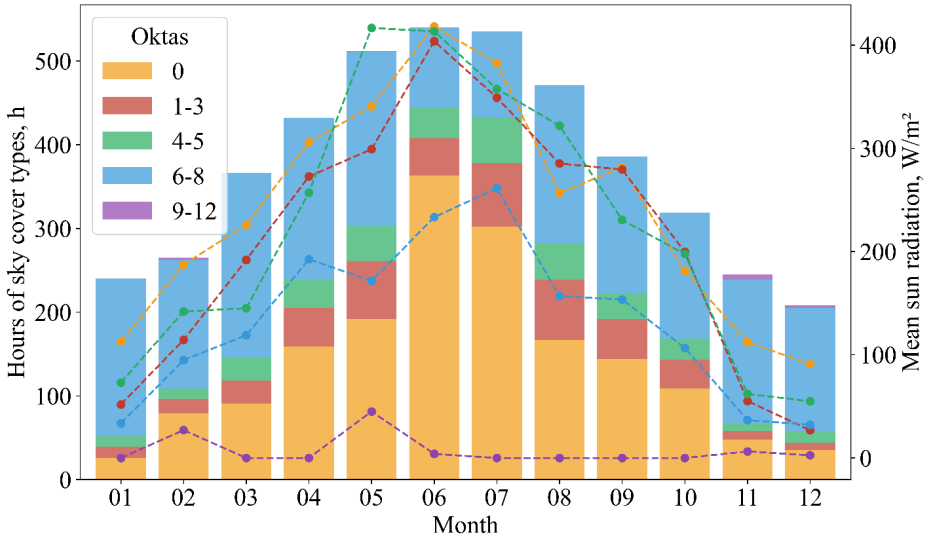

Fig. 1.4. Number of hours of different cloudiness (bars) and the average sun irradiation at this cloudiness (lines) by month for 2021 year based on (Latvian Environment Geology and Meteorology Centre, n.d.) data.

In Fig. 1.4, cloud coverage with corresponding mean sun irradiation in 2021 year is shown for daylight hours (from sunrise to sunset). In summer months, the sky is mostly clear, and solar irradiation is at its highest. However, when the sky is partly cloudy (5 oktas), solar irradiation remains high. In winter months, the number of daylight hours is extremely low, and the sky is mostly covered with clouds (8 oktas), solar irradiation is at its lowest. Weather conditions with the sky covered with rain clouds are relatively rare compared to other cloudiness levels.

Field measurements

To get the representation of the solar thermal collector work under real conditions, the yearly data from the single-family house for one year period was analyzed. Technical parameters of used solar collectors are presented in Table 1.3. Together there were 3 collectors connected in the series. Location: Riga, Latvia. Solar collectors were connected to 500 L hot water tank and were used only for hot tap water preparation. The circulation pump was switched on only when the heat carrier temperature in the collectors reaches 65 °C.

Table 1.3

Technical parameters of the analysed solar collector system

Solar collector type	Amount	Slope	Azimuth	Brutto area, m^2	A, aperture area, m^2	η0 (netto area)	a_1 $W/(m^2K)$	a_2 $W/(m^2K^2)$
Flat plate	3	45°	-17°	2.32	2.13	0.832	3.45	0.014

Measurements of the analyzed system were taken daily from 01.01.2021 till 31.12.2021. The total amount of produced heat energy was 1138.7 kWh (178 kWh/m^2 netto area) but 90.3 % of this energy was produced during 6 months – from 01.04 till 30.09. The maximum daily production was 17.9 kWh (2.8 kWh/m^2) on 25.07.2021. In the winter season, the effectiveness of solar collectors significantly decreases due to low solar radiance and high heating loss.

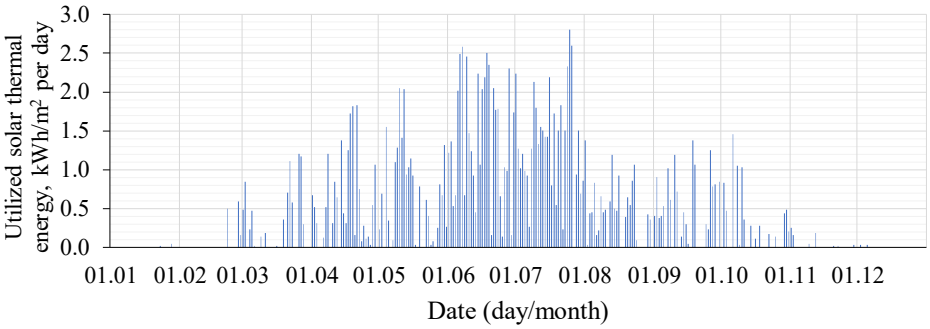

Fig. 1.5. Amount of daily produced heat of analyzed solar collector system.

As it is seen in Fig. 1.5, the main amount of heat energy was produced during June and July. Temperature measurements show that on 25.07.2021 (2.8 kWh/m^2) the average solar collector temperature was approximately +65 °C, but the maximum solar collector temperature (+86 °C) was detected on 15 July, with daily heat production of 1.4 kWh/m^2 and on 16 July, 2.2 kWh/m^2.

The influence of heat carrier temperature on thermal output

Solar collectors (Table 1.3) that are analyzed in this chapter were used for hot tap water preparation. The circulation pump was switched on only when the heat carrier temperature in the collectors reaches 65 °C. According to the eq. (1.1), if the outside temperature is 0 °C (winter conditions), then solar collectors start to produce heat energy ($Q_{coll} > 0$) only when G > 340 W/m^2. If the outside temperature is 20 °C (summer conditions) then solar collectors start to produce het energy only when G > 220 W/m^2. If the solar intensity on the collector plane falls below these thresholds, heat losses exceed heat gain.

Solar thermal collectors convert solar irradiation into heat energy, commonly used for hot water production, space heating, and pool heating. However, efficiency drops during winter months due to reduced solar irradiance and increased heat loss. Reducing the temperature of the heating medium can mitigate heat loss, expand usage to low-temperature heating systems and increase energy production during non-heating periods for domestic hot water preparation.

To improve performance, the heat carrier temperature needs to be reduced. For example, for 30/20 °C temperature regime in winter conditions, with a mean heat carrier temperature of 25 °C, solar collectors start producing heat energy when G > 114 W/m^2, while in summer conditions with G > 21 W/m^2.

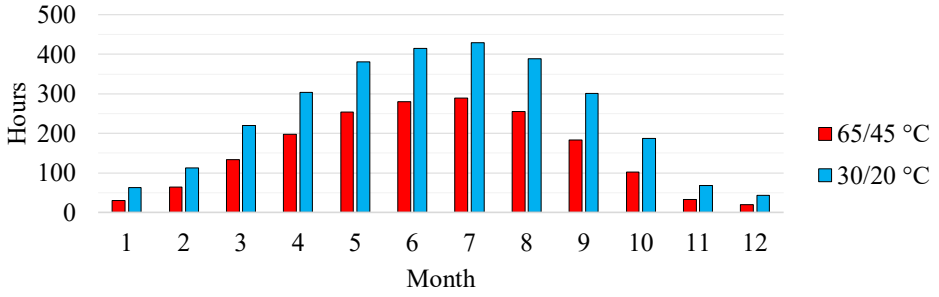

Fig. 1.6. Average amount of hours per month in 2005-2023 years in Riga based on PVGIS-SARAH3 (European Commission, 2024b) database when the thermal output of the solar collector at 45° slope and -17° azimuth is > 0 W according to eq. (1.1).

Analyzing hourly data (Fig. 1.6) on global irradiance and air temperature from 2005 to 2023 in Riga at 45° slope and -17° azimuth (European Commission, 2024b), reveals that the positive capacity (Qcoll > 0) of the solar collectors according to eq. (1.1) is during 21.0 % (1840 hours) of the year at heat carrier temperatures 65/45 °C and 33.2 % (2910 hours) for 30/20 °C. Analyzing only 6 month period (April – September), the capacity theoretically should be positive during 33 % of time for 65/45 °C and 51 % of time for 30/20 °C case.

The maximum theoretical hourly average thermal output of the system, calculated by eq. (1.1), was 762 W/m^2 for 65/45 °C case and 880 W/m^2 for 30/20 °C with maximum solar intensity 1102 W/m^2 on the collector plane.

Theoretically, the 65/45 °C case can produce 554 kWh/m^2 in an average year but 30/20 °C case can produce 841 kWh/m^2 or 1.5 times more energy. To increase the heat carrier temperature from 30 °C to 65 °C, the brine-to-water heat pump or electric boiler might be used.

We can see that this calculated energy amount is much higher compared to field measurements, because it does not consider system inertia and the time which the system needs to reach the temperature before it starts to produce useful energy.

Computer simulation

To get energy calculation results closer to real measurements, the simplified studied system (Fig. 1.7) was modeled in the TRNSYS 18 energy simulation software package. The climate for Riga location was used from the Meteonorm V 5.0.13. database in TMY2 output format. Generic solar collector model using the EN12975-2 efficiency approach (Type1290) from (TESS, 2012) were used to calculate useful produced solar energy for one-year period for two cases: heat carrier temperature 65/45 °C and 30/20 °C (temperatures from/to collectors). Solar collector parameters from Table 1.3 were used. Collector outlet temperature control: modulate flowrate and keep the outlet as close to the setpoint as possible if the collector is gaining energy but turn off the collector if the collector is losing energy. Simulation step: 1 min.

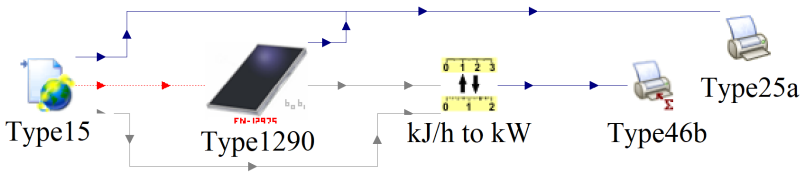

Fig. 1.7. TRNSYS model of flat-plate solar thermal collector.

According to TRNSYS 18 simulations, flat plate collectors in the described conditions can produce 216 kWh/m^2 in the 65/45 °C case and 399 kWh/m^2 in the 30/20 °C case. The total yearly solar energy on the collector plane was 1143 kWh/m^2.

Solar collectors operating on 30/20 °C offer an extended period of positive energy gain, lasting 132 % longer and can potentially generate 85 % more heat energy compared to the 65/45 °C scenario.

To increase the temperature for heating or hot water preparation purposes, the heat pump can be used. While it can raise the temperature, it would require additional electricity consumption, which is considered in next chapter.

Table 1.4

Monthly energy production data of measured and monthly energy and operating hours data of calculated solar thermal (ST) collector with parameter from Table 1.3, located in Riga.

	ST energy measured data (Fig. 1.5), kWh/m^2	TRNSYS calculations (model shown on Fig. 1.7)				
		Energy, kWh/m^2			ST operating hours	
		Solar energy on surface	ST useful energy gain			
			65/45 °C	30/20 °C	65/45 °C	30/20 °C
January	0.1	39.9	2.2	9.2	9.4	46.2
February	1.3	65.7	8.7	21.2	26.8	79.4
March	7.8	108.6	17.7	36.4	41.2	123.7
April	18.5	125.4	22.8	41.9	61.1	135.2
May	24.3	160.5	37.4	61.1	98.2	176.9
June	46.1	163.2	39.3	63.9	99.9	196.7
July	45.2	162.0	38.7	64.1	100.8	200.6
August	13.3	137.1	24.3	47.7	61.0	183.2
September	13.7	97.1	17.4	33.3	57.7	119.9
October	7.3	59.3	7.3	17.9	25.5	73.9
November	0.7	9.4	0.0	0.4	0.0	3.0
December	0.1	15.2	0.1	2.0	0.5	13.1
Total	178.2	1143.4	215.9	399.1	582 (6.6 %)	1352 (15.4 %)

Table 1.4 summarizes the data from solar collector measurements operating in the real system and simulated under two temperature regimes: 65/45 °C and 30/20 °C.

The measured heat energy production of the analyzed system (Fig. 1.5) was 17.5 % lower than the simulated results, with 178 kWh/m^2 compared to 216 kWh/m^2. This discrepancy can be attributed to a key difference between the simulation and real-world conditions: the simulation assumed constant energy consumption, with all produced energy being fully utilized. In reality, energy consumption fluctuates throughout the day, depending on hot water demand. On sunny days with low consumption, surplus heat can lead to collector overheating, reducing the system's efficiency. As mentioned before, the maximum solar collector temperature was measured to be 86 °C, meaning there was low energy consumption during that day.

Based on literature data (Lebedeva et al., 2023; Weiss & Spörk-Dür, 2024) and simplified calculations based on eq. (1.1), it is possible to produce 350–500 kWh/m² per year from solar thermal collectors in Latvia, depending on the collector type, heat carrier temperature, and weather conditions. However, the measured data reveals a significantly lower heat output of 178 kWh/m² per year with a 65 °C heat carrier set point — at least 2 times less than expected. These findings are consistent with dynamic computer simulations, highlighting a clear gap between theoretical potential and real-world performance.

1.2. Solar collectors test facility

To gain more data from solar thermal collectors under different temperature regimes, the test facility (Fig. 1.8) with flat plate and vacuum thermal collectors was designed, constructed and placed on the Riga Technical University roof (Fig. 1.9) in Riga, Latvia, providing the location of solar collectors to the south without shading. The first results were presented in the author's Master's Thesis (Bogdanovičs, 2021) with the title "Decentralized solar thermal collectors integration into district heating system".

Fig. 1.8. The view of the test facility (Bogdanovičs, 2021).

The schematic of the test facility (Fig. 1.10) was based on the scheme from the existing system in Lerum city, Sweden (Lennermo et al., 2019). Flat plate and vacuum tube solar collectors were settled at 45° slope and filled with water-glycol mixture (50%) heat carrier. Pipes, pumps, valves and control devices were placed in a lockable water-resistant cabinet. The water heating unit (heat energy consumer) was located above the cabinet and was protected against rain by a specially designed tin structure. Pipes, accessories and pumps had been selected to ensure the heat carrier flow of 30–150 l/h. The manual balancing valves were set to ensure that the same volume of the heat carrier flows via both collectors.

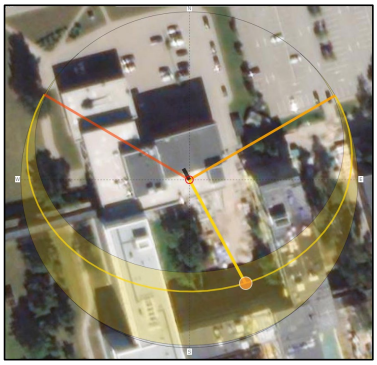

Fig. 1.9. Location of the test facility. Sun position on May 1 at 12:00 (SunCalc.org, n.d.).

The test facility consists of 4 modules (see Fig. 1.10):

- M1: parallel-connected flat plate and vacuum tube solar collectors;
- M2: solar collector connection module for district heating system. The three-way valve controls the temperature of the heat carrier, supplied to the net, based on S12;
- M3: district heating system simulated with electric water heater;
- M4: thermal energy consumer simulated with variable speed water heating unit.

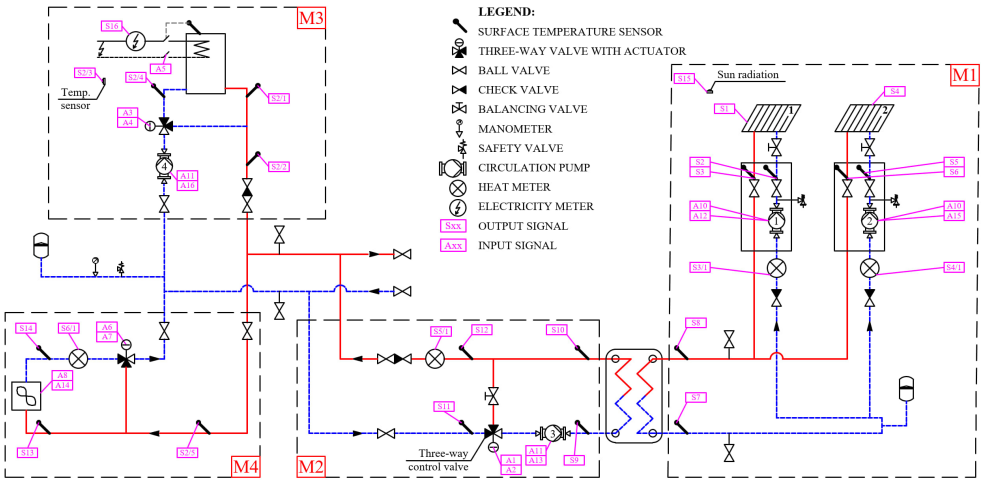

Fig. 1.10. Test facility schematic (Bogdanovičs, 2021).

TRNSYS and TESS component libraries do not have a valve with flow control dependent on system pressure and valve hydronic characteristics. To analyze the influence of valve Kvs coefficient, actuator time constant, hysteresis and inherent characteristics on heat carrier flow and temperature fluctuations in a short period (0.1 s), a Fortran code of "three-way valve with actuator" from TRNLIB was modified and adapted to TRNSYS 18. For the three-way valve it is possible to adjust the response speed, which determines the duration of the transmitted signal for opening the valve and the waiting time between two consecutive opening / closing signals. Three control speeds were investigated: "slow", "normal" and "fast" (see Fig. 1.11). For "fast"

regime, in case of high temperature difference between actual and desired heat carrier temperature, the control valve is moving for longer period of time (so the flow is changed faster) and the pause between moving intervals is shorter comparing to "normal" and "slow" regimes. For "slow" regime, in case the temperature difference is less than 2.3 K, there is no response.

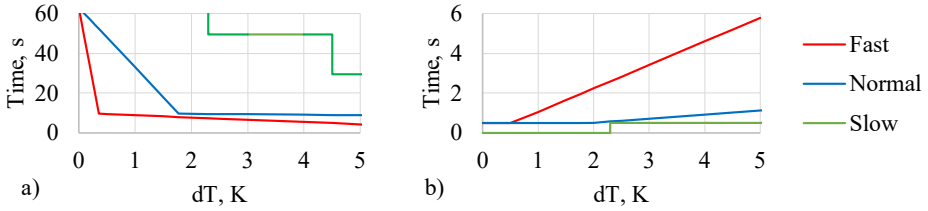

Fig. 1.11. Control signal (a) waiting time and (b) operating time depending on the temperature difference (dT) between actual and specified heat carrier supply temperature.

The operation of the test facility was automated by using the freely programmable controller and was described in the (Zajacs et al., 2022). To improve the quality of measurements, the setpoint values (desired supply and return temperatures) for one day were not changed. Measurement interval: 2 seconds, which allow to notice all temperature fluctuations caused by solar energy variability and control valve operation principle.

The statistical analysis was performed by Python using numpy and pandas libraries and built-in tool of Microsoft Excel "Data Analysis". In order to perform separate analysis on sunny and cloudy hours, the standard deviation (SD) of the solar irradiation intensity during the operation time (from 9:00 till 18:00) of the test facility was calculated and analyzed. The lower the standard deviation, the less fluctuations of the solar irradiation, thus less clouds. If hourly solar irradiation SD < 100 W/m^2, it is assumed that during this hour the weather was sunny, otherwise – cloudy. The standard deviation was selected as one of the major criteria for the analysis because this parameter is closely related to data dispersion. The higher the standard deviation of data sets is, the higher the temperature fluctuations are.

Computer model of the solar collector test facility

For additional in-depth component-level analysis, a test facility model was developed by applying the dynamic simulation computer software TRNSYS 18 (Fig. 1.12). The model was developed based on the parameters of the elements of the experimental test facility and first was presented in the author's Master's thesis (Bogdanovičs, 2021). The main values of every element are described in the Table 1.5.

Input data:

- the outdoor temperature and the solar irradiation intensity during a day from the test facility measurement data; values between input data were linearly interpolated;
- the sun position from Meteonorm data for Riga on the relevant day;
- the heat network supply (P_Supply) and return (P_Return) pressure fluctuations according to Fig. 1.13 (2 scenarios were reviewed, as there were no measurement data regarding the pressure fluctuations in the test facility: 1) supply pipe 63 ±1 kPa, return pipe: 34±1 kPa and 2) supply pipe 60±6 kPa, return pipe: 33±5 kPa).

The model was validated by means of experimentally obtained data.

The simulation step is 0.1 s (minimum possible by simulation software).

Assumptions: no specific data about wind speed, so Meteonorm database data was used. In the model heat carrier flow speed was not considered, so model inertia was lower than in reality.

The heat carrier parameters: water-ethyleneglycol (50 %). The circulation pump with a wet rotor, the efficiency of the pumps depends on the flow volume according to the manufacturers' curves. Inclination of solar collectors: 45°; south direction.

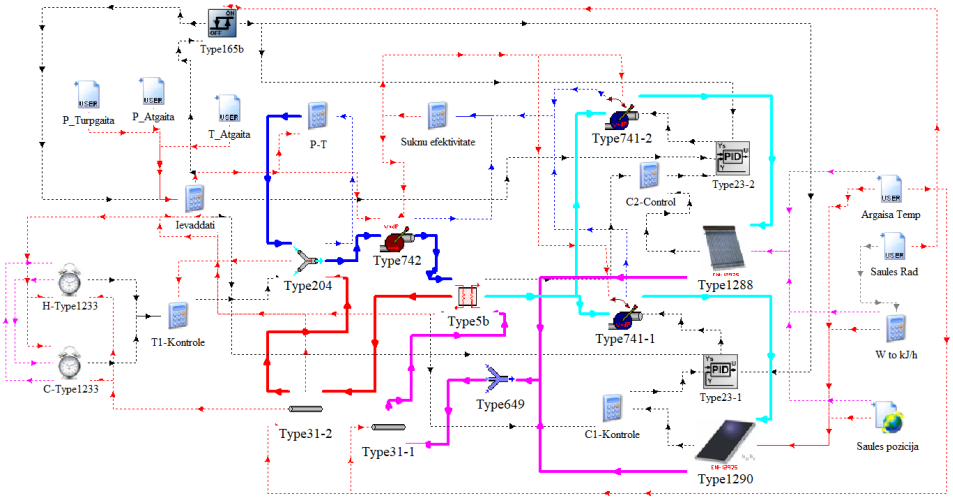

Fig. 1.12. The TRNSYS model (Bogdanovičs, 2021).

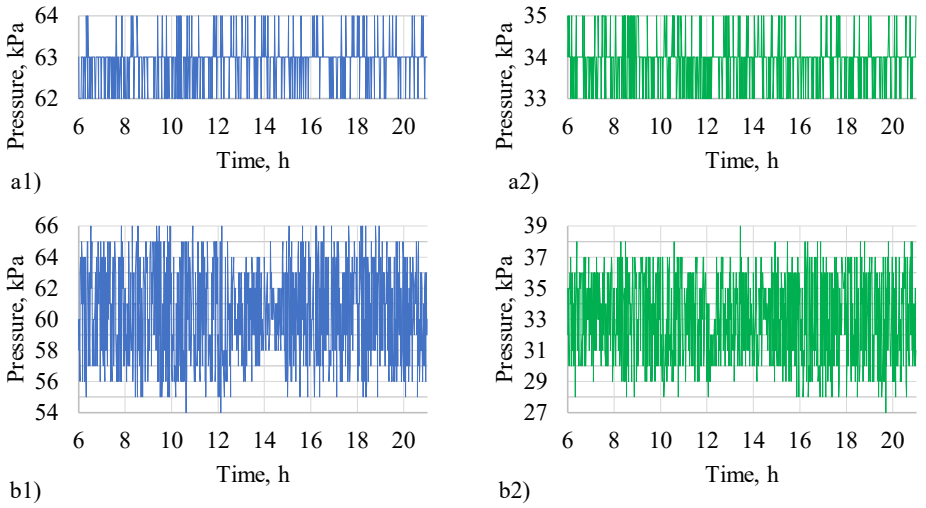

Fig. 1.13. Heat network pressure fluctuation patterns used in simulation. a1) supply pipe, "light" case; a2) return, "light"; b1) supply, "heavy"; b2) return, "heavy" (Bogdanovičs, 2021).

Table 1.5

Variables used in the TRNSYS model (Bogdanovičs, 2021).

Element name	Variable	Value
Heat network parameters (input data)	Supply temperature	65 °C
	Return temperature	approx. 30 °C (measurement data)
	Supply and return pressure	Fig. 1.13
Three-way valve (Type204)	1st and 2nd enclosed Kvs values	0.4 m^3/h
	Leakage at a closed valve	0.001 m^3/h
	Time constant	15 s or 60 s
	Hysteresis	0.05 or 0.025
	Valve curve	Linear / linear
Valve (Type1233)	Operating and waiting time	Fig. 1.11
PID controller (Type23)	Gain constant	3
	Integral time	1 s
	Derivative time	4 s
Circulation pump (Type742)	Pressure	42.7 kPa
	Efficiency	3–19 %, depend. on the flow
Heat exchanger (Type5b)	Heat transfer coefficient	425 W/K
	Kvs value	3.5 m^3/h
Circulation pumps (Type741)	Max flow	100 kg/h
	Pressure	30 kPa
	Efficiency	3–19 %, depend. on the flow
Flat plate solar collector (Type1290)	Area (total)	2.03 m^2
	Efficiency	0.712
	Coefficient α_1	3.18 W/m^2K
	Coefficient α_2	0.01 W/m^2K^2
	Heat capacity of the collector	6.3 kJ/m^2K
Vacuum tube solar collector (Type1288)	Area (total)	1.95 m^2
	Efficiency	0.362
	Coefficient α_1	0.60 W/m^2K
	Coefficient α_2	0.005 W/m^2K^2
	Heat capacity of the collector	6.5 kJ/m^2K

Elements “Type31-1” and “Type31-2” determine the heat loss in the pipelines and fittings of the test facility. The actual heat loss in the system was not known, therefore, for the purpose of the model it was assumed that heat loss was equivalent to the heat loss in a DN15 insulated steel pipe with the heat loss coefficient 10 W/m^2K. The assumed length of the equivalent pipe is 10 m at the side of solar collectors and 4 m at the side of the connection module.

In district heating networks pressure can fluctuate due to the dynamic nature of the system. As part of this research, pressure data from a DH operator was analyzed, covering multiple locations over a one-year period with a one-minute time step. The analysis showed that pressure fluctuations varied even within the same location. Based on these findings, two fluctuation patterns, “light” and “heavy”, were created for a 15-hour period. The absolute pressure in the DH system is higher (up to 6 bar) than in the solar collector test facility, so the pressure values were scaled down, preserving the fluctuation patterns (Fig. 1.13). This adjustment allowed the patterns to be used in computer simulations and can also serve as a basis for future simulations.

Results. Energy production of solar thermal collectors on the test facility

The long-term energy performance measurements of flat-plate (FPC) and evacuated tube (ETC) collectors on the test facility was performed from January to November 2022, with results shown in Table 1.6. TRNSYS simulations were performed using measured solar irradiation, air temperature and heat carrier temperatures as inputs. The calculated and measured values align reasonably well, though monthly variations occur. Annually, the calculated output for the ETC was 11 % lower than measured, while for the FPC it was 8 % higher. In general, the results are comparable to those observed in the field study presented in Chapter 1.1.

Table 1.6

Measured and calculated produced thermal energy by test facility solar collectors by months.

Month	kWh/m^2 solar	kWh/m^2, ETC meas.	kWh/m^2, ETC calc.	kWh/m^2, FPC meas.	kWh/m^2, FPC calc.
January	11.00	0.92	1.01	0.85	1.24
February	32.63	7.74	6.68	9.77	10.62
March	77.81	21.58	18.75	27.51	29.44
April	136.56	36.33	38.65	56.09	70.25
May	194.66	70.54	60.84	101.43	111.15
June	183.42	72.51	55.59	104.38	96.07
July	141.74	23.36	21.94	26.53	28.17
August	119.36	20.13	18.95	24.40	24.60
September	108.93	18.98	21.31	21.89	28.23
October	41.62	3.62	2.36	-2.48	0.00
November	11.72	0.94	0.24	-0.42	0.00

Collectors were tested at two supply temperature setpoints: Low T (35 °C) in March – May, and High T (65 °C) in July – October. As shown in Table 1.7, the difference between measured and calculated thermal output during this period was up to 8 % for ETC and up to 15 % for FTC. At similar levels of total solar irradiation, low-temperature operation enabled up to 94 % more energy use for ETC and up to 163 % more for FPC.

Table 1.7

Total measured and calculated utilized solar thermal energy by test facility flat-plate (FPC) and evacuated tube (ETC) solar collectors in different temperature regimes.

	kWh/m^2 solar	kWh/m^2, ETC meas.	kWh/m^2, ETC calc.	kWh/m^2, FPC meas.	kWh/m^2, FPC calc.
Low T (35 °C)	409.02	128.45	118.24	185.03	210.84
High T (65 °C)	411.66	66.08	64.56	70.33	81.00

Due to high solar intensity, actual heat carrier temperatures sometimes exceeded the setpoint as stated in Fig. 1.14. The thermal output from FPC on two similar sunny days indicates that at high temperature collector produced 2357 Wh/m^2 (32 % of 7360 Wh/m^2 total received solar irradiation), while at low temperature 5041 Wh/m^2 (67 % of 7564 Wh/m^2 solar input).

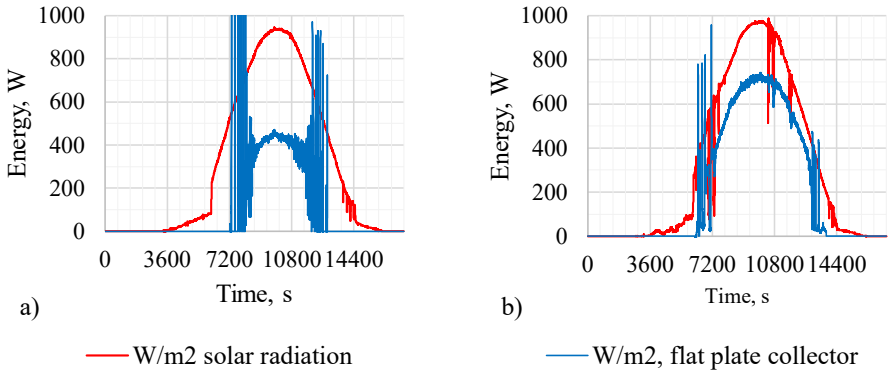

Fig. 1.14. Thermal energy output of FPC and solar irradiation on the collector surface.
a) average heat carrier temperature: 71/64 °C; b) average heat carrier temperature: 44/33 °C.

Overheating measurements

A mismatch between solar energy production and household hot water consumption can result in overheating of the storage tank, stagnation of collectors, solar energy loss and potential equipment damage (Frank et al., 2015; Harrison & Cruickshank, 2012).

To assess the rate of overheating, measurements were taken at the solar collector test facility during four sunny days in June. The results are presented in Fig. 1.15 and Fig. 1.16:

- Day 1: Normal operation with constant energy consumption;
- Day 2: Three short-term energy consumption periods;
- Day 3: No energy consumption;
- Day 4: Two longer energy consumption periods.

A safety algorithm was implemented to prevent equipment damage – activating the circulation pump when the collector temperature reached 140 °C to cool the system. This explains the temperature fluctuations observed near 140 °C.

Fig. 1.16 shows that under sunny conditions:

- on Day 2, in the morning, collector temperatures rose from 50 °C to 140 °C in 2 hours and 30 minutes for FPC and in 50 minutes for ETC;
- on Day 3, with no energy consumption, temperatures remained above 100 °C for 5 hours and 30 minutes (FPC) and 9 hours and 50 minutes (ETC);
- on Day 4, energy consumption appearance rapidly reduced collector temperatures within 1 minute; however, temperatures quickly exceeded 100 °C again once consumption stopped.

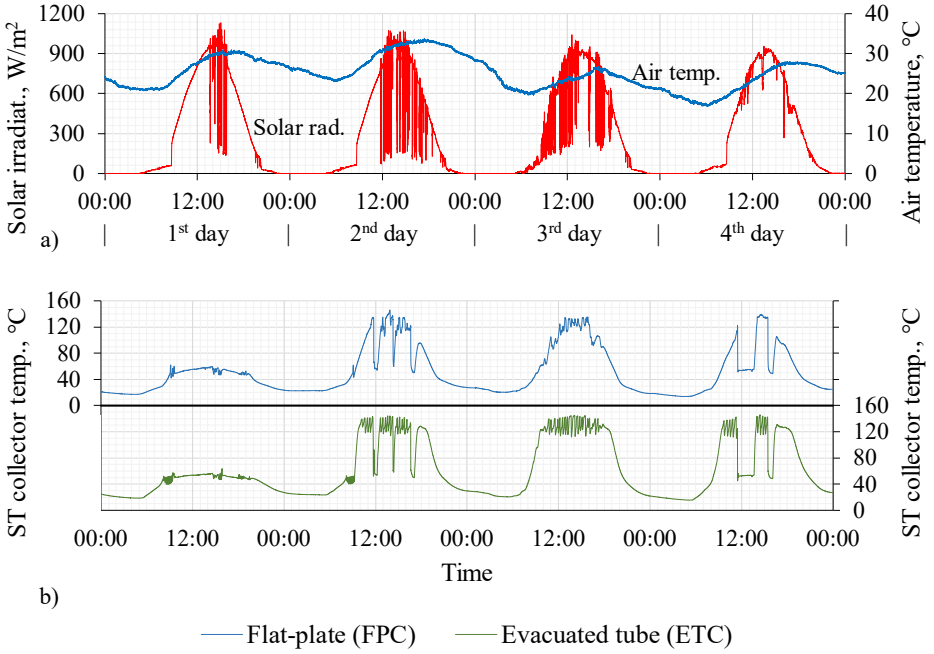

Fig. 1.15. Measured data on the test facility during 4 days. a) Ambient air temperature and solar irradiation intensity on the colletor surface; b) solar collector temperature. Measurement step: 2 seconds.

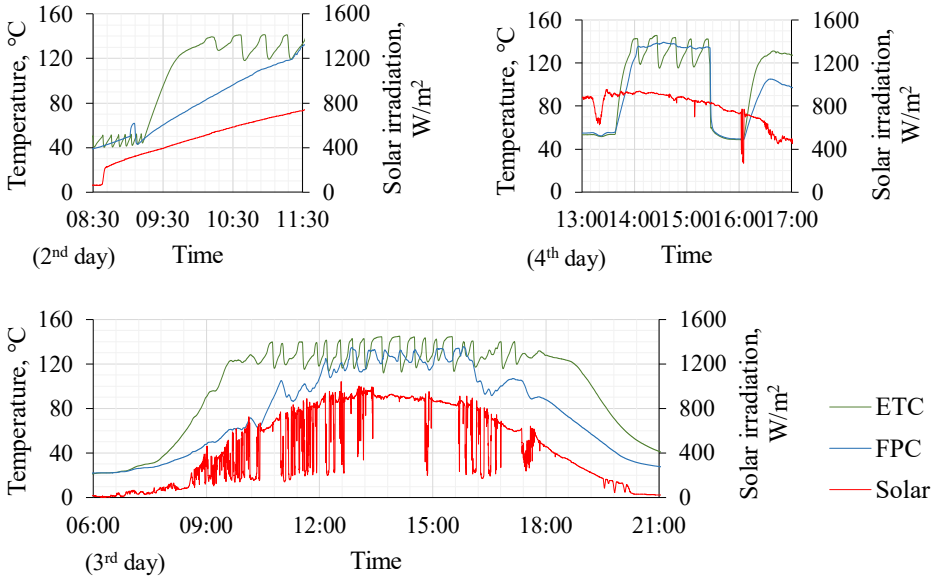

Fig. 1.16. Heat carrier temperature inside flat-plate (FPC) and evacuated tube (ETC) collectors and solar irradiation on collector surface, for 2nd, 3rd and 4th days based on Fig. 1.15.

Temperature fluctuations. Measured and simulated

The research presented in this chapter originated from the author's Master's thesis "Decentralized solar thermal collectors integration into district heating system" (Bogdanovičs, 2021) and was later expanded, completed and published in (Zajacs et al., 2022): Zajacs, A., **Bogdanovics, R.**, Zeiza-Seleznova, A., Valancius, R., & Zemitis, J. (2022). Integration of decentralized solar collectors into a district heating system. *Sustainable Cities and Society*, *83*.

Based on the experimental measurements, data concerning the solar irradiation intensity, outdoor temperature and the heat carrier temperature were selected for two sunny (15.05. and 30.05.) and two cloudy (08.05. and 01.06.) days in 2021, which were used as input data in the TRNSYS computer simulation model. It was assumed that pressure in the networks follows the "heavy" scenario (Fig. 1.13); the valve opening time 60 seconds, hysteresis 5 %.

Values on Fig. 1.17 – Fig. 1.20 are based on the moving average with interval 60 s.

By analyzing the temperature fluctuations on a sunny day (Fig. 1.17 – Fig. 1.18), it can be concluded that the overall trends are very similar to both the data obtained by the experiment and the data obtained in the result of simulation. In both cases the number of temperature fluctuations per hour and the ranges of fluctuations are similar for the measurement and simulation data. In the "normal" mode the period of fluctuation is about 13–15 minutes, while in the "fast" mode the period of fluctuation is about 8–9 minutes with a little lower range.

The temperature values obtained in the result of simulation on the cloudy day at the "fast" control mode are very similar to the ones found in the experiment. By comparing Fig. 1.19 to Fig. 1.20, it can be seen that the range of the temperature fluctuation is considerably less at the "fast" control mode. On cloudy day the measured mean temperature is 1.4 K – 1.7 K lower than simulated (Table 1.8).

The analysis also shows that on sunny days fluctuations are higher approximately before 11:00 and after 16:00 when solar irradiation is below 750 W/m^2.

Table 1.8

Comparison of the experiment measurements and simulation results (Bogdanovičs, 2021).

	Sunny day				Cloudy day			
Date	15.05		30.05		08.05		01.06	
Mode	Normal		Fast		Normal		Fast	
Measurement (M) / Simulation (S)	M	S	M	S	M	S	M	S
Mean value, °C	**63.7**	**64.5**	**63.8**	**64.9**	**62.7**	**64.1**	**63.1**	**64.8**
SD, K	**1.9**	**0.8**	**1.5**	**0.7**	**4.7**	**2.0**	**1.9**	**1.1**
$SD_{meas.} : SD_{simul.}$	2.4		2.1		2.4		1.7	
Kurtosis coeff.	1.3	-1.0	0.0	0.4	-0.7	0.2	1.1	0.1
Assymetr. coeff.	0.1	0.1	-0.4	-0.3	0.1	-0.6	-0.7	-0.3
Range, K	15.6	3.9	8.7	4.7	24.1	12.8	11.4	6.8
Min value, °C	55.2	62.7	59.2	62.2	50.4	55.2	56.3	60.9
Max value, °C	70.8	66.6	67.9	66.9	74.5	68.0	67.7	67.7

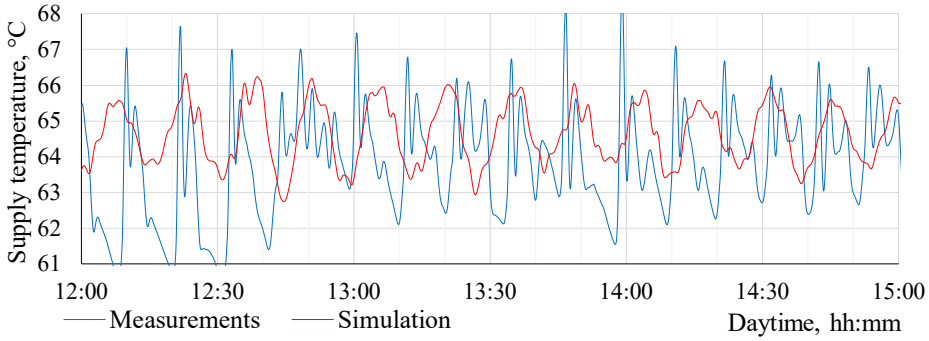

Fig. 1.17. The results of supply temperature measurements and TRNSYS simulation on the sunny day (15.05.2021) from 12:00 to 15:00 at the "normal" mode (Bogdanovičs, 2021).

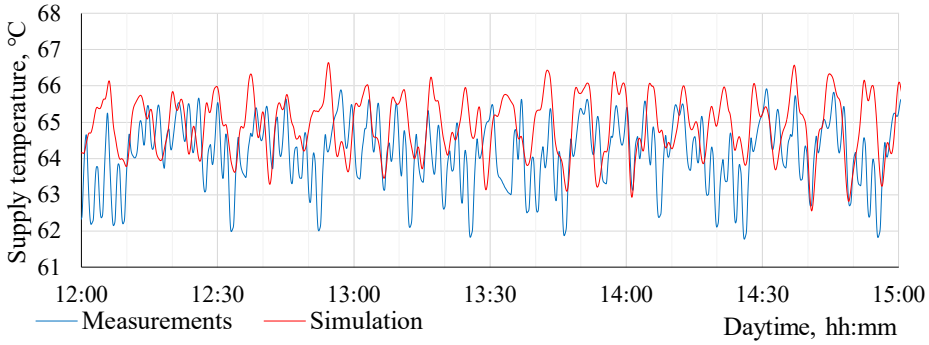

Fig. 1.18. The results of supply temperature measurements and TRNSYS simulation on the sunny day (30.05.2021) from 12:00 to 15:00 at the "fast" mode (Bogdanovičs, 2021).

The statistical analysis (Table 1.8) shows that the measured mean temperature is 0.8 K – 1.1 K lower than the simulated temperature. It can be explained by both the insufficient control degree of the three-way valve and the possible increased heat loss in the pipelines resulting in the heat carrier cooling down faster than predicted. It can also be seen that the maximum and minimum values of the measurement data do not conform with the simulation maximum and minimum values as regards the time, which could be explained by the heat inertia of the systems, which may differ from the value assumed in the model, as well as that the velocity of the heat carrier is not complied with in the model, therefore there is time deviation. Within the simulation the mean supply temperature is by 0.8 K – 1.7 K higher and the standard deviation is by 0.8 K – 2.7 K lower than in the experiment (Table 1.8)

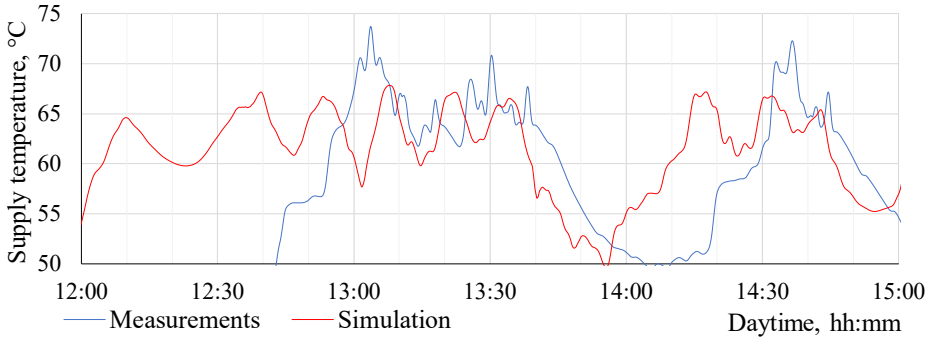

Fig. 1.19. The results of supply temperature measurements and TRNSYS simulation on the cloudy day (08.05.2021) from 12:00 to 15:00 at the "normal" mode (Bogdanovičs, 2021).

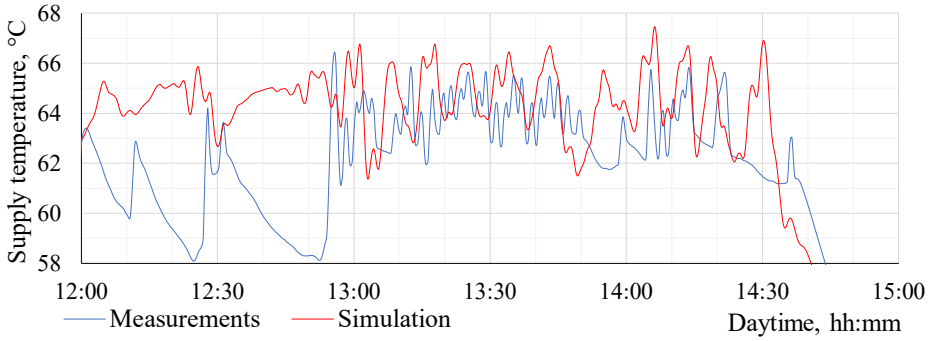

Fig. 1.20. The results of supply temperature measurements and TRNSYS simulation on the cloudy day (01.06.2021) from 12:00 to 15:00 at the "fast" mode (Bogdanovičs, 2021).

However, generally, the trends of the supply temperature fluctuations are similar for the experimentally measured values and the values obtained by simulation. The standard deviations (SD) of the data obtained by experiment and by simulation differ 2.4 times for normal mode and 1.7–2.1 times for fast mode; that can be used as a correction coefficient. In sunny days the SD of measured data obtained in normal mode is 1.3 times higher comparing to fast mode, but the simulation shows the difference of 1.1 times. In cloudy days the SD of measured data obtained in normal mode is 2.5 times higher comparing to fast mode, but the simulation shows the difference of 1.8 times. It can be concluded that the developed TRNSYS model can be used for assessing the effect of the system parameters, but simulated fluctuations are lower.

By using the TRNSYS model, 8 scenarios were simulated for component-level analysis by changing the parameters of the three-way valve. Results summarized in Table 1.9, Table 1.10.

Description of the scenarios: A-B-C-D:

- A: The response speed of the three-way valve: N – "normal"; F – "fast".
- B: Pressure in heat networks (see Fig. 1.13); H – heavy scenario; L – light.
- C: The opening time of the three-way valve: 60 seconds or 240 seconds.
- D: Hysteresis of the three-way valve: 5.0 % or 2.5 %.

Table 1.9

The analysis of the simulation results of the sunny day (15.05.2021) (Bogdanovičs, 2021).

Scenario	N-H-60-5.0	N-H-240-5.0	N-H-60-2.5	N-L-60-5.0	F-H-60-5.0	F-H-240-5.0	F-H-60-2.5	F-L-60-5.0
Mean value, °C	**64.5**	**64.5**	**64.6**	**64.6**	**64.8**	**64.7**	**64.9**	**64.9**
SD, K	**0.79**	**1.04**	**0.53**	**0.65**	**0.35**	**0.71**	**0.26**	**0.30**
Kurtosis coeff.	–1.0	0.2	–0.2	–0.7	0.3	–0.8	1.0	–0.5
Assymetr. coeff.	0.1	-0.2	–0.3	–0.2	–0.2	–0.2	–0.2	–0.1
Range, K	3.9	6.4	3.5	3.3	2.9	3.5	2.4	1.9
Min value, °C	62.7	61.1	63.0	62.8	63.4	62.7	63.6	63.8
Max value, °C	66.6	67.5	66.5	66.1	66.3	66.2	66.0	65.7
Count	13450	13640	13776	13340	13335	13366	13566	13486

Table 1.10

The analysis of the simulation results of the cloudy day (08.05.2021) (Bogdanovičs, 2021).

Scenario	N-H-60-5	N-H-240-5	N-H-60-2.5	N-L-60-5	F-H-60-5	F-H-240-5	F-H-60-2.5	F-L-60-5
Mean value, °C	**64.1**	**63.0**	**64.2**	**64.2**	**64.7**	**64.1**	**64.7**	**64.7**
SD, K	**2.0**	**4.1**	**1.8**	**2.0**	**0.7**	**1.9**	**0.6**	**0.7**
Kurtosis coeff.	0.2	0.5	0.7	–0.2	2.4	–0.1	3.5	2.9
Assymetr. coeff.	–0.6	–0.6	–0.7	–0.5	–0.9	–0.5	–1.1	–1.0
Range, K	12.8	25.5	12.3	10.8	5.2	10.2	5.1	5.2
Min value, °C	55.2	46.3	55.7	57.5	61.5	57.8	61.6	61.6
Max value, °C	68.0	71.8	68.0	68.3	66.7	68.0	66.7	66.8
Count	6294	6776	6714	6349	6390	6180	6681	6519

Based on the results summarized in Table 1.9 and Table 1.10 , it can be concluded that on a cloudy day the standard deviation is 0.3 K – 3.1 K higher than on a sunny day. The change of the control algorithm (reduction of the waiting time of the valve) reduces the standard deviation 1.5–3.0 times. The reduction of the closing speed from 240 s to 60 s reduces the standard deviation 1.3–2.7 times. The reduction of the hysteresis from 5.0 % to 2.5 % reduces the standard deviation 1.1–1.5 times. The reduction of the pressure fluctuations in the networks reduces the standard deviation 1.0–1.2 times. The flow of the heat carrier is almost the same under all the scenarios. On the sunny day it was 32 l/h with SD = 10 l/h; on the cloudy day it was 32 l/h with SD = 17 l/h.

Additional component-level computer simulation analysis was done and presented in (Bogdanovics et al., 2022). A 200 m^2 flat-plate solar collector plant was simulated, at +25 °C ambient temperature, +70 °C heat carrier temperature, and 1000 W/m^2 solar radiation, the solar plant can produce up to 110 kW of thermal power.

The simulation was performed for one day – 02.06.2021 from 7:00 till 19:00. The simulation step was 0.1 s. The outdoor temperature and the solar irradiation intensity on the tilted surface during a day (Fig. 1.21) were taken from the measurement data, values between input data were linearly interpolated. The sun position from Meteonorm data for Riga on a relevant day. The heat network parameters were taken from the existing district heating system (patterns based on Fig. 1.13) with average supply pressure 4.8 bar and average return pressure 2.9 bar. For the "light" pressure fluctuation, in the supply pipe pressure fluctuated in the range 4.71–4.91 bar with standard deviation (SD) = 0.05 bar; in the return pipe 2.81–3.01 bar with SD = 0.06 bar. For the "heavy" pressure fluctuation in the supply pipe pressure fluctuate in the range 4.15–5.35 bar with SD = 0.32 bar; in the return pipe 2.39–3.49 bar with SD = 0.28 bar.

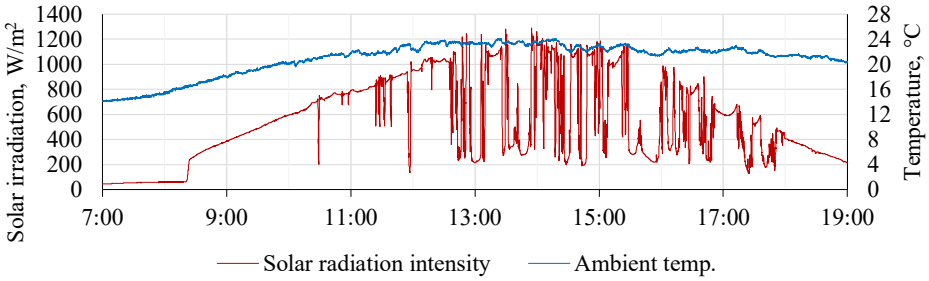

Fig. 1.21. Weather data used in simulation, measured data, step 2 sec.

Table 1.11

Cases description used in the TRNSYS model.

Case	Pressure fluctuation	Response speed	Valve hysteresis	Actuator time constant	Valve Kvs value	Port (from DH) characteristics
0	light	normal	5%	60 s	16 m^3/h	linear
1	**heavy**	normal	5%	60 s	16 m^3/h	linear
2	light	**fast**	5%	60 s	16 m^3/h	linear
3	light	normal	**1%**	60 s	16 m^3/h	linear
4	light	normal	5%	**15 s**	16 m^3/h	linear
5	light	normal	5%	60 s	**4 m^3/h**	linear
6	light	normal	5%	60 s	16 m^3/h	**expon.**

There were relatively high (1.2 K) temperature difference between district heating temperatures with and without solar collectors at the beginning of the day (Fig. 1.25) that might be explained by the solar collector system's heat inertia. From 12:45 to 16:00 the temperature fluctuations were higher than from 10:00 to 12:45 which correlates with solar radiation fluctuations (Fig. 1.21).

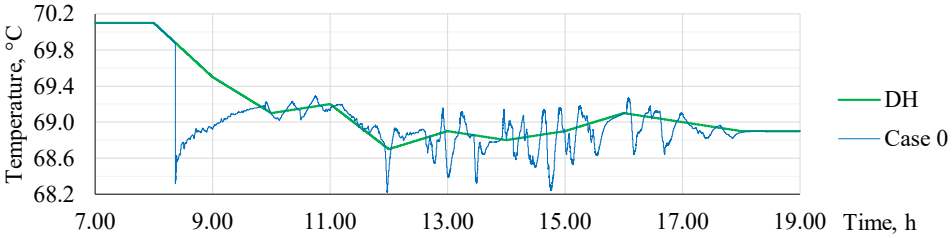

Fig. 1.22. Simulated supply pipe temp. without (DH) and with (Case 0) solar collectors.

Results in Fig. 1.23 show how different control valves and algorithm choices (Table 1.11) may influence the small district heating system heat carrier temperature.

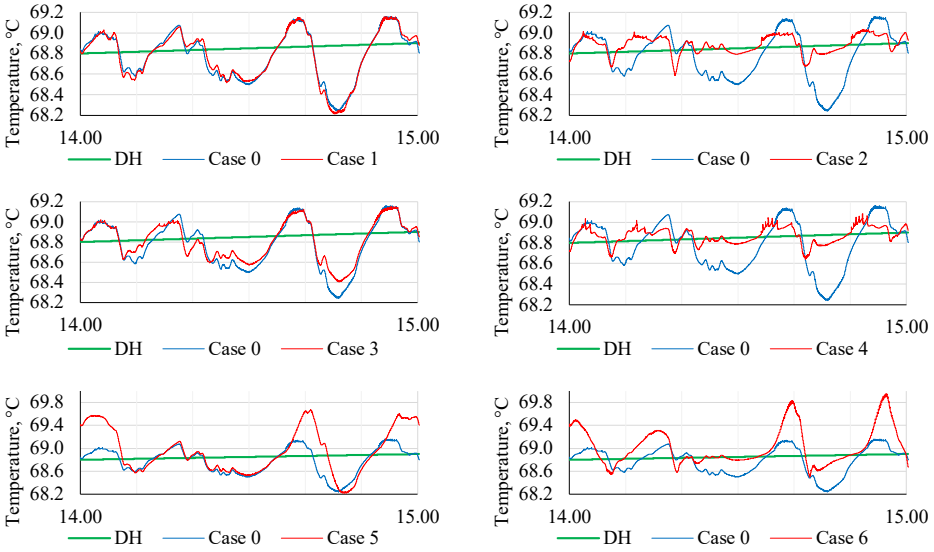

Fig. 1.23. Simulated supply pipe temperature in the district heating system without solar collectors (DH) and with installed 200 m^2 solar collector plant in 0-6 cases (Table 1.11).

The amount of useful heat energy produced by solar collectors 02.06.2021 from 7:00 to 19:00 for Cases 0 – 5 was in the range from 428.0 kWh (Case 2) to 435.0 kWh (Case 1). For Case 6 it was smaller – 419.4 kWh. From 14:00 to 15:00 solar collectors produced only 7.5 % (higher rate) of the whole district heating system energy demand but the heat carrier temperature fluctuates in the range of 0.45 K (Case 2) – 1.47 K (Case 5).

The inappropriate control valve selection can negatively impact system parameters by increasing temperature fluctuations and reducing heat energy output by up to 2 % (based on specific weather and case conditions). Simulations indicate that large pressure fluctuations in the DH system have only a minor effect on temperature stability. Temperature fluctuations can be reduced by increasing the control valve's response speed and lowering the actuator time constant. While reducing valve hysteresis also helps, its impact is less significant. Choosing an undersized valve (low Kvs value) or one with an exponential instead of a linear flow characteristic significantly increases temperature fluctuations.

Long-term measurement results from the solar collector test facility

Results presented here were published in (Zajacs et al., 2022). The experiment took place from 1st June till 16th September 2021 (summer weather). Daytime period: 9:00–18:00. Measurement step: 2.0 s. Data were filtered so that only measurements of the heat carrier from module M2 that were injected into M4 (see Fig. 1.10) were taken into account. Total analyzed data: 505 953. Data were grouped in a way that each hour can be analyzed separately.

During the experiment, different temperature regimes (T1/T2) were used:

- HighT: 80/50 °C, regime usually used in the big scale district heating systems;
- MediumT: 65/42 °C, regime used in the summer in district heating systems;
- LowT: 50/30 °C, regime represent low-temperature district heating.

All temperature regimes were performed both in sunny and cloudy weather conditions and with different control programs ("slow", "normal", "fast", Fig. 1.11). 18 cases were analyzed.

Table 1.12

The statistical analysis of supply temperature measurements

		Sunny hours					Cloudy hours				
Temp	Regime	ΔMean	SD	MAD	Kurt	Skew	ΔMean	SD	MAD	Kurt	Skew
50/30	Slow	1.23	1.34	1.02	6.65	–1.81	0.77	1.29	0.89	5.58	–0.18
	Normal	0.32	0.89	0.47	21.78	–3.67	0.15	1.34	0.88	3.89	–0.87
	Fast	–0.25	1.09	0.88	4.75	–1.55	–0.49	1.11	0.96	–0.65	0.17
65/42	Slow	0.34	1.57	1.07	5.14	–0.57	0.28	2.19	1.58	1.55	–0.36
	Normal	–0.09	1.46	1.03	3.24	–1.12	–0.6	2.09	1.61	0.61	–0.37
	Fast	–0.98	1.46	1.19	1.26	–0.75	–1.07	1.56	1.26	1.46	–0.7
80/50	Slow	–0.65	2.66	2.15	0.42	–0.63	–0.88	2.85	2.20	0.46	–0.8
	Normal	–1.85	2.48	1.84	1.02	0.23	–1.78	2.58	1.98	–0.03	–0.14
	Fast	–2.14	1.49	1.08	2.9	–0.6	–2.07	1.34	1.02	5.8	–0.12

* ΔMean – deviation of measured mean temperature (°C) from supply desired temp.,
SD – standard deviation (K), MAD – mean absolute deviation (K),
Kurt – kurtosis, Skew – skewness of measured values.

The temperature distributions (see Fig. 1.24) seems to be close to the normal distribution but according to Shapiro-Wilk test, they are not. On the cloudy hours the mean temperature in vast majority of cases was lower, and the standard deviation (thus, also the temperature fluctuations) was higher in comparison to the sunny hours. The mean absolute deviation (MAD) of the measured values was also calculated, as it may better represent variability in cases of non-normal distributions, it is more robust to outliers and uses the same units as the data.

For all 18 cases kurtosis is in range -0.6…21.9; asymmetric coefficient (skewness) in range -3.7…0.3. No correlations found between these two coefficients and temperature regimes or control modes. In most cases during sunny hours kurtosis was higher, but skewness was lower, compared to cloudy hours. The best temperature distribution was in the 50-N-S case. In many cases there were two peaks (see 80-L-S, 50-F-C) which is not desirable. The skewness should be close to zero or positive to lower the risks of low temperature supply into the grid. The kurtosis should be higher, indicating more precise control of the feed-in temperature.

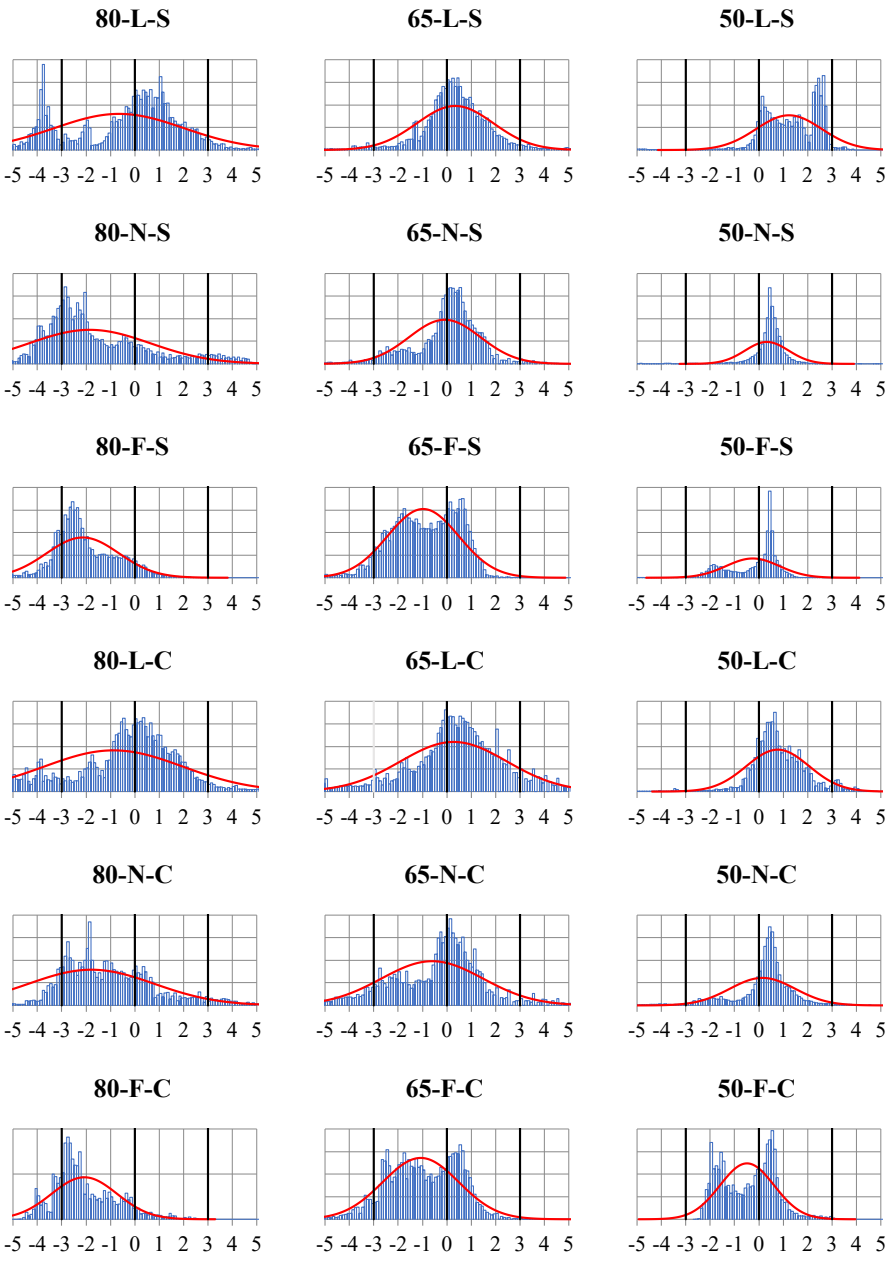

Fig. 1.24. Measured heat carrier supply temperaure distribution
x-axis: heat carrier supply temperature deviation from required temperature
y-axis: number of measured supply temperatures;
red line – normal distribution

80 / 65 / 50 – required supply temperature, °C	L – slow regime	S – sunny hour
	N – normal regime	C – cloudy hours
	F – fast regime	

Quantification of the shape of the probability distributions for supply temperature (Fig. 1.24) could be used as a tool to evaluate the precision of the regulation and control of the supply temperature. Skewness of the distribution shows deviations from the set temperature. According to the technical requirements and DH temperature graphs, supply temperature should deviate within ±3 K. For technical reasons, it is always better to be on the safe side, so skewness should be close to zero or positive to lower the risks of low supply temperature. Kurtosis is a measure of the "tailedness" of the distribution and should be higher, indicating more precise control of the feed-in temperature.

To evaluate if there is a relation between the distribution of supply temperatures and the intensity of solar irradiation, the measurement data were selected based on the solar intensity value at the moment of the measurement. 3 groups were formed as follows: the low solar intensity (100–499 W/m^2), the medium (500–899 W/m^2) and the high (above 900 W/m^2).

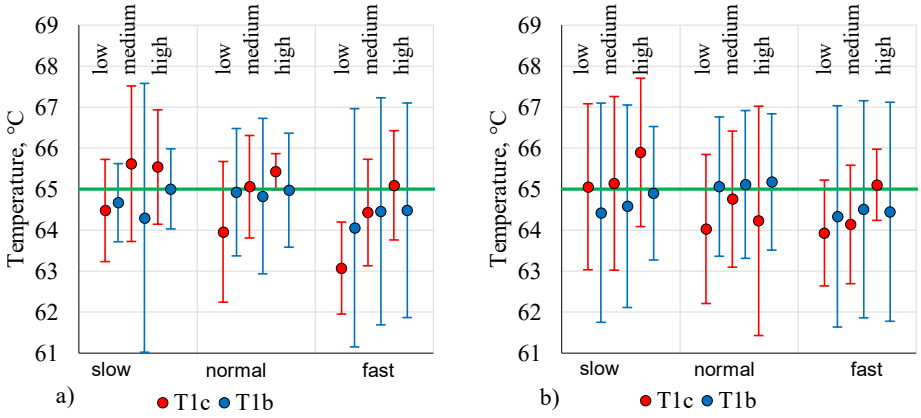

Fig. 1.25. T1/T2 set temperatures: 65/42 °C. a) sunny hours; b) cloudy hours.
Dots – T1 supply temperature mean value; bars – standard deviation.
T1c – temp. from collector module M2; T1b – temp. from el.boiler module M3.
3-way valve control modes: slow / normal / fast.
Solar irradiation [W/m^2]: low (100–499) / medium (500–899) / high (≥ 900).

The mean temperatures and standard deviations of T_{1c} and T_{1b} in different cases were similar, so solar collector connection to “the DH” was not worse than boiler connection, but in many cases solar collector modules provided even higher mean temperature with lower SD.

It was determined by the experiment (see Fig. 1.25) that temperature fluctuations on sunny hours and cloudy hours slightly differ. At the low (100–499 W/m^2) solar irradiation intensity on cloudy hours the mean supply temperature is by 0.1 K – 0.9 K higher with 0.1 K – 0.8 K higher standard deviation than on sunny hours. At the medium (500–899 W/m^2) intensity on cloudy hours the temperature is by 0.3 K – 0.5 K lower with 0.1 K – 0.4 K higher standard deviation but at the high (> 900 W/m^2) intensity there is no evident trend.

Additional analysis shows that T_{1c} and T_{1b} has a moderate positive correlation with T_2 – return temperature from module M4 ($r = 0.51$ and $r = 0.54$, $p < 0.05$). T_{1b} has a moderate positive correlation with T_a – ambient air temperature ($r = 0.57$, $p < 0.05$). There is no correlation between T_{1c} and T_{1b}, between T_{1c} and T_a, between T_2 and T_a.

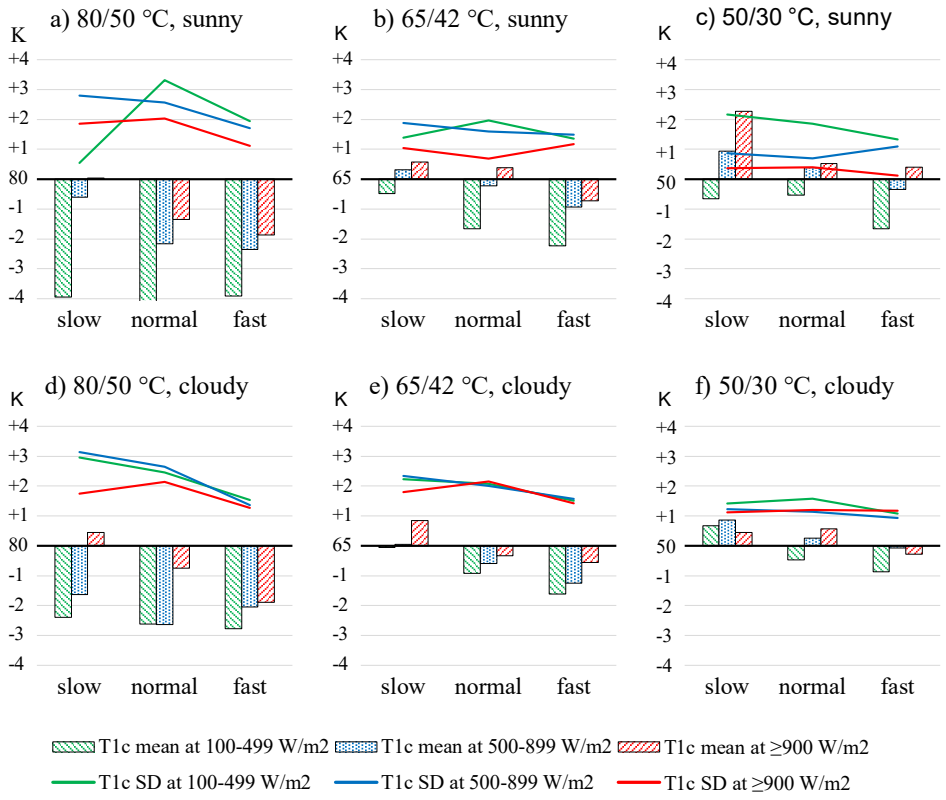

Fig. 1.26. Lines – T_{1c} temperature standard deviation; columns – T_{1c} mean temperature difference from set point temperature

Analysis of Fig. 1.25 and Fig. 1.26 shows the following:

- the measured mean supply temperature is generally lower than the setpoint;
- lowering the supply temperature reduces both the deviation of mean temperature from the setpoint and the standard deviation;
- difference between sunny and cloudy hours are not always clearly noticeable;
- in "fast" control mode, standard deviation is usually lower, but the temperature difference is higher compared to "slow" mode;
- at high solar irradiation level (≥ 900 W/m^2) standard deviation tends to decrease while mean temperature increases.

To ensure the heat carrier temperature from solar collector module reaches a minimum of 80 °C for 98 % of the time without switching control modes, the setpoint must be raised by 12.2 K (to 92.2 °C, +15.2 %), reducing collector efficiency. However, using a dynamic control strategy based on weather can lower the required setpoint to 86.2 °C (+7.8 %).

Similar results apply for other target temperatures:

For 65 °C: 70.6 °C (+8.6 %) without control and 69.6 °C (+7.1 %) with control.

For 50 °C: 55.0 °C (+10.0 %) without control and 54.3 °C (+8.6 %) with control.

1.3. Discussion and conclusions

The investigation of solar energy availability, variability and development potential in Latvia and Northern Europe revealed a steady increase in renewable energy sources and a growing number of installed solar photovoltaic power plants. However, there remains considerable potential for expanding the use of solar thermal (ST) collectors and needs to make this technology more attractive from economical point of view and explore how to maximize solar heating output, providing a foundation for informed decision-making.

Thermal performance

Long-term field measurements and simulations showed that the actual heat output from ST was at least twice as low as reported in the literature. The measured solar heat energy utilization of a ST system in a single family house was 17.5 % lower than the simulated results, with 178 kWh/m^2 compared to 216 kWh/m^2, however heat carrier temperature analysis shows that, in field measurements, temperatures were often higher than expected due to low energy consumption, which may have led to reduced heat utilization.

A seasonal mismatch was observed, with 76 % of total solar irradiation occurring between April and September, during which 90 % of useful solar thermal energy was utilized in field measurements and 83 % in TRNSYS simulations for traditional 65 °C ST applications.

To improve system performance, operating at lower heat carrier temperatures is suggested. Reducing the mean heat carrier temperature from 55 °C to 25 °C can increase energy utilization by 132 %. However, this also raises the challenge of how to effectively use such low-temperature heat – a question addressed in the following chapters.

Overheating risk and the potential of district heating system utilization

During non-heating periods, thermal energy is used only for domestic hot water preparation. However, hot water demand can be irregular – for example, during vacation periods when usage may significantly decrease, leading to a risk of system overheating. The analysis shows that traditional ST systems with local storage tanks can reach a temperature above 100 °C within 30 minutes of stopped energy consumption in the middle of a sunny summer day. Evacuated tube (ETC) solar collectors reach high temperatures faster than flat-plate (FPC) collectors, making them more exposed to overheating risks.

The suggested solution for making solar heating an attractive solution for consumers and reducing the risk of overheating is to connect collectors to existing or newly constructed district heating (DH) systems with significant volume and energy storage potential, if a building already has a connection to DH. Integration of decentralized solar collectors into the networks could be more expensive in comparison to large-scale centralized solar collector plants. However, this solution does not occupy the city's and agricultural lands, and the total potential area for solar collectors on roofs in a city is huge. The decentralized heat source is also located closer to the heat consumer, thus the energy for district heating pumps and heat losses can be reduced.

In Riga, the DH system operates at 65/45 °C during the non-heating season with a defined supply temperature variation of 65 ± 3 °C. Measurements at the solar test facility on such a setpoint showed that small-scale solar collectors can meet the required supply temperature. To ensure a supply temperature of 65 °C for at least 98 % of the time, the setpoint should be 69.6 °C, but in case of a minimum supply temperature of 62 °C for at least 98 % of the time, the setpoint should be 66.5 °C. In this case, the supply temperature will exceed 68 °C for 2–8 % of the time.

The main challenges for thermal solar prosumer units are as follows:

- changing solar intensity during a day;
- the fluctuating differential pressure in the district heating networks;
- the necessity to maintain the stable supply temperature, according to the technical regulations of the district heating operator.

Component-level simulation analysis

To make detailed solar collector performance and temperature fluctuations measurements, the test facility was built, and the TRNSYS computer model was developed and validated. The validation showed that the model predicts similar thermal energy output at high (65 °C) heat carrier temperatures, but at lower temperatures (35 °C), lower output for ETC and higher for FPC.

The system behavior simulation shows that it is possible to make temperature fluctuations in the TRNSYS computer model with a similar fluctuating period, but the standard deviation of simulated fluctuations is 1.7–2.4 times lower. Taking into account all assumptions and simplifications, the model can be used for component-level simulations.

In the results of the simulation, it has been found that the selection of the control algorithm has the most considerable effect on the supply temperature fluctuations. It is suggested to reduce the waiting time of the three-way valve so that the valve responds faster to the temperature change. However, too long an operation time of the valve could contribute to additional fluctuations of the flow and temperature. To reduce fluctuations, it is recommended to select a valve with a lower closing speed and lower hysteresis. Choosing an undersized valve (low Kvs value) or one with an exponential instead of a linear flow characteristic significantly increases temperature fluctuations.

Fluctuation analysis

To describe temperature fluctuations, the standard deviation (SD) and mean absolute deviation (MAD) statistical parameters might be used. The observed fluctuations showed non-normal distribution, so for the further analysis is suggested to use the MAD.

To describe temperature fluctuations, standard deviation (SD) and mean absolute deviation (MAD) can be used. However, since the observed temperature fluctuations show a non-normal distribution, MAD is preferred for further analysis. This is because SD is sensitive to outliers and assumes a symmetric, bell-shaped (normal) distribution, while MAD is more robust and provides a more accurate representation of variability in skewed or irregular data.

The measured MAD of heat carrier temperature from ST collectors varied based on temperature levels, control regime, and weather conditions. At high temperatures (80/50 °C),

MAD ranged from 1.02 K to 2.20 K; at medium temperatures (65/42 °C), it ranged from 1.03 K to 1.61 K; and at low temperatures (50/30 °C), it was between 0.47 K and 0.96 K. In general, MAD is higher during cloudy hours and at the beginning and end of the daytime.

Typical fluctuation period was measured to be about 13–15 minutes in "normal" control mode and about 8–9 minutes in "fast" control mode.

There is no single universal control mode that would be the best in all temperature regimes and weather conditions, but it is clear that with the decreasing supply temperature setpoint, it becomes easier to control the heat carrier temperature.

Limitations

The capacity of the system examined within the scope of this research is very small compared to the systems described in the literature. Smaller systems have lower thermal inertia, which might affect the choice and performance of control algorithms.

Although (Schäfer & Thomas, 2018) highlight the impact of differential pressure fluctuations in heat networks, such fluctuations could not be physically replicated on the test facility. Instead, they were simulated in TRNSYS software, showing that high pressure variations increase the supply temperature's standard deviation by only 1.2 times compared to "normal" conditions. This aspect should be explored further in future studies using systems connected to actual DH networks.

Measurements were carried out under real outdoor conditions, which varied daily (solar irradiation, air temperature, wind). As a result, control strategies and temperature setpoints could not be tested under identical conditions. However, this variability was mitigated by conducting long-term measurements to ensure reliable results.

Future studies

Further research should involve connecting the solar thermal unit to a real district heating system and conducting long-term performance measurements. Future studies should also explore the use of variable set temperatures and control algorithms based on the time of the day, weather conditions, meteorological forecasts, and differential pressure. Additionally, the potential of machine learning algorithms to improve system control and efficiency should be evaluated.

Based on the current findings, several recommendations can guide future development to enhance solar collector performance and reduce temperature fluctuations.

- The developer of the control algorithm of solar collector systems should take into account not only the temperature difference between the setpoint and actual values but also weather conditions, especially cloud cover.
- Technical regulations issued for connection to the district heating system should consider the limitations of the small-capacity solar thermal collectors. The district heating system operator can consider providing a more flexible temperature schedule by defining a higher temperature deviation. For example, +65 ± 5 °C instead of +65 ± 3 °C, unless it can compromise the reliability of the whole DH network, which needs to be investigated in the future research.

2. Solar district heating system

The European Union (EU) has set ambitious goals to become the first climate-neutral region on the planet by 2050 (European Commission, 2020). There are numerous possibilities for generating and transferring heating energy for domestic and industrial needs. One of the environmentally friendly, financially reasonable and cost-effective solutions for populated areas is a district heating (DH) system (Lake et al., 2017). According to the statistical survey by Euroheat & Power on the district heating and cooling sector, there were around 6000 DH networks in the EU, providing approximately 11–12 % of the total heat demand. Some counties do not have district heating at all, but some provide more than 50 % of heat energy by this system (Buffa et al., 2019; Werner, 2017). DH systems are being proposed as the future solution for urban heating in Europe, with high potential to boost the integration of renewable energy in the heating sector. In Riga, there is a wide DH system, which provides heating for 70 % of the Riga building sector with an overall energy demand of 3 TWh, which ought to implement energy efficiency improving activities in this field.

Implementation of the carbon-neutral policy which 195 countries have undertaken to achieve by 2050 according to the Paris Treaty is among the solutions to slow down the climate change rate (Debbarma & Choi, 2022). Decarbonizing the heating and cooling sector is crucial for advancing the energy transition – a priority recognized by the European Green Deal and the "Fit for 55" package. Increasing the share of renewables in this sector is essential to achieving energy and climate targets cost-effectively (Heating and Cooling, n.d.). According to the EU Strategy on Heating and Cooling (EUR-Lex - 52016DC0051 - EN - EUR-Lex, n.d.), this involves renovating the existing building stock, improving energy efficiency, and integrating renewable energy sources, supported by decarbonized electricity and district heating.

2.1. State-of-the-art

Northern and Eastern Europe have relatively high district heating (DH) market penetration rates, ranging from 30 % to 65 % (wedistrict.eu, 2020). DH networks, which supply heat to multiple buildings from centralized heating plants, are continuously expanding. According to the International Energy Agency reports (IEA, 2020), the total length of operational DH pipelines in Europe grows by approximately 3000 km each year, highlighting the potential for integration of new technologies and sustainable concepts. DH networks play a crucial role in advancing local energy communities and supporting the transition to 100 % renewable societies. By facilitating the exchange of surplus heat produced by decentralized renewable energy sources, DH systems help meet the needs of consumers with high heat demand and reduce reliance on fossil fuels (Dino et al., 2023).

Despite progress in using renewable and sustainable energy sources, such as waste materials, waste heat, solar thermal, and geothermal resources (Arabzadeh et al., 2019; H. Lund, Vad Mathiesen, et al., 2014), a significant portion of heating demand still relies on fossil fuels (Barco-Burgos et al., 2022). Many district heating systems in Europe remain heavily dependent on these conventional energy sources. To accelerate decarbonization, the European

Commission has identified heating and cooling as one of the three core areas targeted in the Renovation Wave strategy. In support of this goal, a Heat Pump Action Plan was introduced in 2023, aiming to enhance the adoption of renewable heating technologies (European Commission, 2023, 2024a).

The Baltic region has widespread DH systems that need to be transformed according to EU regulations by increasing the share of renewable energy sources and reducing greenhouse gas emissions (Grzegórska et al., 2021). Latvian mid-term and long-term heating sector planning documents foresee the increase of solar energy use, electrification of the heating sector by increasing the share of heat pumps (HP) and implementation of the renovation measures for building stock (Cabinet of Ministers Republic of Latvia, 2022; Directorate-General for Communication, 2024; International Energy Agency, 2024). There are several initiatives for the transition towards low-temperature DH in the Baltic (LowTEMP project, 2020), where different approaches and strategies were proposed, and pilot projects were implemented. Nordic Energy Research (Volkova et al., 2021) aimed to map and quantify excess heat sources for three Baltic states – Latvia, Lithuania and Estonia – to evaluate the potential of integration of the heat pumps in the DH systems. Current development plans of the biggest DH provider in the city of Riga include the goal of becoming an energy exchange platform (Dienas Bizness, 2023), allowing the excess heat from production processes to enter the networks.

In recent years, the DH industry has increasingly embraced more sustainable energy sources, including heat pumps, condensing biomass boilers, solar thermal collectors, and excess heat utilization (Jodeiri et al., 2022; Johansen & Werner, 2022). This transition has been accompanied by a shift towards low-temperature district heating (LTDH), which offers significant benefits in energy conservation during both production and transmission stages, providing a wide set of economic benefits which are broadly addressed in the study (Averfalk et al., 2021), and more heat obtained from solar collectors are among them. As was discussed in the previous chapter, both flat plate and evacuated tube solar collectors achieve their maximum heat output at lower DH supply temperatures, reinforcing LTDH as a promising concept for broad integration of prosumers and developing high-capacity heat storage solutions.

Solar thermal energy and heat pumps are both well-suited for DH systems; however, their implementation comes with certain limitations related to temperature requirements and operational regimes (Migla et al., 2020). In the Baltic countries, ST collectors are primarily used by individual single-family homes in combination with storage tanks for domestic hot water preparation. Their application within DH systems remains limited, with only one example of a centralized ST field integrated into a DH plant (Lebedeva et al., 2023). Although some multi-apartment and municipal buildings use solar collectors (Gendelis & Mikelsons, 2022), these systems often rely on storage tanks which are not connected to the DH system. This approach raises several challenges, including increased capital investment and potential risks to domestic hot water hygiene during periods of low water consumption. Furthermore, small storage tank volumes combined with limited hot water usage can result in system overheating, ultimately reducing efficiency. To overcome these issues, it is proposed to connect ST systems to LTDH networks. This integration would allow excess energy to be stored within the grid and shared with neighboring households, improving system flexibility and performance.

District heating system generations

In Latvia, the majority of residents receive heat supply through district heating systems. The existing system in Riga is a 3rd generation system (3GDH). It operates with pre-insulated pipelines and heat carrier temperatures typically below 100 °C (65 °C during the non-heating period, averaging 70 °C – 80 °C during the heating season, and reaching up to 118 °C during extreme cold conditions (–20 °C ambient temperature)). In response to policies promoting decarbonization and energy efficiency, Latvia's DH system is undergoing transformation, with various development scenarios under consideration (Zajacs et al., 2021; Zajacs & Borodiņecs, 2019). Research indicated that existing DH networks can be cost-effectively converted into 4th generation district heating systems, which operate at lower supply temperatures and offer benefits such as reduced grid losses and lower production costs (H. Lund et al., 2018a).

According to (H. Lund et al., 2021; H. Lund, Werner, et al., 2014), 4th generation district heating (4GDH) systems are classified as low-temperature district heating (LTDH) networks, operating with heat carrier temperatures of 50 °C – 60 °C in the supply pipe and approximately 25 °C in the return pipe. 5th generation (5GDH) systems are ultra-low temperature district heating (ULTDH) networks, operating at close-to-ground temperatures (below 30 °C) with distributed heat pumps. Importantly, 5GDH is not a direct continuation of 4GDH but rather a parallel, complementary approach within the broader family of advanced district heating technologies. The 5th generation district heating and cooling systems, which are gaining traction in Europe, particularly in Germany and Switzerland, operates at a natural feeding temperature of 4 °C to 25 °C. They can also function at lower temperatures, even down to -5 °C, with the aid of a brine mixture. The 5GDHC system introduces the “prosumer” concept, where energy is both consumed and produced. This innovative system also incorporates solar collectors in some instances (Buffa et al., 2019; H. Lund et al., 2021; Millar et al., 2021a; Revesz et al., 2020).

LTDH is a promising heat supply technology with strong potential for integrating renewable and waste energy (D. Schmidt, 2018). A survey of over 50 DH experts from 13 countries (Guzzini et al., 2020) identified high distribution heat losses as a major drawback of traditional systems, while highlighting LTDH’s ability to reduce these losses. Key barriers included high investment costs, limited retrofitting options, supply temperature restrictions, and the need for new business models. Despite these challenges, many experts believed LTDH could see widespread implementation within the next 20 years.

Transforming existing district heating systems into LTDH or ULTDH networks is a complex process that requires coordinated actions at multiple levels to balance heat source and network temperatures. The transition should start at the consumer level, where building renovation and demand reduction enable the use of lower heating temperatures. Once consumers are prepared, pipeline temperatures can be reduced, making it possible to integrate low-temperature energy sources, such as decentralized heat pumps and solar thermal systems, as alternatives to a single central plant (Averfalk et al., 2021; Stock et al., 2024). Heat pumps powered by renewable electricity are expected to play a crucial role in future DH systems, shifting from a few centralized fossil fuel-based heat generators to a more flexible network of smaller plants combined with energy storage (Wittenburg et al., 2023).

While transitioning from the existing 3GDH to the 5GDH model in the Baltic countries presents challenges – particularly due to the significant capital investments required – the region's ambitious energy and climate goals (Volkova et al., 2022) open the door to integrating certain key elements from the 5GDH approach. This could improve Latvia's DH system's efficiency without necessitating substantial capital investments.

Modifications of existing DH systems are preferable due to possibilities of improving their efficiency by combining and integrating different components and reducing dependency on fossil fuels by increasing renewable energy use. From the point of view of reducing the impact on the environment and human health, DH modernization projects have great potential (Lake et al., 2017; Nannou et al., 2016; Sernhed et al., 2018).

Currently, DH in the EU remains extremely dependent upon fossil fuels (Sayegh et al., 2018). In Riga heat is produced both by Combined Heat and Power (CHP) plants and Heating plants using for this purpose natural gas as well as biomass. One of scenario how to integrate renewable resources in DH and increase its efficiency is by using heat pump (HP) technology that is recognized as a renewable resource in most EU legislation (Sayegh et al., 2018). However, (Tamasauskas et al., 2015) argue, that the method of calculating renewable energy from heat pumps from different heat pump technologies provided by the 2009/28/EU Directive and guidelines 2013/114/EU does not take into account the primary energy input for transforming electric power. Therefore, the calculated amount of renewable energy generated by heat pumps is higher than it should be.

Solar thermal in district heating system

Thermal solar collectors are a technology used to capture renewable energy, but their potential is often limited by fluctuations in heat production, as they generate no heat at night and produce less during cloudy weather. To meet heat demand, more solar collectors can be installed, with excess heat stored in local accumulation tanks. However, an oversized collector system can result in surplus heat that cannot be stored, causing the heat carrier's temperature to rise, leading to system overheating and reduced efficiency (Kolsi et al., 2021).

One solution is to integrate solar collectors into the DH systems, allowing surplus heat to be transferred to the DH network. When solar collectors produce insufficient heat, energy can be drawn back from the DH system, eliminating the need for large local accumulation tanks. It will be possible to install the highest possible number of solar collectors on the roof to produce more heat by using solar energy.

There is growing research interest in integration of decentralized energy sources and prosumers, as well as developing positive energy districts. However, some researchers (Brozovsky et al., 2021) highlight that existing definitions often lack methodological clarity, meaning that key performance indicators, system boundaries and targets are not always clearly defined. This makes it hard for policymakers, researchers and planning professionals to carry out an independent assessment of reported performance.

It is important to find out which solar collector system and approach is more efficient and more profitable from the economic point of view: centralized or decentralized. There was an attempt to find an answer to this question (Rämä & Mohammadi, 2017) using computer

simulation. In the research, it was concluded that the pay-back time of the centralized systems of solar collectors with lower initial investment is 10–11 years, and the decentralized system is not profitable from the economic point of view. The main reason for this is the high initial investment. With high investment costs in the decentralized solar collector system, the total heat price will increase. To improve the attractiveness of the decentralized system, it is necessary to reduce initial investment and to improve efficiency. Within the scope of the research, a very low number of solar collectors were installed in every building (only 6 m^2). If the area of collectors per roof is increased, the initial investment per collector 1 m^2 will decrease. In the decentralized system, a 500 L accumulation tank was used in every building. If the collectors are connected to the district heating via a heat exchanger without using the accumulation tank, the initial investment will decrease, and the surplus heat will be transferred to the network where it can be used by neighbors.

The world energy sector is going to change from its present state of centralized energy generation to a future state with a larger share of distributed generation. Transient performance assessment and techno-economic analysis should serve as a basis for justified decision making and reasonable integration of decentralized energy sources. The research (Cao et al., 2022) shows the TRNSYS potential for the abovementioned purposes, showing the lowest and highest exergy values for the examined hybrid solar-geothermal system.

Some other investigations were made both with TRNSYS dynamic simulation software and by experimental analyses for Warsaw, Lisbon, Madrid, etc. Most systems show primary energy and CO_2 reduction in hybrid solar heating and cooling system, however high investment costs and a high payback period (10–35 years) might be a problem (Calise et al., 2022; Figaj & Żołądek, 2021).

For the solar-driven district heating and cooling system, both time and space mismatches between supply and demand are two key problems to be solved (Sun et al., 2023). This issue can be mitigated by implementing a large-scale heat storage system and allowing for the expansion of storage capacity in response to an increase in the size of the solar collector plant. In this context, utilizing a district heating system for heat storage emerges as a potential solution. However, dynamic exergy and economic assessment of the seasonal underground thermal storage shows that charging the seasonal thermal energy storage at low temperatures increases the specific cost of the heat stored (Veyron et al., 2022).

Prosumers

District heating networks usually have centralized thermal energy production sources at a sole location and energy sources are limited by the installed heating units, while decentralized district heating system allows using and adding multiple energy sources and technologies, such as solar thermal, moderate geothermal resources, industrial waste heat, backup boiler and seasonal storage (Bertelsen et al., 2021). Furthermore, the inclusion of prosumers might be the best way to enhance an existing grid that has been pushed to its technical or economic limits (Lichtenegger et al., 2017). The concept of the 5GDH system includes the possibility to use the network as an energy storage system and simultaneously as a source of heat and cold for buildings' heating and cooling using heat pumps, as well as introducing the concept of

"prosumer" – an individual who both consumes and produces energy (Buffa et al., 2019; Millar et al., 2021b; Revesz et al., 2020).

Despite the apparent usefulness of prosumers in the DH grid, even pioneering countries such as Sweden have not seen a general uptake in prosumer integration in the DH sector. The study (Selvakkumaran, Axelsson, et al., 2021) investigates the drivers and barriers for prosumer integration in the Swedish DH sector and among other barriers such as regulations and policies indicate technical barriers which may affect the enabling of prosumer integration. Explicit literature review shows that most of the articles studied mention the following barriers (Brand et al., 2014; Brange et al., 2016, 2017, 2019):

- a risk that the heat produced by prosumers does not match the heat demand in the heating network. This is dependent on the type of prosumer and the heat source and may act as a barrier from the DH company's side;
- the 'bottlenecks' are caused by the integration of prosumers. Bottlenecks are areas in DH networks in which it is difficult to maintain a sufficiently high differential pressure;
- lack of technical control over the heating units belonging to the prosumer;
- malfunctions of technical solutions may disrupt the power balance in the DH network.

Operational analysis

The analysis of integration of decentralized renewable thermal energy production sources in the district heating system (Brand et al., 2014; Brange et al., 2017; Huang et al., 2020), show that the physical control of the prosumer unit should meet the following principles:

- should be robust and reliable;
- precise temperature control, to meet DH network requirements;
- remote access in order to be able to adapt to different business models and to reduce human interference;
- low maintenance costs and efforts.

The analysis of the data from existing case studies (Lennermo, 2020) give strong evidence that prosumer problems are mostly depending on two parameters:

- the DH system characteristics, where a prosumer unit is going to be integrated (differential pressure and pressure oscillations);
- distributed generation source characteristics (source capacity, stability of heating power and feed-in temperature).

However, limitations found in the operation of one unit might not be the same when operating in another environment.

There are 4 basic schemes for connecting solar collectors to the district heating system, all of them explicitly addressed by the study of (Lennermo et al., 2019). To minimize heat carrier temperature fluctuations, the optimal approach is to use solar collectors to heat the heat carrier from the return pipeline of the network and then deliver it to the supply pipeline.

The data concerning the operation of the current systems indicate that considerable temperature and flow fluctuations are possible. In Düsseldorf (Germany), an experimental solar collector farm with a total area of collectors 232 m^2 (gross) was constructed on a roof of an apartment house and connected to the existing city district heating system. The supply

temperature in the heat networks is 70 °C – 100 °C in summer, the temperature difference between supply and return pipes is 20 °C – 30 °C in summer and above 40 °C in winter. The pressure difference is within the range of 1.5 bar – 4.2 bar. The experimental connection was constructed in such a way that it would be possible to examine 4 different connection variants. Within this experiment (Schäfer & Thomas, 2018) it was concluded that there was potential for improving by reducing the flow and responding faster to the necessity of changes of the flow volume, by the optimum setting of the PID controller.

The study (Heymann et al., 2018) analyzed two different operating connections of solar collectors to the district heating system in Dresden (Germany). The system FP1 with the designed capacity of 30 kW (83 m^2) was connected to high-temperature heating networks (the temperature setting of 110 °C) via a heat exchanger, and the system FP2 with the designed capacity of 61 kW (143 m^2) was connected to heating networks directly (without a heat exchanger) with the temperature setting 75 °C. The authors found the high heat loss in the FP1 system (20.2 %), caused by the high temperature of the heat carrier in collectors and pipes. Power consumption for the operation of pumps amounts to 1.4 % of the heat delivered to the network. The maximum pressure difference in the network amounts to 7.35 bar. The heat loss was very low in the FP2 system (1.9 %). Power consumption for the operation of pumps amounts to 0.2 % of the heat delivered to the network, which can be explained by low-pressure difference in the network – only 0.59 bar. Although it was mentioned in the article that the supply temperature in FP1 system was controlled with sufficient accuracy, the analysis of the temperature graph shows that the supply temperature during the day has been constantly fluctuating from 104 °C to 112 °C, and before 18:00 hours temperature reached 95 °C in the beginning and then 118 °C. The temperature at solar collectors was within the range from 122 °C to 130 °C, thus 18 °C above supply temperature. Based on the graph, it can be concluded that the flow was mainly fluctuating within the range from 0.08 m^3/h to 0.39 m^3/h – which is almost a 5-fold difference. In FP2 case the temperature fluctuations were minimum because the temperature was mainly higher (up to 82.7 °C) than the set temperature (65 °C), which was explained by a too small circulation pump. Thanks to a lower temperature, the heat production at FP2 was 1.5 hours longer in comparison to the plant FP1.

Temperature control issues were observed at the decentralized solar collector installation in Göteborg (Sweden) (Lennermo et al., 2019). The range of temperature fluctuations was within 20 °C for the supply line and 30 °C for the return line. It was concluded in the article that the control issues were caused by using a three-component regulator (a PID controller) with a considerable time delay. In the scientific article (Lennermo et al., 2019) it was proposed to use a three-way valve with model predictive control, which, based on the intensity of the solar irradiation (R1), the outdoor temperature and the differential pressure in the network, calculates the necessary temperatures T3 and T5, the speed of the pump P2 and the opening positions of the valves V3 and V4. The three-way valve (V3) with the PID controller is also used for achieving the desired supply temperature (T4) to the heat network, however, if the pressure drop in the network (PE4) is not stable, it is difficult to control the flow using the three-way valve, therefore the motorized two-way valve (V4) is installed on the bypass line ensuring that the pressure drop PE2 is equal to PE3. The speed of the pump P2 depends on the differential

pressure difference PE4. The speed of the pump P1 is permanent. (Lennermo et al., 2019). From this study it can be seen that before the introduction of the model predictive control, the supply temperature fluctuations amounted to approximately ±5 K, and after the implementation of the model predictive control the temperature fluctuations almost disappeared; however, this is probably not related to modification of the control function only. Compared figures present the data collected on a cloudy day and on a sunny day, therefore, the fluctuations of the flows of the heat carrier differ a lot. To be able to exclude the influence of clouds, it is necessary to make measurements in similar weather conditions, as well as to use computer simulations with equal input data.

Study (Pipiciello et al., 2021) focused on the hydraulic configuration and the control strategies of prosumer units. The test unit was designed for supply and return temperatures equal to 80 °C and 50 °C, respectively. Other design values were the heat supply temperatures of the DH system (90 °C), and to the user (60 °C). The test confirmed the reliable operation of the substation, which could handle simultaneous heat exchanges with the user's heating system and the DH network at pressure loss lower than 0.2 bar and at temperatures within ±0.6 K of the prescribed setpoint after transients shorter than 5 min, even with ±10 K step changes in the inlet fluid temperatures. However, the authors identify that for optimal operation, the control system of the substation must properly interact with the controls of the distributed energy source and the user's heating plant. Such interaction, however, is out of the scope of the present work.

Based on the analysis of literature sources it can be concluded that large-scale solar collector farms are actively built and operated in Denmark, Sweden and Germany, where they are connected to the district heating system by mainly using the "Return-Supply" method. Fluctuations of the temperature and flow of heat carriers are observed in the existing plants and are caused by the changes in the solar irradiation intensity, the changes of the temperature regime and pressure difference in heat networks. There are few examples when small-scale solar collector systems are connected to heat networks, however, this solution could resolve the issue of overheating of solar collectors in households which is topical also in the climate conditions of Latvia. The main knowledge gaps identified in the existing studies are as follows:

- lack of experimental data from small-capacity prosumer units (below 10 kW);
- lack of unit prototypes with remote access and control options;
- lack of recommendations regarding controller set values to ensure precise feed-in temperature;
- lack or limited data from small-capacity units connected to the real DH system.

The current study addresses the first three identified knowledge gaps. Within the next research activities, after all necessary adjustments and maintenance of the unit will be performed, it is planned to connect the prototype unit to the university campus DH network.

2.2. District heating system as heat storage for solar thermal collectors

The research presented in this chapter has been published in (Bogdanovics et al., 2024): **Bogdanovics, R.**, Zemitis, J., Zajacs, A., Borodinecs, A. (2024). Small-scale district heating system as heat storage for decentralized solar thermal collectors during non-heating period. *Energy*, 298.

Background

The integration of solar thermal collectors into existing district heating systems eliminates the need for local heat storage tanks, which require additional space and investment. It also minimizes the risk of collector overheating and provides an opportunity to maximize the capacity of solar collector plants by utilizing all available roof areas (Zajacs et al., 2022).

District heating systems have a thermal energy storage capacity that can be used for reducing peak demand (Kuosa et al., 2022), balancing renewable energy fluctuations and storing surplus energy when there's a mismatch between demand and supply. In situations where the capacity of the solar district heating system is insufficient, one or several seasonal water thermal storages can be added, depending on the number of installed solar collectors (Hiris et al., 2022). Solar district heating systems were found economically feasible for most regions from low to high latitudes (Jiang et al., 2022). In the context of Danish conditions, the combined use of a seasonal heat accumulation system and a solar collector farm can significantly enhance the heat contribution from solar collectors. This combination can increase the solar heat contribution from 20 % to as much as 70 % (Tian et al., 2019). However, if the peak heat production from solar collectors remains below 10 % of the total heat demand, no central or decentralized storage tank is necessary when the pipe system is used for short-term storage (Heymann et al., 2017). This approach optimizes the use of solar energy while reducing the need for additional infrastructure when the solar contribution is relatively low.

Centralized solar thermal plants, typically large-scale and ground-mounted, require extensive land areas, while decentralized or distributed plants with roof-mounted collectors are beneficial in urban areas with high land costs. Decentralized solar plants have collectors located closer to the heat consumption point, serving individual buildings or blocks and also can be connected to a district heating network. The most common connection for such systems is return/supply. Decentralized feed-in systems are not fully commercial yet, and there is no standard design for such installations (Perez-Mora et al., 2018). While solar thermal collectors are a mature technology, they remain a subject of ongoing research, especially concerning the optimization of the solar field size and the utilization of various collector types. Despite the existence of numerous pilot systems and theoretical studies, this area continues to be actively explored (Jodeiri et al., 2022). The pipe network in the decentralized solar plant system exhibits bidirectional flow characteristics, making it incompatible with the existing unidirectional network design approach, which goes from heat source to users. A parametric analysis revealed that the cost of pipelines significantly influences design outcomes when annualized network construction costs, operating costs, and heat loss costs are comparable. In contrast to the conventional design method, the suggested optimization model led to a 4.9 % reduction in total annualized costs (Liu et al., 2022). Latest studies (Martin et al., 2024) show projections of the

future district energy systems which are predicted as multi-source systems with different enthalpy levels, which make network optimization problems more complex and actual.

The study (Monsalvete Álvarez de Uribarri et al., 2017) investigated a branch of the existing district heating system in Germany, featuring solar thermal collectors, local heat storage tanks, and a connection to the district heating system for excess heat injection. It found that larger solar systems do not necessarily yield higher savings due to the mismatch between periods of high demand and high solar energy conversion. Increasing the tank volume up to a certain point lead to an increase in collected solar energy and a reduction in imported energy. However, if the volume is too large, the extra solar energy is mainly used to reach operation temperatures, leading to higher tank losses. The study concluded that network thermodynamics and the influence of the first prosumers on the others must be considered for more realistic values of exported energy.

Suggested solution / novelty

In Latvia, the heat energy is mostly consumed for space heating showing a monthly variation, with a general trend towards reduction by improvements in building and grid energy efficiency and efforts towards balancing the energy consumption of buildings. On the other hand, the heat consumption for the preparation of hot tap water remains relatively constant throughout the year (Krumins et al., 2022). As a result, it is projected that the proportion of hot tap water preparation in the total energy balance of buildings will increase in the future.

Taking into account the high difference between heating energy demand in winter and summer months, certain small-scale district heating systems do not supply heating energy during the summer due to relatively high heat losses in the pipelines. Instead, local electric boilers are used for the preparation of domestic hot water. However, given that the volume of the district heating system is larger than a typical hot water storage tank, and considering the absence of temperature regime requirements and pressure differences between supply and return pipelines during summer, these district heating systems can be effectively used as heat energy accumulators.

This setup allows for the storage of energy produced by decentralized solar collectors. Consequently, a household equipped with solar collectors becomes a ‘prosumer’, storing heating energy in the grid. This stored energy can be used later or shared with neighboring households, optimizing energy use and promoting a more sustainable and community-oriented approach to heating and domestic hot water preparation. By using the DH system as a heat storage system without any other heat source, the solar collector can operate at a lower temperature and the final desired temperature for heating or hot water production can be achieved by local electrical heaters or heat pumps at each household. This approach can be applied not only to existing DH systems but also to new small-scale networks that are located too far from a larger DH system but want to integrate renewable energy sources, store energy and share it among neighboring houses.

By 2050, the business model will have shifted from economies of scale to a decentralized heat supply technology that makes use of locally available heat without burning fossil fuels and prosumers will become one of the key partners in this new model (Lygnerud et al., 2023). The

study (D. Wang et al., 2021) found that prosumer-based district heating systems typically outperform individual heating systems in terms of solar fraction, costs, and greenhouse gas emissions, given the right storage volume to solar area ratio. However, the size of the district and load densities as well as the design of thermal storage capacities significantly impact the system's performance. Increasing the size of thermal storage tanks improves solar fractions up to a point beyond which additional storage volume is not utilized and becomes cost-inefficient. This turning point varies depending on the district and heating system design, making it challenging to define a universal rule for the optimal design of solar-based thermal storage systems. Reducing heat losses is an important factor in improving the performance of district heating networks. The study (Martin-Du Pan et al., 2019) reports that high heat losses are often the result of poor design, partly due to oversized pipes. The current study aims to numerically assess how the pipe diameter affects the heat losses in the untraditional usage of DH system as heat storage.

Numerous studies address thermal energy storage in DH networks and consider it an important asset for improving the performance of DH networks (Chicherin & Anvari-Moghaddam, 2021). The main benefit of integration of any kind of thermal storage is the unlocking the flexibility in district multi-energy systems. The study using a linear programming approach and including a physical model of the district heating network shows that thermal storage installation can reduce costs by about 1.5 %, while its integration with demand-side management leads to a cost reduction of up to 4 % and allows reducing the storage size (Capone et al., 2021). The study (Angelidis et al., 2023) highlights the problem of hydraulic instabilities and control complexities when dealing with decentralized prosumers. The same problem is noted by the (Jebamalai et al., 2022) when trying to optimize the district heating network configuration with ring topology and concluded that ring topology is around 23 % costlier and such a concept is economically attractive only if there is a free waste heat source. The abovementioned facts confirm the need for a detailed assessment of the DH network storage capacity especially for the excess heat from renewable sources. A few latest studies have addressed this issue. Heat accumulation of district heating network to improve performances of integrated energy system under source-load uncertainties was studied by (J. Wang et al., 2022) using Kirchhoff law and constructing the dynamic model of district heating network. Also (He et al., 2023) studied integrated power and thermal systems for flexibility improvement based on evaluation and utilization of heat storage in district heating systems. But both works were focused on wind energy accommodation and considering the heat accumulation characteristics of the district heating network the economic performance can be improved by 2.4 % to 15 %.

A significant trend observed in the literature is the use of system multi-objective optimization (Mertz et al., 2016; Morvaj et al., 2016; Vesterlund et al., 2017), considering both economic and ecological factors. However, social factors and end-consumer economic decisions have not been included in the optimization process, indicating a potential research gap (Sporleder et al., 2022). This is particularly relevant when it comes to the decision of whether or not to connect a building to the district heating system. Addressing this, our paper presents a comparative analysis between a local solar thermal collector solution and a system that is connected to the district heating network. We also analyze the influence of solar collector

distribution among different buildings in the network, taking into account the heat load profile and distance between buildings.

The study (Lee et al., 2023) used TRNSYS simulation to investigate heat trading between two large prosumers using solar and ground energy systems in Korea. The results showed that heat trading allowed the prosumers to increase their renewable energy provision and reduce total costs compared to a scenario without heat trading. However, the study also highlighted the need for differential heat trading costs to ensure benefits for both prosumers. Various studies have employed TRNSYS for optimization purposes, including the modeling of solar thermal collectors for domestic hot water production (Harrabi et al., 2021), the optimization of building-integrated solar thermal systems with seasonal storage optimization (Antoniadis & Martinopoulos, 2019), the optimization of district heating systems (Lu et al., 2021), and developing modeling tools that can be used for the optimization of solar thermal storage applications in the future smart thermal grids (L. Yang et al., 2017).

The aim

The main goal of this study is to present the parametric study for evaluating the effectiveness of utilizing a small-scale district heating system to store heat absorbed by decentralized solar thermal collectors during summer in colder climates when solar thermal collectors are the only source of heating energy in the grid. Additionally, the research aims to explore the feasibility of distributing the generated energy to nearby houses by analyzing the energy balance and comparing the described District solution to the traditional Local system.

This paper introduces a comprehensive model, developed using TRNSYS 18 software, that explores the potential of the suggested DH system. The model takes into account various factors that could influence the system's energy efficiency, including the diameters and lengths of pipelines. Furthermore, it examines how alterations in heating load demand profiles could impact the system.

Methods

The research was based on dynamic computer simulations with the TRNSYS 18 software. The simulation timestep: 2 min. Simulated period: 5 months (May–September). Fig. 2.1 shows the principal drawings of the studied systems, based on which 2 models (Fig. 2.2 and Fig. 2.3) were created. The initial conditions for the temperatures of the heat carrier in the solar collectors, thermal storage tank, and pipelines are set at 20 °C.

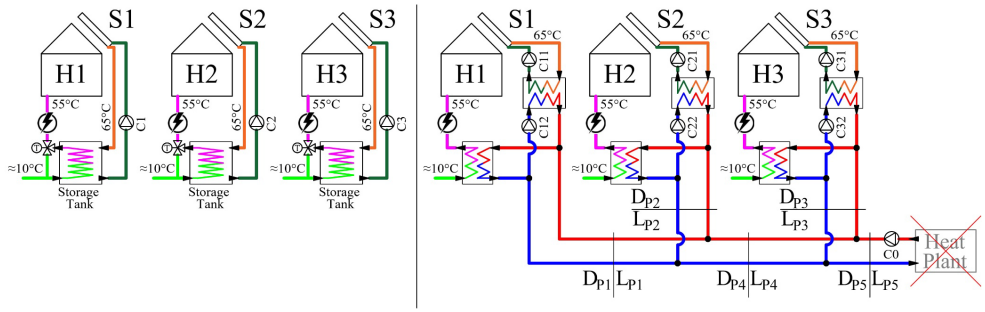

Fig. 2.1. Principal drawing of the studied "local" system (left) and "district" system (right).

Table 2.1

Case description. Symbols based on Fig. 2.1.

Parameter	Unit	Case 1	Case 2	Case 3	Case 4
System	-	Local	District		
Storage tank volume	m^3	1 / 2 / 3	no storage tank		
H1, heating load profile	-	residential	resid. / rest. / office	residential	
H2, heating load profile	-	restaurant	resid. / rest. / office	restaurant	
H3, heating load profile	-	office	resid. / rest. / office	office	
S1, solar collector area	m^2	0 / 40 / 60 / 120		40	0
S2, solar collector area	m^2	0 / 40 / 60 / 120		40	0
S3, solar collector area	m^2	0 / 40 / 60 / 120		40	120
Total solar collector area	m^2	S1 + S2 + S3 = 120			
Pipeline diameter	mm	no pipelines	DP1 = DP2 = DP3 = 50		
			DP4 = DP5 = 125	DP4 = DP5 = 80 / 100 / 125 / 150 / 200 / 250	
Pipeline length	m		LP1 = 150; LP2 = 50; LP3 = 50		
			LP4 = 500; LP5 = 1500	LP4 = 0 / 100 / 500 / 1000 / 1500; LP5 = 2000 – LP4	
Number of simulations	-	21	189	30	30

Description of the "local" system (case 1):

The heating energy produced by solar collectors is accumulated in a storage tank. The tap water is preheated by solar collectors through the heat exchanger in the storage tank and then heated by an electric flow heater up to 55 °C. In case of too high tap water temperature leaving the storage tank, there is a 3-way mixing valve which ensures that the hot tap water temperature entering the house is not higher than 55 °C.

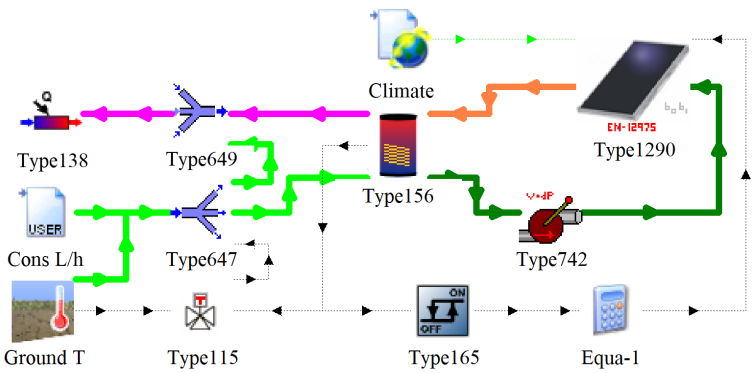

Fig. 2.2. Part of the TRNSYS 18 model of the studied "local" system.

The model (Fig. 2.2) consists of:

- H1: hot water load profile (input file “Cons L/h”) based on Fig. 2.4;

S1: solar collectors (Type 1290), parameters described in

- Table 2.2;
- C1: circulation pump (Type 742), pump efficiency 50 %, motor efficiency 60 %, pressure 50 kPa;
- Storage tank with heat exchanger (Type156), height 2 m, loss coefficient 0.28 W/(m^{2}K), volume dependent on case (Table 2.1);
- Three-way valve actuator (Type115);
- Cold water temperature = ground temperature (Type 77) at 1 m depth;
- Electric auxiliary heater (Type 138) with unlimited power capacity and setpoint 55 °C.

Description of the “district” system (cases 2, 3 and 4):

The simulation represent only non-heating period in the small town when the main heat plant in the DH system is switched off. Typically, during such periods, hot water preparation is provided by auxiliary heaters (usually electrical) installed on the secondary side to reach a desired temperature of 55 °C. Our simulation tests the feasibility of utilizing the primary side of heating networks as an underground heat accumulation storage for solar thermal collectors. The decentralized solar collectors serve as the only source of heating energy in the primary side. In these situations, with an increased heat carrier temperature on the primary side, the tap water is preheated through a heat exchanger from the DH system and the energy consumption of auxiliary heaters on the secondary side decreases.

- Case 2 – the solar collector distribution influence on produced useful solar energy on 3 houses with different heat load profiles with fixed DH system pipelines diameter and length and fixed total solar collector area, which ensures that initial installation costs in all cases are similar.
- Cases 3 and 4 – the DH system main pipelines diameter and length influence on produced useful solar energy on 3 houses with fixed load profiles and fixed solar collector areas: 40-40-40 m^2 or 0-0-120 m^2.

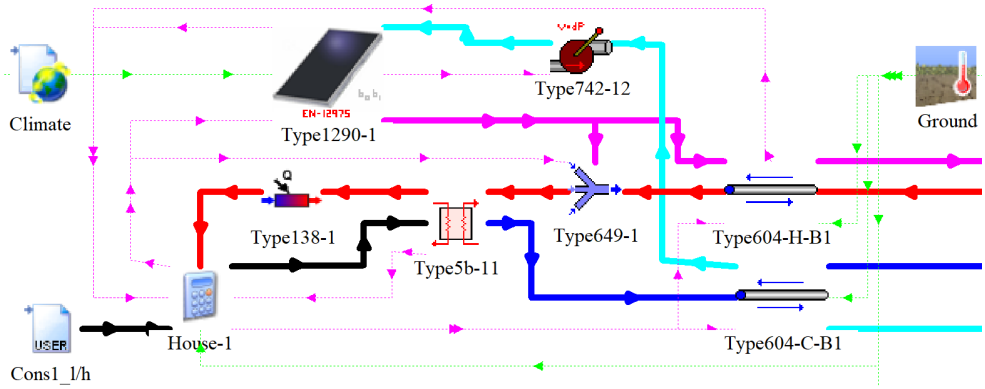

Fig. 2.3. Part of the TRNSYS 18 model of the studied system No.2 “district”.

The model (Fig. 2.3) consists of:

- H1, H2, H3: hot water load profile (input file "Cons L/h") based on Fig. 2.4;
  S1, S2, S3: solar collectors (Type 1290), parameters described in
- Table 2.2;
- P1 – P5: bidirectional pipeline (Type 604); D – diameter [mm]; L – length [m];
- C0, C12, C22, C32: circulation pump (Type 742), overall pump efficiency 50 %, motor efficiency 60 %, pressure 200 kPa; C11, C21 and C31 pumps are not included in the model;
- Heat exchanger (Type5b), overall heat transfer coefficient of exchanger 20000 kJ/(h·K);
- Cold water temperature = ground temperature (Type 77) at 1 m depth;
- Electric auxiliary heater (Type 138) with unlimited power capacity and setpoint 55 °C.

Heating load

Simulation time: May 1 – September 30 (non-heating season), so the heating load was defined only by hot tap water consumption, based on three different building types (Fig. 2.4). It was assumed that the simulated residential building floor area is 400 m^2 and total hot water consumption = 0.03 m^3/month/m^2 x 400 m^2 x 6 stores = 72 m^3/month = 2.4 m^3/day. All three buildings' total daily hot water consumption was assumed to be equal to simplify the simulation by reducing the number of variables and allowing for a clearer understanding of the effect of other variables.

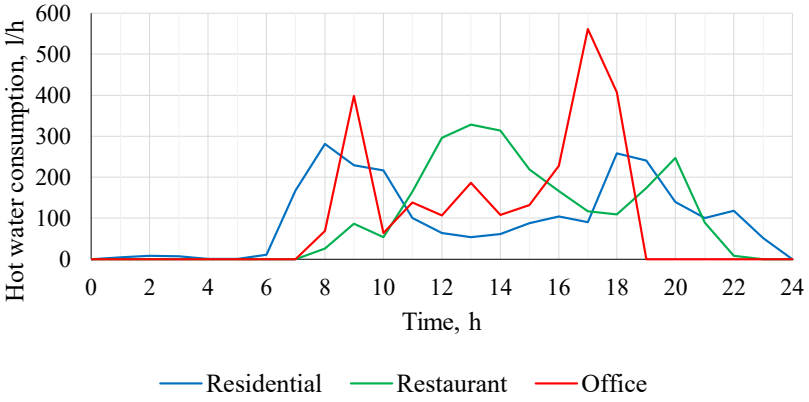

Fig. 2.4. Hot water consumption profile for calculating heating load; data based on (Fuentes et al., 2018).

The hot water consumption [l/h] was read from a text file with a one-hour time interval from 00:00 to 23:00 (including). Data was linearly interpolated.

The heat carrier flow rate is calculated by the equation:

$$Q_{\text{load}} = V \cdot \rho \cdot c \cdot (T_{in} - T_{out}) / 3600, \quad (2.1)$$

where

Q_{load} – heat load, kW;

V – flow, l/h;

ρ – density, 1 kg/l;

c – water heat capacity, 4.18 kJ/(kg·K);

T_{in} – inlet flow temperature = ground temperature, °C;

T_{out} – outlet flow temperature, 55 °C.

Solar collectors

For the simulation, the parameters of flat plate solar collector were used (see

Table 2.2). Glazed flat plate collector (Type 1290) from TESS Component Libraries is based on the EN12975-2 dynamic efficiency approach. The climate for Riga location was used from the Meteonorm V5.0.13. database in TMY2 output format.

As the peak hot water consumption is 562 l/h (see Fig. 2.4), it requires 29.4 kW heating power to heat this flowrate from 10°C up to 55°C. According to equation (1.1) to produce this power at the ambient air temperature of 25 °C, heat carrier temperature 65 °C, and solar irradiation on the surface 1000 W/m^2, it is needed 52 m^2 solar collector plant.

Table 2.2

Solar thermal collector system parameters.

Parameter	Unit	Value
η_0, maximum efficiency	-	0.712
α_1, heat transfer coefficient	W/m^{2}K	3.18
α_2, temp.-dependent heat transf.coeff.	W/m^{2}K^2	0.01
b_o, beam IAM coefficient	-	0.09
Heat capacity of solar collectors	kJ/m^{2}K	6.3
Maximum flowrate	l/(h·m^2)	100
Inclination of solar collectors	-	30°
Facing of solar collectors		equator
Desired collector outlet temperature	°C	65

For the simulation, different collect areas from 0 to 120 m^2 were investigated. According to eq. (1.1), the thermal output of the 120 m^2 collector plant at described conditions is 68.3 kW. Lower network temperatures could significantly enhance collector efficiency, e.g. at 45 °C mean fluid temperature, 120 m^2 plant thermal output increased by 13 % up to 77.3 kW.

Pipelines

Bi-directional noded pipe (Type 604) from TESSLibs 17 (TESS, 2012) was used to model district heating pipelines. It considers the effects of the pipe and insulation mass and performs an energy balance on each fluid node, annular pipe node, and annular insulation node in the pipe.

The number of fluid nodes in circular pipes in branches (P1, P2, P3 in Fig. 2.1) is one fully-mixed node per one meter, but in main pipes (P4, P5) is one fully-mixed node per two meters. The number of pipe and insulation nodes in branches (P1, P2, P3) is one fully-mixed node per five meters, but in main pipes (P4, P5) is one fully-mixed node per ten meters.

Energy balance of a node depends on fluid flow (2.2), energy transferring due to axial conduction (2.3) and energy transferring between fluid, pipe wall, insulation and environment (2.4), (2.5), (2.6). The flow can enter the pipe from the "left" end or from the "right" end but cannot enter from both ends at the same time.

$$Q_{\text{in,fluid}} = m \cdot Cp \cdot (T_{\text{fluid,n}} - T_{\text{fluid,n-1}}) / 3600 , \tag{2.2}$$

where

$Q_{\text{in,fluid}}$ – energy transferred into a fluid node, kW;
m – mass flow rate of fluid entering a fluid node, kg/h;
Cp – specific heat of fluid, kJ/(kg·K);
$T_{\text{fluid,n}}$ – temperature of a fluid node, K;
$T_{\text{fluid,n-1}}$ – temperature of the adjacent fluid node, K.

$$Q_{\text{in,axial}} = \frac{k_{\text{node}} \cdot A_{\text{node}}}{L_{\text{node}}} (T_{\text{node,n}} - T_{\text{node,n-1}}) / 3600 , \tag{2.3}$$

where

$Q_{\text{in,axial}}$ – energy transferred into a node ue to axial conduction, kW;
k_{node} – thermal conductivity of a node (fluid / pipe / insulation), kJ/(h·m·K);
A_{node} – cross sectional area of a node, m^2;
L_{node} – length of a node, m.

$$Q_{\text{fluid,pipe}} = \frac{1}{R_{\text{fluid}} + R_{\text{pipe}}} \cdot (T_{\text{fluid,n}} - T_{\text{pipe,m}}) / 3600 , \tag{2.4}$$

$$Q_{\text{pipe,insul}} = \frac{1}{R_{\text{pipe}} + R_{\text{contact}} + R_{\text{insul}}} \cdot (T_{\text{pipe,m}} - T_{\text{insul,m}}) / 3600 , \tag{2.5}$$

$$Q_{\text{surface}} = h_{\text{outside}} \cdot A_{\text{surf}} \cdot (T_{\text{surf}} - T_{\text{env}}) / 3600 , \tag{2.6}$$

where

$Q_{\text{fluid,pipe}}$, $Q_{\text{pipe,insul}}$ and Q_{surface} – energy transferred from fluid to pipe node, from pipe to insulation node and from pipeline surface to environment, kW;
$T_{\text{fluid,n}}$, $T_{\text{pipe,m}}$, $T_{\text{insul,m}}$ – temperature of a fluid, pipe, insulation nodes, K;
T_{surf}, T_{env} – temperature of surface of the insulation jacket; environment in which the pipe is immersed, K;
R_{fluid}, R_{pipe} and R_{insul} – thermal resistance of the fluid, pipe and insulation material, K·h/kJ;
R_{contact} – thermal contact resistance between the pipe and insulation, K·h/kJ;
h_{outside} – heat transfer coefficient off the outside of the pipe, kJ/(h·K·m^2);
A_{surf} – surface area, m^2.

Table 2.3

Pipeline system description.

D_{P4}, D_{P5}	Pipe inner diameter, mm	Pipe outer diameter, mm	Insulation thickness, mm	Total DH system volume, m^3
50	54.5	60.3	36.9	10.5
80	82.5	88.9	42.6	22.5
100	107.1	114.3	52.0	37.2
125	131.7	139.7	51.6	55.7
150	160.3	168.3	52.0	81.9
200	210.1	219.1	63.5	139.8
250	263.0	273	83.3	218.5

The small-scale district heating system is built with high-performance pre-insulated steel pipes buried at one-meter depth. Insulation thermal conductivity 0.026 W/(mK), density 70 kg/m^3, specific heat 1.5 kg/(kJK). Soil thermal conductivity 2.0 W/(mK), soil density 1500 kg/m^3, soil specific heat 0.84 kJ/(kgK). Other parameters are in Table 2.3.

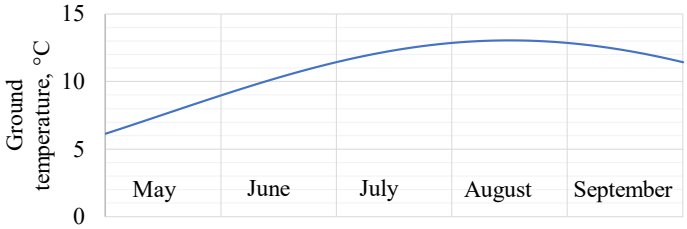

Fig. 2.5. Ground temperature used in simulation calculated by Type77 (Solar Energy Laboratory University of Wisconsin-Madison & Thermal Energy Systems Specialists LLC, 2023) in TRNSYS 18 at 1.0m depth.

As all pipelines in all simulated scenarios are buried underground, their heat losses are reduced due to the surrounding backfill (sand), which acts as additional insulation. However, the bi-directional noded pipe model in TRNSYS (Type 604) consists of two layers – a steel pipe and insulation – and does not allow for the addition of an extra insulation layer. To overcome this limitation, an additional simulation was conducted using the HTFlux program. The goal was to find a way to compensate for the lack of additional insulation from the surrounding backfill. This was achieved by reducing the thermal conductivity of the insulation without changing its thickness, thereby preventing an increase in the surface area of the pipeline. The thermal conductivity of the pipe insulation in the model was reduced by 6 %, as illustrated in Fig. 2.6, resulting in a value of 0.0245 W/(mK). In the TRNSYS model, the temperature around the pipe is determined based on Fig. 2.5, without the influence of wind.

To simplify the model and increase the calculation speed, the solar collector circulation pump and heat exchanger were not included in the model as they have a minor influence on the final energy balance result. The flow rate of the pump was controlled by the solar collector (Type1290) – it modulates the flowrate and keeps the outlet as close to the setpoint as possible if the collector is gaining energy but turns off the collector if the collector is losing energy.

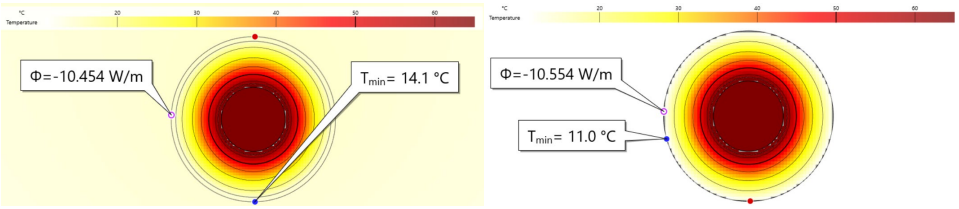

Fig. 2.6. HTFlux simulation results.
Left: buried pipe in the ground (2.0 W/(mK), 1500 kg/m^3, 0.84 kJ/(kgK)) at one meter depth with 0.0260 W/(mK) pipe insulation thermal conductivity and HDPE outer casing. Right: pipe in the air (+11°C) without wind influence with 0.0245 W/(mK) pipe insulation thermal conductivity without HDPE outer casing.

Results

Simulation results are presented separately for "local" and "district" solution and then compared to make a conclusion about the most efficient solution from energetic point of view.

"Local" solutions

The annual energy demand for hot tap water preparation for one house is 48.0 MWh. With 10 m^2 solar collectors, the energy production covers 3.8 % – 4.2 % (1.82 – 2.02 MWh) of the demand, while with 120 m^2, it covers 20.4 % – 29.8 % (9.82 – 14.36 MWh), depending on storage tank volume and load profile. The circulation pump for solar collectors at one household consumes up to 85 kWh of electricity; however, in the case of a wet rotor pump, this energy is partly converted into heating energy.

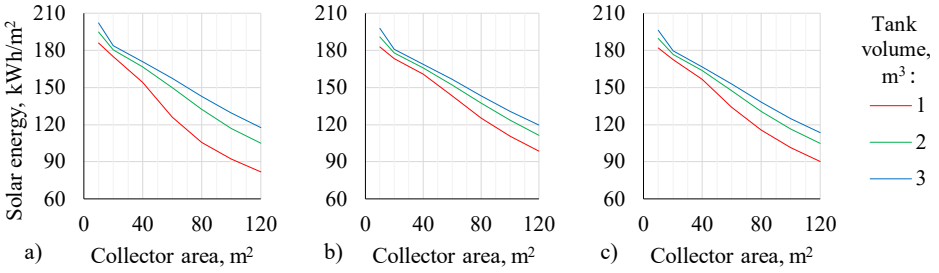

Fig. 2.7. Case 1. Utilized annual solar energy amount depending on collector area for "local" studied system. Load profile: a) residential, b) restaurant, c) office. Storage tank: 1, 2, 3 m^3.

According to Fig. 2.7, as the solar thermal collector area increases from 10 m^2 to 120 m^2, the amount of solar energy utilized per m^2 decreases by 40 % – 56 %, with a larger decrease observed in the case of 1 m^3 storage tank volume. According to equation (1.1), solar collector performance is dependent on the heat carrier temperature: higher temperature results in lower performance. With a smaller storage tank volume, the temperature of the heat carrier in the tank increases more rapidly, potentially leading to decreased performance, so in the case of residential hot tap water profile, 60 m^2 solar collectors with 3 m^3 storage tank absorb 9457 kWh, which is 1902 kWh or 25 % more than with a 1 m^3 storage tank. Additionally, the hot water

profile has an influence: with a 3 m^3 storage tank, the curve (blue line) for all 3 profiles is nearly identical, but with a decrease in the storage tank volume, the reduction in produced energy is more significant, especially in the case of a residential profile.

"District" solution

The simulation covered a 5-month period from May to September (non-heating period), during which the heat demand for a single building was 18.8 MWh. The total heating energy demand for hot tap water preparation for all buildings included in the simulation was 56.4 MWh. Solar collectors were installed on one, two or three buildings in different cases with a total of 120 m^2 area and produced between 10.2 MWh and 18.6 MWh useful energy. This resulted in a reduction of the total auxiliary heating load by 18.2 % – 35.1 %.

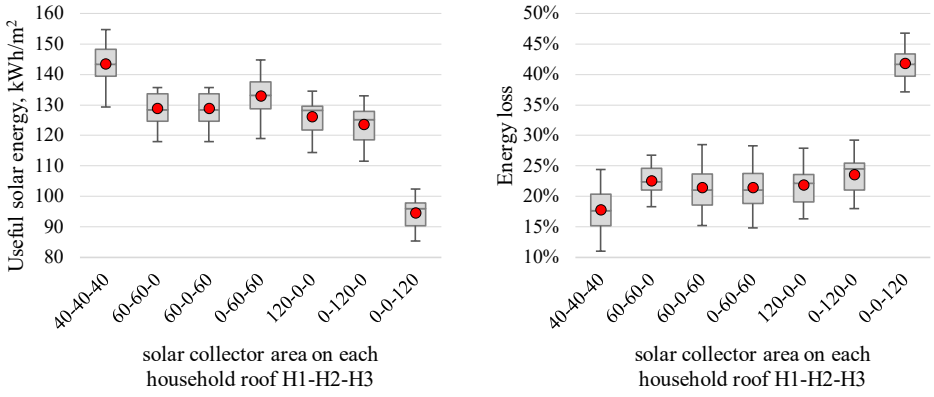

Fig. 2.8. Case 2. Left: produced useful solar energy amount for three households, kWh/m^2 collector area and Right: percentage of solar energy loss depending on the solar collector on each household roof. May 1 – September.

According to Fig. 2.8, a higher amount of solar energy (129–155 kWh/m^2, 143 kWh/m^3 average) is produced when the collectors are evenly distributed between all buildings (40-40-40 m^2). If it is only possible to install collectors on two buildings, it is preferable to install them on H2 and H3 (see Fig. 2.1). However, if it is only possible to install collectors on one building, it is advantageous to do so on the roof of the H1 building rather than H3. This is because H3 is located far from H1 and H2, resulting in the highest heat losses of solar energy, up to 47%. In the best-case scenario, heat losses in pipelines are only 11%.

Comparing "local" and "district" cases during 5-month period, where 40 m^2 solar collectors are installed on each building (40-40-40 m^2), the "local" scenario produces 114.1–127.1 kWh/m^2 (13.69–15.25 MWh for all 3 buildings), whereas the "district" scenario yields 129.3–154.7 kWh/m^2 (15.52–18.56 MWh for all 3 buildings), representing a 13 % – 22 % increase. The yearly energy production in the "district" case depends on the heating system demand and the heat carrier temperature regime in the pipelines. However, the heating period is not investigated within the scope of this paper.

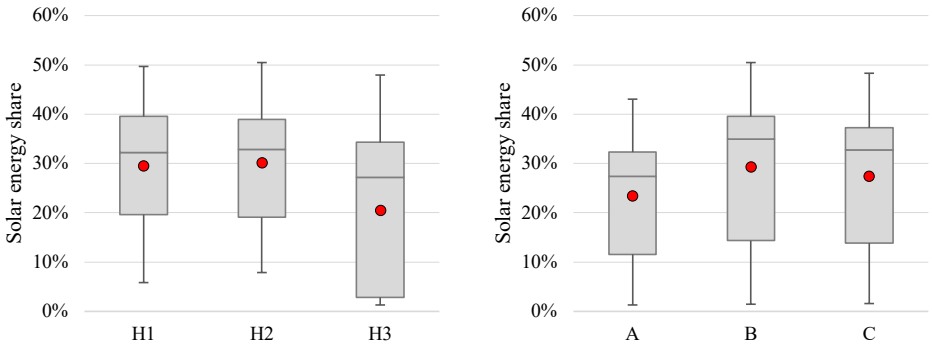

Fig. 2.9. Case 2. Left: percentage of total required energy for hot water heating received from solar collectors for H1, H2 and H3 households. Right: percentage of total required energy for hot water heating received from solar collectors for each household with specific loaf profile: A – residential, B – restaurant, C – office. May 1 – September 30.

As showed in Fig. 2.9, the H2 building derives the greatest benefit from solar collectors, especially when considering a restaurant profile (up to 51%). The difference between H1 and H2 buildings is minimal and statistically insignificant ($p = 0.62$) according to a two-tailed t-test with equal variance. However, the differences between H1 and H3, as well as between H2 and H3, are statistically significant ($p < 0.05$). The difference between B and C profiles is not significant ($p = 0.24$), but between A and B and between A and C are significant ($p < 0.05$).

Various scenarios were investigated by changing the heating energy demand profile of households, the installed solar collector area on each household, and the diameter (DN80 – DN250) and length (0 m – 1500 m) of the district heating system pipeline between buildings.

According to Fig. 2.10, as the P4 pipeline length increases (the distance between H2 and H3 buildings, see Fig. 2.1), the total energy from solar collectors transferred to the end users decreases. In Case 3 with a 250 mm diameter for P4 and P5 pipelines, the total transferred energy decreases from 32.9 % to 30.9 %, and for an 80 mm diameter, it decreases from 31.0 % to 29.5 %. This decline is attributed to increased heat losses in the pipelines. With P4 pipeline lengths exceeding 1000 m, further increases do not yield significant differences.

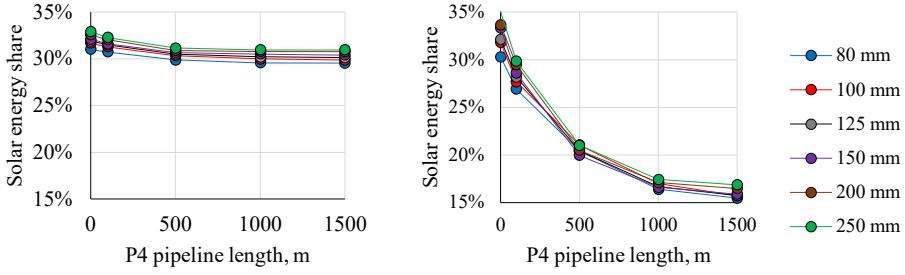

Fig. 2.10. The total solar energy share depending on P4 pipeline length and diameter (80 – 250 mm). Left: Case 3. Right: Case 4. May 1 – September 30.

When all solar collectors are installed on the roof one house (Case 4), the impact of length significantly increases, with losses reaching up to 54.8 % of solar energy in an 80 mm, 1500 m length main pipeline, resulting in a 15.5 % solar energy share.

The system benefits more from larger main pipeline diameters due to reduced heat losses: smaller pipelines experience greater heat losses because the same volume of heat carrier in a smaller pipeline must travel a longer distance, increasing the total contact area between the hot heat carrier and the colder pipe wall. To accommodate 1000 liters of water in a DN250 pipeline, it would require a length of 18.4 meters, with a surface area of 15.2 m^2. However, for a DN80 pipeline, the required length would be 187 meters, with a surface area of 48.5 m^2. The study (Quirosa et al., 2022) also concluded that district heating systems utilized as storage can benefit from larger pipeline diameters.

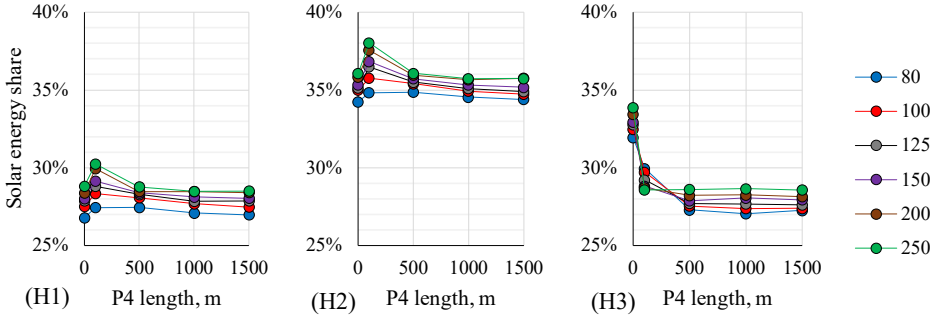

Fig. 2.11. Case 3. The solar energy share for each household (H1, H2, H3) depending on P4 pipeline length and diameter (80–250 mm). May 1 – September 30.

Fig. 2.11 shows that in Case 3, the greater benefit is received by H2 building with a restaurant solar energy profile. The length of the P4 pipeline has a variable effect on the amount of useful solar energy received. For the H3 building, the amount decreases with increasing length, while for H1 and H2, it increases up to L_{P4} = 100 m before decreasing.

In Case 4, if buildings without solar collectors (H1 and H2) are located more than 1000 m from the prosumer, they each receive less than 4 % of the utilized solar energy (Fig. 2.12).

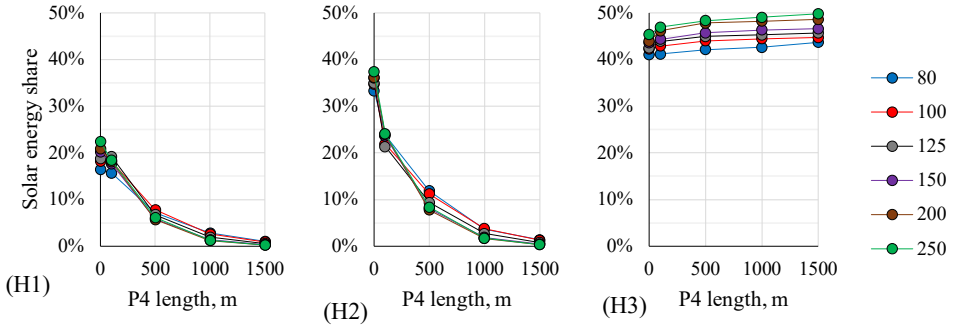

Fig. 2.12. Case 4. The solar energy share for each household (H1, H2, H3) depending on P4 pipeline length and diameter (80–250 mm). May 1 – September 30.

Comparison

The study examined two systems: a local solution and a theoretical district heating system connecting three buildings. Over the simulated 5 months (May–September), solar collectors utilized 67 % – 75 % of all year energy production, but since the studied "district" system is simulated only during the non-heating period to avoid the influence of building heating energy demand, the analysis and comparison are limited to this 5-month period. The energy demand for one house during the 5-month period is 18.8 MWh. Solar energy share refers to the percentage of total energy consumption by end-users that is derived from ST collectors. Energy is absorbed by solar collectors on the primary side and auxiliary heaters on the secondary side.

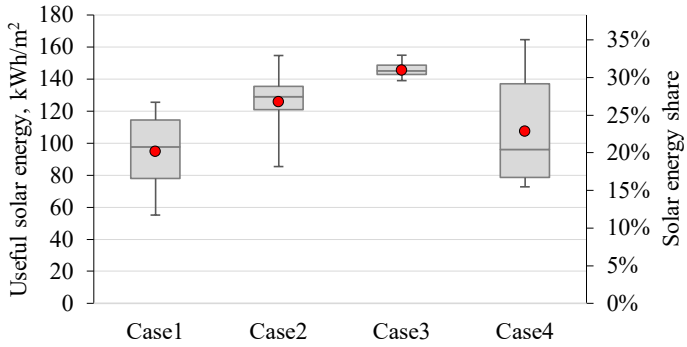

Fig. 2.13. Utilized useful solar energy for three households, kWh/m^2 collector area and % of total required energy for hot water heating received from solar collectors. May–September.

Fig. 2.13. illustrates the significant variation in useful solar energy [kWh/m^2] produced by solar thermal collectors based on different variables. Case 1, representing a "local" solution, shows the lowest average value (94.8 kWh/m^2, indicated by the red dot) and a wide range (55.1 kWh/m^2 to 125.5 kWh/m^2) depending on storage tank volume and the quantity of installed solar thermal collectors in each household. In contrast, Case 3, where solar collectors are evenly distributed among households, demonstrates the highest average value (145.7 kWh/m^2) and a narrower range (139.0 kWh/m^2 to 154.9 kWh/m^2). The maximum solar energy production (164.6 kWh/m^2) occurs in Case 4 with parameters $DP_4 = DP_5 = 250$ mm and $LP_4 = 0$ m. Throughout the examined period, the solar energy share in domestic hot water production ranges from 11.8% to 35.1%.

The heat carrier temperature

The TRNSYS simulation not only allows to calculate energy balance of the system but also enables the examination of heat carrier temperatures at various points within the system.

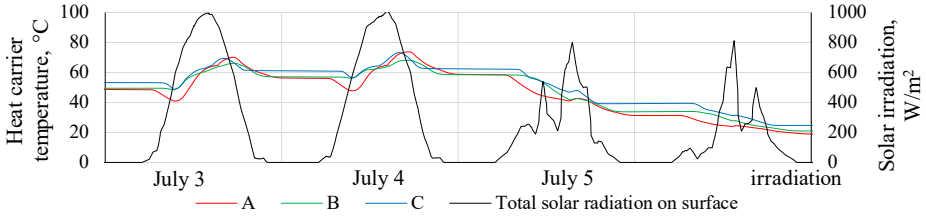

Fig. 2.14. Case 1. Heat carrier temperature in the 2 m^3 storage tank at 0.75 fraction (1.5m) of tank height. A – residential; B – restaurant; C– office heat load profile.

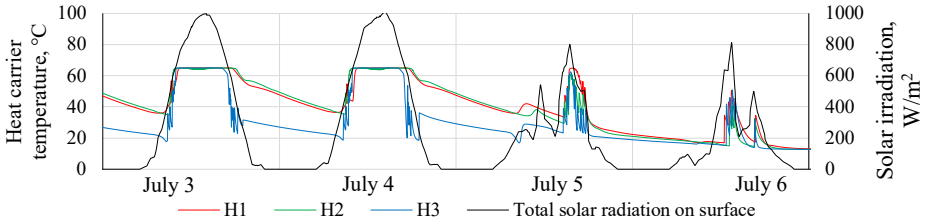

Fig. 2.15. Case 3. Heat carrier temperature in the district heating supply pipeline collectors near H1, H2 and H3 households. $DP_4 = DP_5 = 125$; $LP_4 = 500$; $LP_5 = 1500$.

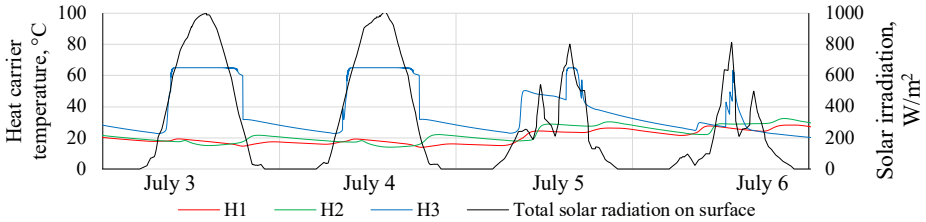

Fig. 2.16. Case 4. Heat carrier temperature in the district heating supply pipeline collectors near H1, H2 and H3 households. $DP_4 = DP_5 = 125$; $LP_4 = 500$; $LP_5 = 1500$.

In the “local” system (Fig. 2.14) the volume of the heat storage tank is limited, and the temperature in the morning might exceed 50 °C, leading to reduced solar energy utilization due to the high heat carrier temperature. In contrast, in the “district” solution (Fig. 2.15, Fig. 2.16), heat carrier temperatures in pipelines remain stable during sunny weather, lower during the night, resulting in lower energy losses, but can oscillate in the morning and evening and cloudy days if here are many solar collector in the system (Case 3). With a large district heating system volume (55.7 m^3), the heat carrier temperature never exceeds 65 °C. Due to the smaller cross-section of pipelines compared to the local storage tank, the heat carrier temperature increases rapidly in the morning, and during cloudy days (such as July 5 and 6), temperatures in the “district” solution are higher than in the “local” solution.

To analyze heat carrier temperature fluctuations entering the building, additional simulations were conducted for Case 3 (H1: H2: H3 = Residential : Restaurant : Office profiles). Since 40 m^2 solar collector area is not sufficient to provide the daily building consumption during cloudy day, for these simulations it was assumed that each building has 120 m^2 of solar collectors per roof and district heating parameters DP4 = DP5 = 80; LP4 = 100, meaning that all three buildings are located near each other. The simulations varied the solar collector orientation, represented as S1:S2:S3, with the following configurations: E:S:W and W:E:S, where S – south, E – east and W – west facing collectors. Simulated period: June 16–17. Simulation time step: 5 sec.

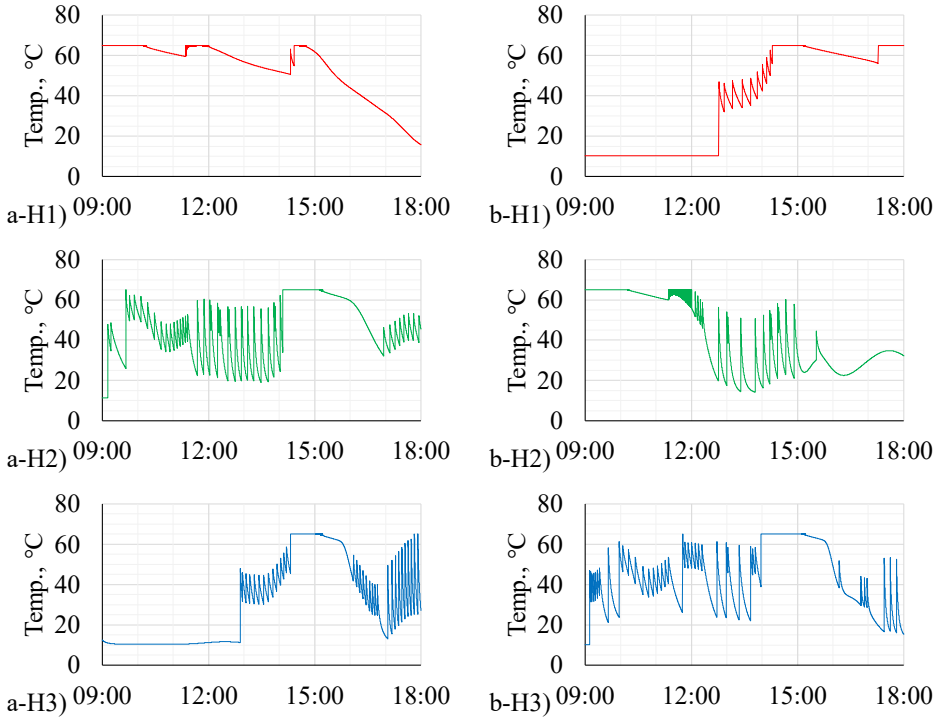

Fig. 2.17. Heat carrier temperature entering H1, H2 and H3 households on June 17 (cloudy day) for different solar collector surface orientation: S1:S2:S3 (a) E:S:W; (b) W:E:S.

Simulation results presented in Fig. 2.17, showing different heat carrier temperature patterns which depends on building energy consumption pattern and solar collector orientation. It is clearly seen that solar collectors can cause temperature fluctuations in all cases with fluctuation period 6–12 minutes.

2.3. Discussion and conclusions

The large-scale solar collector plants connected to the district heating (DH) system have been successfully operating for a long time in Denmark, Sweden, Germany, as well as in Latvia (in Salaspils). However, there are a few examples when households are connected to a district heating system as prosumers. The stagnation and overheating problems are crucial for small-scale solar collector plants in a local system with uneven heat demand and limited heat accumulation capacity. Integration of solar thermal collectors into the 4th or 5th generation district heating system allows to minimize these risks and to provide an opportunity to maximize the capacity of solar collector plants by utilizing all available roof areas.

Integrating decentralized renewable thermal energy sources into DH systems requires robust, reliable solutions with precise temperature control, remote access, and low maintenance costs. To minimize heat carrier temperature fluctuations, solar collectors can heat the return pipeline and deliver energy to the supply pipeline according to the defined temperature regime. Since DH systems provide both domestic hot water and space heating, it is essential to consider factors like building energy consumption reduction through renovations (Hamburg et al., 2020), forecast-based heating control (Cholewa et al., 2022), and combining solar energy with other sources. Converting existing 3rd generation DH networks to 4th or 5th generation is complex and costly. In Latvia, small-town DH networks often are not operated during the non-heating period due to low demand and high pipeline heat losses, so domestic hot water is heated locally by electric boilers. In such cases, integrating solar thermal collectors could transform DH networks into large heat storage systems, reducing reliance on local electric boilers.

Economic evaluation is crucial for the practical implementation of low-temperature district heating systems. It must account not only for investment and operational costs but also for technical, climatological and demand-supply profile data to ensure accurate assessment. While various economic evaluation approaches exist (Calise et al., 2022; Topal & Arabkoohsar, 2024; Ziemele et al., 2021), applying these findings directly to specific cases is challenging due to numerous variables, uncertainties and system configurations. As a result, economic evaluation is beyond the scope of this study but is considered a subject for future research.

For decentralized energy production, a major barrier for heat prosumers is the lack of economic incentives to feed surplus heat into DH networks, as current pricing models do not support reverse heat flow (Li et al., 2022). Lessons from the electricity sector, such as dynamic pricing (Taşcıkaraoğlu, 2018) and peer-to-peer energy trading (Park et al., 2022; Samuel et al., 2022), could help prosumers maximize financial benefits. Additionally, feed-in decisions will depend heavily on real-time energy prices (Selvakkumaran, Eriksson, et al., 2021), highlighting the need for policy and utility-level efforts to establish appropriate tariff structures to accurately assess economic feasibility.

The presented study introduces a method for evaluating the impact of key parameters – including hot water usage profiles, solar collector area, and district heating system pipeline diameter and length – on the useful amount of received solar energy. It conducts a parametric study to assess the efficiency of using an existing small-scale DH system as heat storage for prosumers with decentralized solar thermal collectors in northern climatic conditions during the non-heating period. By comparing TRNSYS 18 simulation results of the "district" solution with the "local" system, the study highlights the potential for energy sharing with neighboring houses, providing insights for future simulations, decision-making processes, and system optimization.

Results show that production of useful solar energy depends on the amount of installed solar thermal collectors, the size of thermal storage and the heating load profile and can vary from 55.1 kWh/m^2 to 164.6 kWh/m^2 for a 5-month period (May–September). Increasing the solar collector area in the "local" solution results in a reduction of energy production per square meter, but this effect can be mitigated by increasing the volume of the storage tank. In the "district" solution, there is no need for a local storage tank due to the substantial volume of the DH system. The useful solar energy received in the "district" solution surpasses that of the "local" solution thanks to the lower heat carrier temperature in the DH system compared to the temperature in the local storage tank. Implementation of a 40 m^2 collector area on each house in the "district" solution can increase the amount of solar energy received by 13–22 % in comparison to the "local" solution with 40 m^2 collectors on each house and 1 m^2, 2 m^2 or 3 m^3 storage tank.

The study found that the building domestic hot water demand profile can have an impact on the amount of energy received from the district heating system: it is more beneficial to install solar collectors on a restaurant roof rather than on a residential building, and the difference between residential and restaurant or office building is statistically significant ($p < 0.05$), but the difference between restaurant and office building is not statistically significant ($p = 0.24$).

More solar energy is produced when the collectors are evenly distributed between all buildings. However, even if the building does not have solar collectors, it can receive up to 38 % of solar energy through the district heating system. If this building is located too far (P4 length = 500 m), it will receive only 1–4 %. A larger main pipeline diameter and more compact consumer locations were found to result in higher efficiency. If the neighboring building without solar collectors is located further than 500 m from a prosumer, it receives a very small amount of solar energy through the district heating system.

Limitations and assumptions

During the research, it was concluded that the TRNSYS might not be the best tool to model the entire town DH system because of the high level of detail and the necessity to define parameters for each building. This issue may be minimized by combining several households into groups or using results from TRNSYS simulations in other software. The key objective of the model was to assess relationships between crucial parameters. This information serves as a foundation for discussions on the practicality of implementing this approach in a case study. It is crucial that the model remains simple enough, providing clear identification of the influence of each parameter on the result.

The study concentrates on three distinct hot water consumption profiles, intentionally avoiding any weekly variations. This approach aims to minimize the number of variables, allowing for a clear examination of the specific profile's influence on the final results. It is crucial to note that the primary emphasis lies in the diversity of these profiles rather than their representation as real residential, office, or restaurant profiles. While future work considers utilizing real case studies with reference profiles for specific buildings, this study employs numerical modeling for the purpose of comparing and analyzing the profiles and their interplay. The model can be easily adapted to any other thermal energy consumption profiles.

The presented model was based on the previously described situation, with a small-scale district heating system in the non-heating period, which is not used, so there are no defined temperature regime and pressure requirements. As the heat carrier temperature in the pipelines is not stable and changes frequently, it may cause unnecessary thermal stress on the affected district heating pipes that may decrease their lifetime and need to be considered in future studies.

If the district heating system is operated during the summer period with the main plant and stable heat carrier temperature, it is needed to insert all the information about each building location and heating energy consumption in the real system, because the absence of some consumers will result in the high heat losses in the pipelines and simulation results will be incorrect. As this is an initial study of a newly proposed solution with potential application in a large-scale DH system, which requires significant investment, validation of the system is currently not feasible. In future studies, the presented model can be used with real data related to pipeline diameters, length, depth and building hot water and heating energy consumption.

Increasing the depth of pre-insulated pipelines has the potential to lower heat losses, but it simultaneously raises the installation costs. Consequently, identifying the optimal solution for each specific situation becomes important. This research focuses on integrating the proposed solution into an existing district heating system. Following recommendations from pipeline manufacturers and based on our real-world experience, pipelines usually range in depth from 0.6 m to 2.0 m, with an average of about 1.0 m. Therefore, a one-meter depth was chosen in the simulation, aligning with the practical limitations of the current infrastructure.

3. Solar-assisted heat pump in district heating system

According to Directive 2010/31/EU of the European Parliament and of the Council of 19 May 2010 on the Energy Performance of Buildings, "heat pump" means a machine, a device or installation that transfers heat from natural surroundings such as air, water or ground to buildings or industrial applications by reversing the natural flow of heat such that it flows from a lower to a higher temperature. For reversible heat pumps, it may also move heat from the building to the natural surroundings.

3.1. Overview of solar-assisted heat pump design

Heat pump operating principles

Heat pump (HP) is a part of environmentally friendly technologies, widely used for domestic purposes even in cold climates. It does not produce exhaust gases while heating any space, especially if the compressor of HP is driven by green electricity. HPs can provide both space heating and cooling as well as hot water preparation by transforming low potential energy from air, ground or water to high potential energy. HP works based on refrigerant cycle, it consists of 4 main components and additional valves, thermostats, measurement tools, pumps, fans, or extra heaters (Çakir et al., 2013; Gaigalis et al., 2016):

- evaporator (uses the thermal energy from the outdoor source to boil the refrigerant and turns it into a gaseous state);
- compressor (compresses the refrigerant, which is in gaseous state, to a high pressure, that by consequence increases its temperature);
- condenser (the refrigerant moves from gaseous into liquid state by releasing the heat into the heating system for the house);
- expansion valve (decrease refrigerant pressure and temperature).

Heat pump performance is based on the second law of thermodynamics, so it depends on the system's temperatures and especially on the temperature lift (Meggers et al., 2010). COP can be increased by decreasing the temperature lift – the difference between HP condensation temperature T_H and evaporation temperature T_C – according to Eqs. (3.1) and (3.2).

$$\mathrm{COP_{ideal}} = \frac{T_H}{T_H - T_C}\,, \tag{3.1}$$

$$\mathrm{COP_{real}} = \eta_{Carnot} \cdot \frac{T_H}{T_H - T_C} = \frac{Q}{E}\,, \tag{3.2}$$

where

$\mathrm{COP_{ideal}}$ – maximal (theoretical) coefficient of performance;
$\mathrm{COP_{real}}$ – real coefficient of performance;
T_H – condensation temperature, K;
T_C – evaporation temperature, K;
η_{Carnot} – Carnot factor (or Carnot efficiency);
Q – produced heating power, W;
E – consumed electrical power, W.

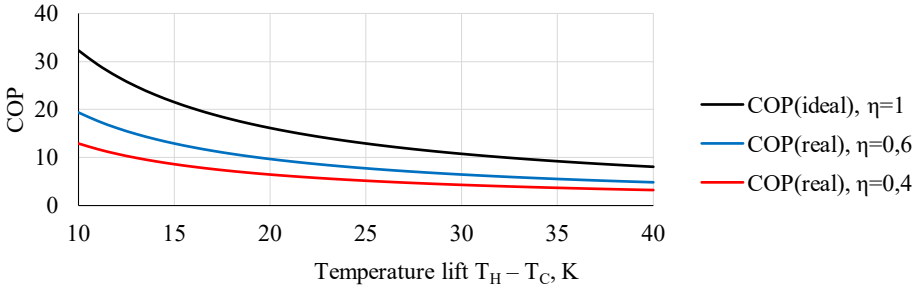

Fig. 3.1. COP dependence on temperature lift with different Carnot efficiency

The most popular are air source heat pumps and ground source heat pumps with a COP varying from 1 to 5 (Bogdanovičs et al., 2018), but almost all heat pumps are designed for internal temperature lifts of about 20 °C – 60 °C (Wyssen et al., 2010). The typical Carnot efficiency is in the range from 0.4 to 0.6. Decreasing the temperature lift from 40 K till 10 K, can increase COP in 4 times from 3.2–4.8 till 12.9–19.4 (see Fig. 3.1), but in reality it is hard to achieve low temperature lift, which depends on the temperature difference between heat source and sink temperatures as well as on the temperature difference between the heat transfer medium and the refrigerant fluid which can be approximated by 4 °C for water-based components and up to 15 °C for air-based (Gasser et al., 2017; Zirngibl, 2020).

Systems with low temperature lift can be used for low exergy building systems, but such HP must be specially designed for these purposes to achieve high Carnot efficiency with low-temperature lift (Gasser et al., 2017; Meggers et al., 2010). The low-temperature lift heat pump was designed and tested at the ETH Zurich. COP of 11 was experimentally achieved for a full-scale heat pump with temperature lift of 15 °C (Wyssen et al., 2010).

(Xu et al., 2024) explores the coupling effects of combining a solar collector field with an air-to-water heat pump in Ørum (Denmark), showcasing significant improvements in thermo-economic and environmental performance, noting that electricity-driven heat pumps are most effective in regions with abundant renewable electricity and fluctuating electricity prices. Air-source heat pumps perform poorly in cold climates due to decreased COP at low temperatures, so replacing air-source heat pumps with brine-to-water heat pumps can lower the return water temperature of the solar collector field, improving its efficiency.

Heat pump and photovoltaic-thermal collector

Photovoltaic-thermal solar-assisted heat pump (PVT-SAHP) is a promising technology that allows achieving very high renewable energy use, increasing heat pump efficiency, and producing both heating and cooling energy for domestic heeds.

There are a lot of different ways to combine a PVT system with a HP. Review of technologies were made by (Miglioli et al., 2021). There are the direct-expansion (DX) systems where the solar collector is operated as an HP evaporator with refrigerant circulation and the indirect-expansion (IDX) systems, where water-glycol is circulated through the PVT collector. It was concluded that the dual-source indirect-expansion system represents the most promising

solution; it is the system where the heat can be gained not only from PVT collectors but also from ambient air by using outdoor unit with the fan or from the ground loop.

The ground source heat pump (GSHP) has higher efficiency compared to air source heat pump but one of the main problems of GSHP in cold regions with dominant heating load is soil thermal imbalance causing the average soil temperature to decrease by 3 K – 12 K in 10 years and as a result, heat pump COP decreasing by 0.5–2.2 (You et al., 2016). The dual source heat pump with PVT and ground loop is a promising, noise-free alternative to air-source heat pump, which allows to store the solar heat in the ground and regenerate it in such a way avoiding soil thermal imbalance (Chhugani et al., 2023; Hengel et al., 2020).

Photovoltaic (PV) systems are commonly used to produce electricity, but technology efficiency depends on panel temperature. One-year measurements of two multi-crystalline silicon (m-Si) PV systems in Greece show that the efficiency temperature coefficient is about –0.44 %/K for roof-mounted system (low wind speed installation) and –0.30 %/K for the open area farm (high wind speed installation). The difference in panel temperatures between the two cases was 10 K thanks to the wind cooling effect. An average panel temperature on the roof was 35 °C but values up to 70 °C have been recorded (Kaldellis et al., 2014).

A combination of PV, GSHP and ST working in a low-temperature regime allows for improving the performance of all mentioned technologies. There are various existing and potential PVT-GSHP systems (You et al., 2021): with PVT for direct heating; with PVT for temperature increasing; with multiple energy sources; with energy storage/borehole recharge. The most widely used and suitable type of PVT-GSHP system for residential applications in heating-dominant regions is the hybrid PVT-GSHP with energy storage/ground recharge.

To optimize the performance and minimize the cost, the specific tool to properly model the system should be developed in correspondence to different sizes, climatic conditions and building loads, as well as real case-study should be investigated (Miglioli et al., 2021).

Solar energy and heat pumps in district heating system

According to calculations by (Larsen et al., 2020), based on low (RCP 2.6) and medium (RCP 4.5) climate change scenarios, a 10-year average heating demand in Latvia is expected to decrease to 91 % of 2010 year levels by 2050. The average cooling demand will be increased significantly, by a factor of 1.40 to 3.07. The cooling demand change ratios are seen to be highest in Northern Europe. The research did not account for changes in building insulation standards, indoor temperature settings, occupant behavior and heating and ventilation habits.

In practice, heating demand in Latvia is likely to drop even more due to stricter energy efficiency regulations. Starting from the 2021 year all new buildings must be nearly zero-energy buildings with yearly heating energy consumption ≤ 40 kWh/m^2 for residential buildings with area > 250 m^2 compared to allowed 70–80 kWh/m^2 before the 2017 year (Cabinet of Ministers Republic of Latvia, 2019, 2021).

The district heating system in Latvia continues to be developed. While a full transition from the existing 3rd generation DH to 4th (LTDH) or 5th (ULTDH) generation is unlikely in the short term, it might be possible to design or modernize smaller DH networks for newly built or renovated buildings, where lower temperature regimes can be implemented more easily.

Heat pumps, powered by electricity from renewable sources (e.g., hydro, solar, wind), offer strong technical potential for renewable energy integration into Latvia's DH system (Lauka et al., 2015). At least twelve possible configurations exist for integrating heat pumps into DH, with smaller networks showing the highest potential (Barco-Burgos et al., 2022). Waste heat from industrial processes, exhaust gases and ambient or wastewater sources can also be utilized in combination with heat pumps (David, 2016; Meggers & Leibundgut, 2011).

The main challenge for ULTDH is meeting domestic hot water (DHW) temperature requirements Booster heat pumps or electric heaters are required to meet hygienic and comfort standards above 50 °C. Simulations show that booster heat pumps reduce the operation costs for the DH system due to lower heat losses in the pipes and outperform individual HPs during non-summer period (P. A. Østergaard & Andersen, 2016), but their high capital costs can limit economic feasibility (Degelin et al., 2024; X. Yang et al., 2016). Neighborhood-scale booster heat pump systems may offer a more cost-effective and energy-efficient alternative, outperforming LTDH systems without heat pumps (Topal & Arabkoohsar, 2024).

Speaking about solar collectors, the integration of large scale solar collector farms with the district heating systems is not complicated from the technical point of view, and this issue has been sufficiently studied (Paulick et al., 2018; Sørensen et al., 2012; Winterscheid et al., 2017), however, regardless of the interest of integration of solar collectors with the city heat networks has been increasing globally during recent years, the total installed capacity of these systems is low. By the end of 2023, 336 large scales (> 350 kW_{th}, 500 m^2) centralized solar collector farms were in operation worldwide delivering heat to the district heating system, with a total area of 2.73 million m^2 (1908 MW_{th} installed capacity), accounting for only 0.35 % of the total global area of solar collectors (Weiss & Spörk-Dür, 2024).

The district heating system in Latvia is well developed and 65 % of the residents receive heat supply to buildings by using this system. Latvia ranks 2nd in Europe according to this parameter (*Statistics Overview, Country by Country, 2015 Survey*, 2015), therefore a majority of residents have an opportunity to connect solar collectors to DH system. In district heating, it is also possible to construct seasonal heat accumulation tanks which allow using the heat accumulated in summer during the autumn season (Nielsen & Möller, 2012; T. Schmidt et al., 2018). Use of the seasonal heat accumulation system jointly with a solar collector farm in Danish conditions allows increasing the contribution of heat by solar collectors from 20 % up to 70 % (Tian et al., 2019), however, if the maximum heat production of solar collectors does not exceed 10 % of the heat demand, no accumulation tank is necessary (Heymann et al., 2017).

It is not always justified from the economic point of view to connect rural territories with low population to the existing city district heating system, considering the costs of construction of long pipelines and large heat loss there, therefore, quite often decentralized energy sources, like heat pumps, thermal solar collectors, micro-cogeneration plants, could be a better choice from the technical and economic point of view and also more environmentally friendly (Dalla Rosa et al., 2014), however, such regions can build their own small-scale DH system with solar energy utilization and heat pump technology usage to benefit from energy storage and sharing potential.

3.2. Maximizing specific thermal heat from solar energy

Background

Riga, the capital city of Latvia, has an extensive district heating (DH) system with approximately 800 km of pipelines. This system distributes 3 TWh annual thermal energy or 76 % of all thermal energy needed by Riga's building sector. Around three-quarters of this energy is used for residential building heating and domestic hot water (DHW) preparation. Heat energy is supplied in nearly equal proportions by burning biomass and natural gas, but by 2030 it is planned that 90 % will be produced from renewable energy resources, reducing the dependence on natural gas (Rīgas Siltums JSC, 2024). The system can be classified as a 3rd generation district heating (3GDH) system with monthly average supply temperature 70 °C – 80 °C during heating period, a peak 118 °C supply temperature at –20 °C ambient air temperature, and constant 65 °C during non-heating period. The system is constantly refurbished by replacing old pipelines inside deep-bury small concrete tunnels with pre-insulated pipelines. Heat network refurbishment during the period from 1996 to 2012 made system more reliable and resulted in heat loss reduction from 20 % to 13 % (Rīgas Siltums JSC, 2013). The new development strategy anticipates that DH needs to be transformed into an energy sharing platform with allowing users to sell excess heat to the system, transforming it into a 4th generation district heating (4GDH) system (Dienas Bizness, 2023).

4GDH systems supply low-energy buildings efficiently, minimizing grid losses and integrating low-temperature heat sources with smart energy system operations. The heat carrier temperature typically ranges from 30 °C to 50 °C for ultra-low-temperature DH and from 50 °C to 70 °C for low-temperature DH (H. Lund, Werner, et al., 2014; D. S. Østergaard et al., 2022).

To get maximum benefit from heat loss reduction and low-temperature heat sources, the DH supply temperature should be reduced as much as possible until electric boosting of DHW becomes necessary (R. Lund et al., 2017). Maintaining a DHW temperature above 51 °C is crucial to prevent Legionella growth, as lower temperatures promote its dominance by enabling it to outcompete other bacteria and rapidly occupy the newly formed environmental niche (Ji et al., 2017). According to Latvian regulations regarding the sanitary maintenance of a residential house (Cabinet of Ministers, 2010), “the administrator of a residential house has an obligation to ensure continuous hot water exit temperature from heat exchanger which is not less than 55 °C”. Measurements in multistorey residential buildings with hot water recirculation systems in Riga, Latvia (Zemīte et al., 2023), showed average DHW circulation temperatures of 46.3 °C and 47.6 °C at the entry to the heat exchanger, despite a DHW supply setpoint of 57 °C. This indicates a risk of Legionella growth even when the DHW supply temperature exceeds 55 °C.

The analysis of transition of existing 3GDH system to 4GDH system with supply temperature 65 °C or below has been analyzed using planning tool (Zajacs & Borodiņecs, 2019) and showed that it is possible even for non-renovated building district, allowing to reduce transmission losses, but may cause thermal discomfort for a short period of time. It was concluded (D. S. Østergaard et al., 2022) that building full renovations are not essential for operating low-temperature heating systems; for example, mechanical ventilation with heat recovery can significantly reduce heat demand and support lower temperature operation in

airtight homes, so supply temperatures below 55 °C are generally sufficient to maintain comfort for most of the year. The ultra-low temperature district heating suggests lower temperatures with local temperature boosting of DHW with local heat pumps, but this is questionable from an economic perspective and will rely on a very low investment cost in the units but under the right circumstances in small areas it might be feasible (R. Lund et al., 2017).

Many countries have made progress in using renewable and sustainable energy sources for heating and cooling, including waste materials, waste heat, solar thermal and geothermal resources (Arabzadeh et al., 2019; H. Lund, Vad Mathiesen, et al., 2014), however, a significant portion of heating demand still relies on fossil fuels (Barco-Burgos et al., 2022). Among the underutilized renewable options for district heating in the Baltic states is geothermal energy, which has the potential to support decarbonization efforts. A spatial assessment of geothermal energy potential for district heating networks in the region, along with aggregated data, is provided in the study (Zajacs et al., 2025).

Heat pump technology has gained popularity in countries with cold climates and is actively used for space heating. Ground source heat pumps are more suitable than air source heat pumps due to maintaining a higher coefficient of performance during cold periods. However, more than 90 % of heat pump installations in Norway are air source heat pumps. Compared to air source heat pumps, ground source heat pumps face many challenges, such as high initial cost, lack of public awareness, and insufficient professional workforce (Sadeghi et al., 2022).

Many studies have addressed the solar energy use in the DH networks, focusing on the ground centralized solar thermal parks (Lebedeva et al., 2023; Lepiksaar et al., 2025; Tian et al., 2019), however existing urban environment lacks free land space, while available rooftop space with low or zero shading is not used effectively.

Photovoltaic-thermal (PVT) technology is a promising solution for integration into DH systems. In colder Northern European climates, large-scale PVT systems can achieve a relatively high solar fraction, making them an efficient renewable energy option (Pakere et al., 2018). The integration of PVT collectors with DH systems in urban areas is increasingly relevant due to the shift toward 4GDH, advancements in solar and storage technologies, cost reductions, synergy with heat pumps and supportive green policies (Chen et al., 2025; Kang et al., 2022). (Pardo García et al., 2017) examined the integration of a heat pump supported PVT system with a 4GDH network for a multi-family house in Central Europe, finding that system energy efficiency is highest when produced heat is supplied directly to the district heating system rather than stored in local thermal storage.

This study aims to describe distributed renewable heating supply potential for district heating using rooftop solar technologies. The main objective is to identify the solar plus heat pump system that produces the most heating supply for a given roof area; a critical limitation in dense urban areas. Three solar heat generation solutions (ST, PV + HP, and PVT + HP) are modelled under Latvian climatic conditions, utilizing a solar power-to-heat concept. The secondary objective is to describe the capacity for solar to cover local heating demands.

Novelty

While interest in integrating PVT collectors, HP and DH systems has grown in recent years, few studies have examined this combination from a technical perspective at the local scale, considering available roof area, manufacturer-reported heat pump performance data, circulation pump electricity consumption and heat losses in pipelines. This study applies a systems solution where rooftop solar is utilized exclusively by the DH network; while not a novel concept for solar thermal there are no studies the authors are aware of where ST, PV, and PVT are directly compared in this application. This is uniquely manifest in the heat pump controls, which are dedicated to conversion of solar electricity to heat rather than building or network heat demands. The research focuses on maximizing solar heat generation within a DH network using limited roof space, with the broader goal of integrating solar energy into DH systems and decarbonizing the heating sector.

Scope

Since all building heating stations in Riga are designed to provide the heating load at –20 °C when the DH supply temperature is 118 °C, it seems quite challenging to lower the temperature in the whole system at once. A modular approach is needed (H. Lund et al., 2018b), retrofitting parts of the DH network (Fig. 3.2) by isolating branches with substations that supply low temperatures to small districts of new and renovated buildings with low energy consumption. These isolated districts will integrate renewable energy sources, utilize excess heat and benefit from energy sharing. As refurbishment expands across districts, the concept can gradually transition the entire network to low-temperature DH.

Fig. 3.2. Zoning scheme of DH system (red lines – main pipelines) for some Riga districts.

As the zoning approach is proposed, a substation is required to isolate the zone from the main DH network. This can be achieved either by installing a heat exchanger to create an independent hydraulic zone or by implementing a mixing system to lower the heat carrier temperature. The target zone of this study primarily consists of multi-apartment buildings, with limited ground space due to playgrounds, recreation areas, parking and shading from buildings and trees. Therefore, the solar technologies are limited to roof areas for heat generation.

This study does not consider operations of the entire DH system. Focus is placed on the local building scale, treating the DH network as the thermal grid for excess energy export. Analysis focuses on technical potential and performance.

Methods

Solar energy can be converted to heat through two methods: (1) directly using solar thermal (ST) collectors, or (2) generating electricity with photovoltaic (PV) panels and using it to produce heat via electric heaters or heat pumps. Photovoltaic-thermal (PVT) systems combine these approaches, simultaneously generating both electricity and heat.

The produced heat can be supplied to 4th or 5th-generation district heating (DH) systems, where it may be stored and redistributed as needed. This study investigates three configurations for integrating solar energy into DH systems (see Fig. 3.3):

1. Connecting ST collectors to the DH system through a heat exchanger.
2. Using a brine-to-water heat pump powered by electricity and heat from the PVT system.
3. Using an air-to-water heat pump powered by electricity generated by PV panels.

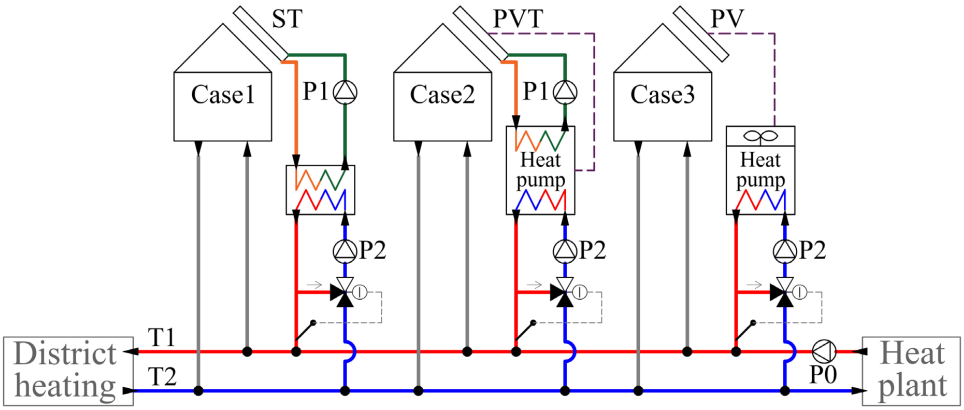

Fig. 3.3. Principal drawing of the studied system with 3 cases.

This study does not investigate the dynamic behavior of the greater DH system, including temperature and pressure fluctuations or heating capacity of the system. It is assumed that the DH network is sufficiently large to accumulate all produced heat.

To evaluate and compare cases, the following key performance indicators were used:

- produced useful heating energy per unit area of ST, PVT or PV system [kWh_{th}/m^2];
- thermal output ratio – the ratio of produced useful heating energy relative to total solar irradiation on the surface;
- system operating hours;
- heat losses in pipes (connect ST with the heat exchanger and PVT with the heat pump);
- circulation pump electricity consumption;
- heat pump coefficient of performance (COP).

Several scenarios were simulated for each case, varying ST, PV and PVT parameters under two DH temperature profiles (see Fig. 3.4):

- low-T with supply temperature 30–50 °C and return 20 °C;
- high-T with supply temperature 60–70 °C and return 40 °C.

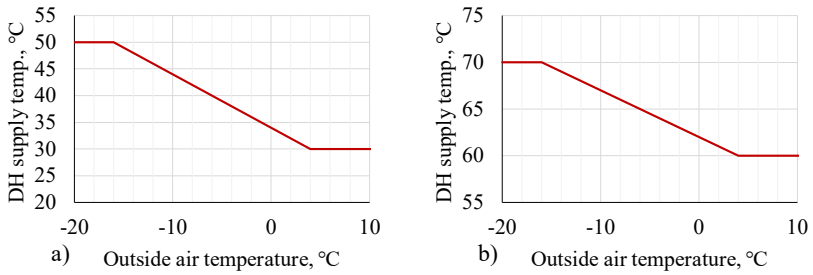

Fig. 3.4. DH supply temperatures for two cases: a) low-T, b) high-T.

It was assumed that the ST, PV or PVT system is installed on the flat roof of the building with the longer side positioned horizontally, resulting in a side length of 1.0–1.2 m depending on manufacturer. The optimum slope of the surface to receive maximum annual solar energy for the Riga location based on PVGIS data (European Commission, 2024b) is 42° but in this case the shadow created by the surface on December 21 at 12:00 is 5.64 m (solar altitude 9.6°). With the width of a typical multi-apartment building in Riga of 10 meters, this would result in 2 rows of panels. To maximize the useful usage of the roof space and reduce the mechanical stress created by wind, the slope of the surface is chosen to be 15° with the distance between surfaces of 2 meters (see Fig. 3.5), facing south. According to PVGIS data (European Commission, 2024b), this slope reduces the yearly in-plane irradiation on the surface by 7 % compared to the optimal slope. The ground coverage ratio (GCR) in this case is 1.2 / 2.0 = 0.6, which results in a partial shading during winter months but is optimal from the land usage perspective (Tonita et al., 2023).

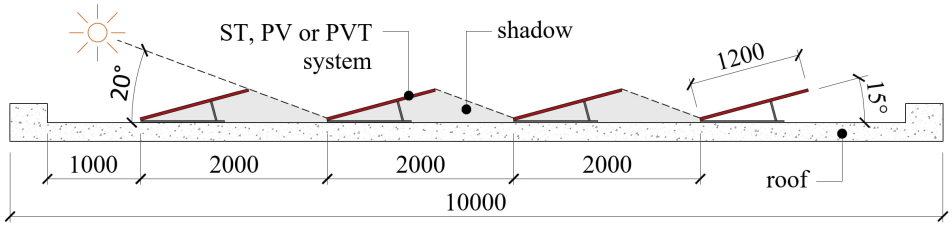

Fig. 3.5. Section drawing of ST, PV or PVT system installation and shading on December 21 at 12:00 in Riga.

The length of the typical multi-apartment building is between 30 and 100 m but usually it is not possible to fully use all the roof area. The analysis shows that taking into account obstacles, on the 10 x 53 m roof it is possible to install 64 panels with 1.2 x 2.0 m dimensions in accordance to Fig. 3.5 and Fig. 3.6 layout which results in total 153.6 m^2 ST, PV or PVT area used in the simulation model (roof utilization ratio about 29 %).

The heat exchanger or heat pump was in the basement near the DH system connection. The total piping distance between the solar collectors and the heat exchanger or heat pump on each side of the collector was set to be total 250 m: 100 m inside the building and 150 m on the roof.

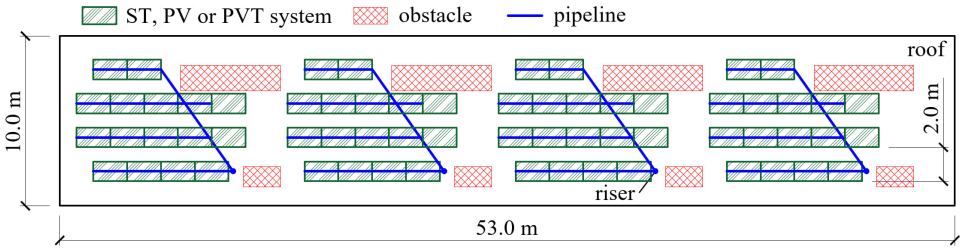

Fig. 3.6. Roof area of a typical house with possible installed ST, PV or PVT system.

The analysis was conducted using dynamic systems simulations in TRNSYS 18 with a one-minute timestep. Fig. 3.3 shows the principal drawings of the studied systems, based on which three models were created. The climate for the Riga location was used from the Meteonorm V 5.0.13. database in TMY2 output format.

The simulated systems included two circulation pumps, P1 and P2, with motors mounted within the fluid stream. The overall pump efficiency was 50 %, and motor efficiency was 60 %. P1 maintained a source-side pressure of 80 kPa using water-ethylene glycol (40 %) as the heat carrier with specific heat 3.6 kJ/(kg·K) and density 1066 kg/m^3. P2 pump controlled the load-side flow to meet the required DH supply temperature, using water as the heat carrier specific heat 4.18 kJ/(kg·K) and density 996 kg/m^3 and maintaining a pressure of 200 kPa. The required supply temperature from the heat exchanger or heat pump to the DH system is regulated by the P2 pump speed and a mixing 3-way control valve. For simplicity, the valve was not simulated; instead, a constant temperature difference on the DH side was assumed.

Case 1 – Solar Thermal (ST)

Flat plate solar collectors and evacuated tube solar collectors were simulated (see Fig. 3.7) using Type539 and Type538. Both models consisted of 100 nodes and an initial temperature of 10 °C. The solar collector model controlled the flowrate to maintain the outlet temperature near the setpoint, defined as the DH supply temperature plus 3 K to compensate for heat loss in pipelines and heat exchanger efficiency. The collector shut off when it began losing energy.

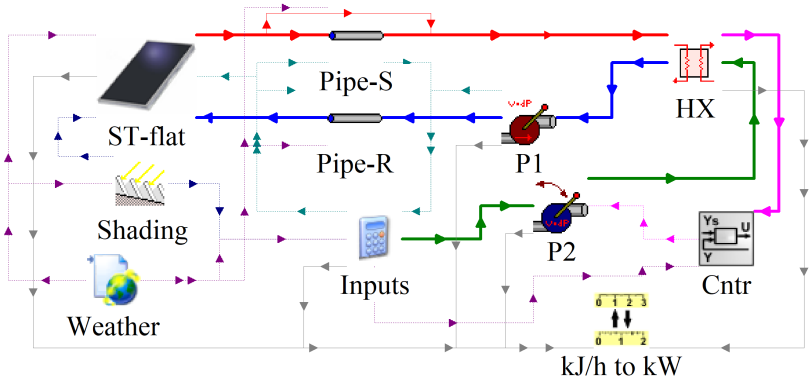

Fig. 3.7. TRNSYS 18 model of the studied system Case 1.

Collector parameters taken from (SPF Institute for Solar Technology, n.d.) and summarized in the Table 3.1. Efficiency as a function of the average temperature; to gross collector area.

Table 3.1

Flat-plate (FPC) and evacuated tube (ETC) solar collector parameters used in simulations, data based on (SPF Institute for Solar Technology, n.d.) database.

ST collector	Efficiency, η_0	a_1, W/(m^{2}K)	a_2, W/(m^{2}K^2)	IAM T/L	Heat capacity, kJ/(m^{2}K)	Heating power*, W/m^2	
						30/20°C	60/40°C
FPC1	0.649	3.51	0.0062	0.87 / 0.87	2.6	649	557
FPC 2	0.736	3.84	0.0079	0.95 / 0.95	2.4	736	635
FPC 3	0.812	2.94	0.0091	0.97 / 0.98	4.8	812	733
ETC1	0.368	0.61	0.0046	1.07 / 0.93	5.3	368	350
ETC 2	0.398	1.29	0.0014	1.47 / 0.96	6.6	398	365
ETC 3	0.608	1.14	0.0012	1.00 / 0.93	1.9	608	579

* At T_a = 25°C and G = 1000 W/m^2.

Pipes between the solar collector and heat exchanger were simulated using Type709 and were sized to ensure pressure drop below 200 Pa/m, with 50 mm insulation thickness and 0.033 W/(m·K) thermal conductivity. The collectors are installed into 4 clusters with 4 different risers connected in parallel. The external pipe temperature was connected to the weather file dry bulb air temperature for 150 m of pipe on each side of the collector and set to a constant 20°C for the remaining 100 m. Pump P1, simulated using Type742, operated with an input-specified flowrate. Pump P2 was simulated using Type741, with flow control implemented via an iterative feedback controller (Type22). This controller regulated the heat exchanger outlet temperature to match the DH setpoint. Pump P2 activated only when Pump P1 was operating, and when the heat exchanger source side inflow temperature exceeded the district heating temperature, ensuring energy transfer occurred always from the source side to the load side.

Case 2 – Photovoltaic-Thermal (PVT)

Photovoltaic-thermal (PVT) collector parameters based on previous research (Francisco et al., 2024) and summarized in the Table 3.2 and Table 3.3. Model (Type 203) of an unglazed photovoltaic thermal collector for TRNSYS 18 developed by Institute for Solar Energy Research in Hamelin (ISFH) and described in (Chhugani et al., 2020; Stegmann et al., 2011).

Table 3.2

Empirical thermal performance coefficients of the studied PVT collectors (Francisco et al., 2024).

PVT system	Efficiency, η_0	a_1, W/(m^{2}K)	a_3, J/(m^{3}K)	a_6, s/m	Heat capacity, kJ/m^{2}K
PVT 1	0.400	9.926	4.653	0.043	6.4
PVT 2	0.410	13.345	4.012	0.027	3.2
PVT 3	0.490	13.925	4.026	0.021	9.5
PVT 4	0.428	34.502	6.066	0.027	6.2
PVT 5	0.566	27.105	5.637	0.017	6.3

Table 3.3

Electrical specifications of the studied PVT collectors (Francisco et al., 2024).

PVT system	Eff. (η_{el})	Open-circuit voltage (V_{oc})	Short-circuit current (I_{sc})	Voltage at Pmax (V_{mp})	Current ar Pmax (I_{mp})	Temp. coeff. P_{max}
PVT 1	17.5%	38.8 V	9.3 A	32.4 V	8.8 A	–0.40 %/K
PVT 2	19.2%	40.9 V	10.2 A	33.2 V	9.6 A	–0.34 %/K
PVT 3	20.0%	48.9 V	9.9 A	40.4 V	9.3 A	–0.34 %/K
PVT 4	20.5%	37.0 V	13.7 A	30.9 V	12.9 A	–0.35 %/K
PVT 5	21.5%	38.6 V	13.8 A	32.2 V	13.2 A	–0.31 %/K

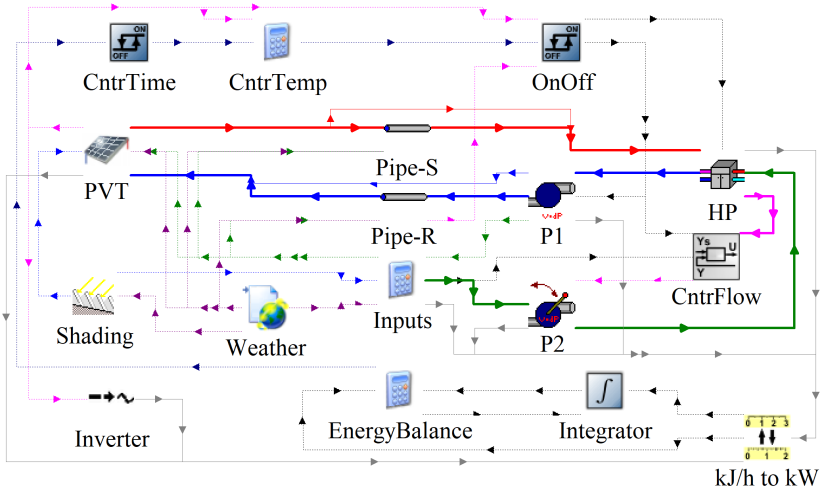

Fig. 3.8. TRNSYS 18 model of the studied system Case 2.

The photovoltaic-thermal (PVT) system produces direct current (DC), while the heat pump operates on alternating current (AC), so the invertor is needed. In the computer model the inverter efficiency of 95 % was defined. Accumulators for electricity storage were not included; instead, it was assumed that any surplus or deficit in electricity is balanced via the grid.

To ensure that the heat pump's annual electricity consumption does not exceed the electricity generated by the PVT system, an integrator tracks cumulative electricity production and consumption. The total consumption includes the electricity used by both the heat pump and the circulation pumps.

Since the PVT area was fixed, the first step was to determine the optimal capacity of the brine-to-water heat pump [kW], because it is not directly connected to the number of PVT collector installed. The goal was to minimize heat pump capacity while ensuring that all the electricity produced by the PVT was effectively used. Therefore, the total annual electricity consumption by the heat pump and circulation pumps must match the total annual electricity production of the PVT system. The same approach also was implemented to the Case 3 with air-to-water heat pump capacity.

To determine where heat pump is turned on and turned off, the following control logic was implemented in the TRNSYS model: controller activates the heat pump when the PVT outlet temperature exceeds the PVT inlet temperature by 2 K. It deactivates the heat pump when the PVT outlet temperature falls below the PVT inlet temperature, preventing energy losses. To reduce the risk of frost formation on the PVT surface and increase the overall heat pump COP, the heat pump is also turned off if the PVT outlet temperature drops below 0 °C. The heat pump minimum run-time is 15 minutes and a minimum reset time is 15 minutes.

Pumps P1 and P2 are synchronized with the heat pump, switching on and off together. Pump P1 operates at a constant flow rate, while pump P2's flow is adjusted by an iterative feedback controller to achieve the desired supply temperature from the heat pump to the DH system.

As mentioned before, the PVT area was set to be constant, while the heat pump capacity was varied to determine the optimum capacity. Lower capacities may fail to utilize all the electricity produced by the PVT, whereas higher capacities demand more electricity.

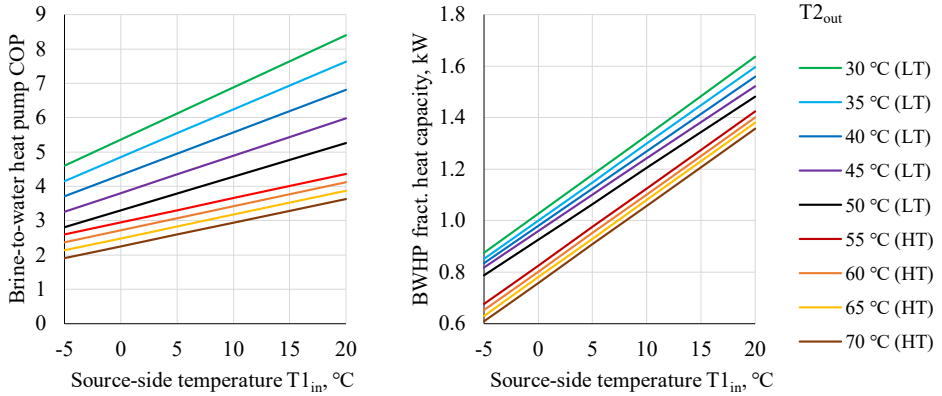

Fig. 3.9. Brine-to-water heat pump (BWHP) COP and fractional heat capacity for different heat sink supply temperatures dependence on ambient air temperature used in Case 2.

The COP is equal to 4.85 and the heat capacity is equal to 1 kW at B0/W35 conditions. The heat pump performance (Fig. 3.9) was based on manufacturers data for 2 heat pumps: data for $T2_{out}$ = 30 °C – 50 °C was for low-temperature brine-to-water heat pump and was used in low-T case simulations, but data for $T2_{out}$ = 55 °C – 70 °C was for high-temperature heat pump from the same manufacturer and was used for high-T cases. The flow rate on the source side was calculated to provide a 4 K temperature drop at a source temperature of 0 °C and a sink temperature of 30 °C. Pipes were selected to ensure a pressure drop below 200 Pa/m, with insulation thickness of 19 mm and thermal conductivity of 0.033 W/mK to prevents condensation risks at a flow temperature of 0°C and ambient conditions of 22 °C with 80 % relative humidity.

Case 3 – Photovoltaic (PV)

For better comparison, PV panel performance was based on PVT panel electrical data from Table 3.3 (PV1 = PVT1). PV panels were simulated using the same Type203 as in case 2 but without heat carrier flow and with reduced heat panel heating capacity. In general, the TRNSYS model was similar to the model from Case 2, but the heat pump was simulated by Type941 with performance data based on Fig. 3.11.

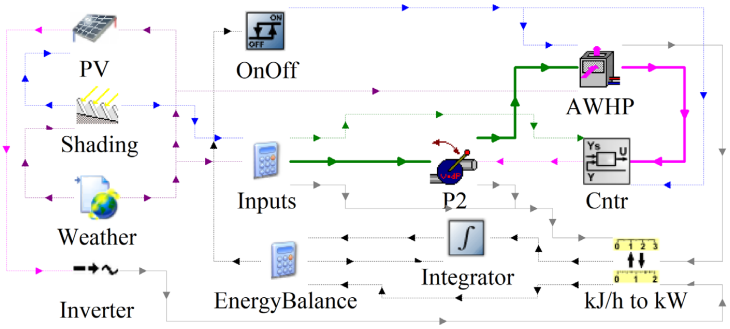

Fig. 3.10. TRNSYS 18 model of the studied system Case 3.

Air-to-water heat pump COP was based on the manufacturer data (Fig. 3.11). The COP is equal to 5 and the heat capacity is equal to 1 kW at A7/W35 conditions.

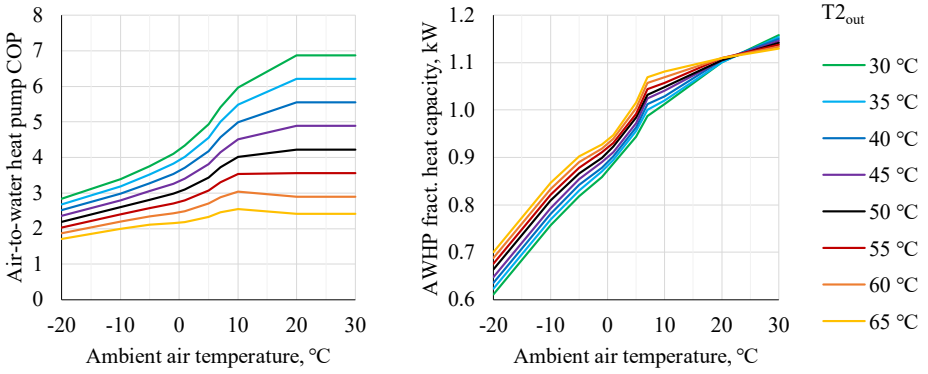

Fig. 3.11. Air-to-water heat pump (AWHP) COP and fractional heat capacity for different heat sink supply temperatures dependence on ambient air temperature used in Case 3.

Two approaches are considered for the heat pump operation:

- **Constant operation scenario ("constant")**: The heat pump operates continuously throughout the year at a constant heat capacity. In this scenario, the annual electricity consumption is balanced with the annual electricity production.
- **Solar availability scenario ("solar")**: The heat pump operates only when solar energy is available (if cumulative electricity consumption exceeds production, the heat pump and circulation pumps are turned off.) with a defined minimum run-time of 15 minutes and a minimum reset time of 15 minutes.

Results

The study examined three systems. Results of calculations are presented for each case and at the end all cases are compared together.

The annual solar irradiation on the ST, PV or PVT surface in all cases was 1033 kWh/m^2.

Case 1 - ST

According to Fig. 3.12, in the low-T case, FPC demonstrate higher performance, with annual useful heat utilization reaching up to 592 kWh/m². In the high-T case, the difference between FPC and ETC is minimal, with maximum annual useful heat production reaching 378 kWh/m². Results indicate that lowering the operating temperature can increase heat utilization by 31 % to 88 %, depending on the type and properties of the collectors.

Table 3.4

Case 1 simulation results, low-T district heating temperature profile.

	FPC1	FPC2	FPC3	ETC1	ETC2	ETC3
Useful heating energy, kWh/m^2	431	495	592	297	366	496
Thermal output ratio	41.7 %	47.9 %	57.2 %	28.7 %	35.4 %	48.0 %
Total operating hours	513	521	567	631	701	644
% of annual hours	5.9 %	5.9 %	6.5 %	7.2 %	8.0 %	7.4 %
Heat losses in pipelines	4.6 %	4.1 %	3.8 %	6.8 %	5.2 %	4.4 %
Pump electricity cons., kWh/m^2	6.4	7.3	8.8	4.4	5.4	7.5

Table 3.5

Case 1 simulation results, high-T district heating temperature profile.

	FPC1	FPC2	FPC3	ETC1	ETC2	ETC3
Useful heating energy, kWh/m^2	228	269	370	168	206	387
Thermal output ratio	22.1 %	26.0 %	35.8 %	16.3 %	19.9 %	36.6 %
Total operating hours	274	284	336	288	344	428
% of annual hours	3.1 %	3.2 %	3.8 %	3.3 %	3.9 %	4.9 %
Heat losses in pipelines	11.8 %	10.4 %	11.1 %	22.3 %	17.8 %	12.1 %
Pump electricity cons., kWh/m^2	1.6	1.9	2.6	1.1	1.4	2.7

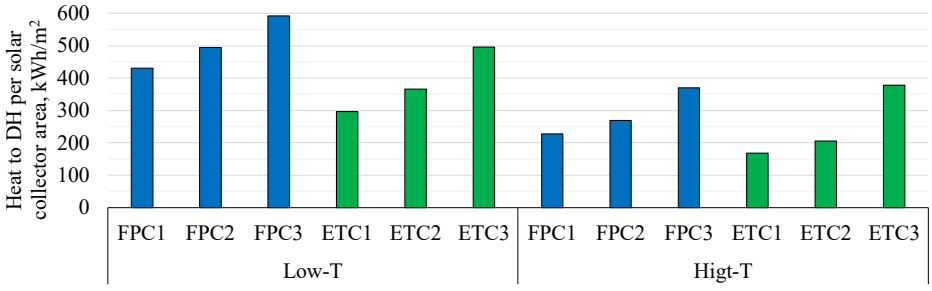

Fig. 3.12. Annual heat delivered to DH for different ST collectors (Table 3.1) and two DH temperature regimes (Fig. 3.4).

On Fig. 3.13 the monthly data for flat-plate collector FPC3 in low-T case is presented. 88 % of thermal energy delivered to the grid is during 6 months (April – September).

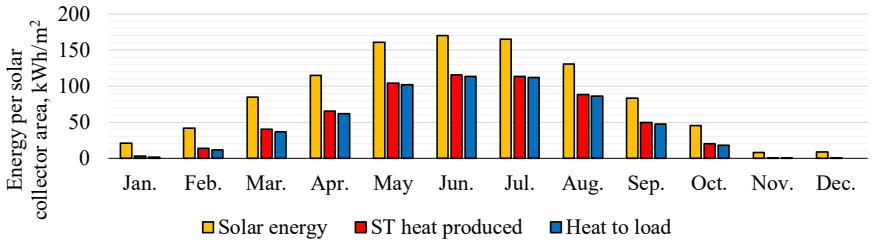

Fig. 3.13. Monthly solar energy irradiation, heat production and delivered by FPC3 collector in low-T system.

Case 2 - PVT

According to Fig. 3.14, heat pump in combination with PVT annually produce up to 1361 kWh/m² in the low-T case and up to 753 kWh/m² in high-T case. Results indicate that lowering the operating temperature can increase heat production by 77 % to 83 %.

Table 3.6.

Case 2 simulation results, low-T district heating temperature profile.

	PVT1	PVT2	PVT3	PVT4	PVT5
Useful heating energy, kWh/m²	1040	1149	1180	1274	1361
Thermal output ratio	100.6 %	111.2 %	114.2 %	123.3 %	131.8 %
Total operating hours	4229	4245	4329	4407	4512
% of annual hours	48.3 %	48.5 %	49.4 %	50.3 %	51.5 %
Heat gains* in pipelines	4.7 %	4.4 %	4.1 %	2.8 %	3.0 %
PVT electricity produced**, kWh/m²	181	201	205	210	228
Circ. pump electricity cons., kWh/m²	26.2	29.0	29.7	31.3	33.7
Heat pump COP (average)	5.76	5.74	5.78	6.09	5.99

* heat carrier temperature is in general lower than ambient air temperature, so PVT extracts additional heat from the air; % from PVT system produced heat (before heat pump).

** all produced electricity is used to power heat pump and both circulation pumps.

Table 3.7.

Case 2 simulation results, high-T district heating temperature profile.

	PVT1	PVT2	PVT3	PVT4	PVT5
Useful heating energy, kWh/m²	589	651	663	697	753
Thermal output ratio	57.0 %	63.0 %	64.2 %	67.5 %	72.8 %
Total operating hours	3527	3912	3993	4072	4051
% of annual hours	40.3 %	44.7 %	45.6 %	46.5 %	46.2 %
Heat gains* in pipelines	4.9 %	4.8 %	4.7 %	3.8 %	3.6 %
PVT electricity produced**, kWh/m²	180	199	203	209	227
Circ. pump electricity cons., kWh/m²	15.5	17.1	17.5	18.2	19.7
Heat pump COP (average)	3.28	3.27	3.27	3.34	3.33

* heat carrier temperature is in general lower than ambient air temperature, so PVT extracts additional heat from the air; % from PVT system produced heat (before heat pump).

** all produced electricity is used to power heat pump and both circulation pumps.

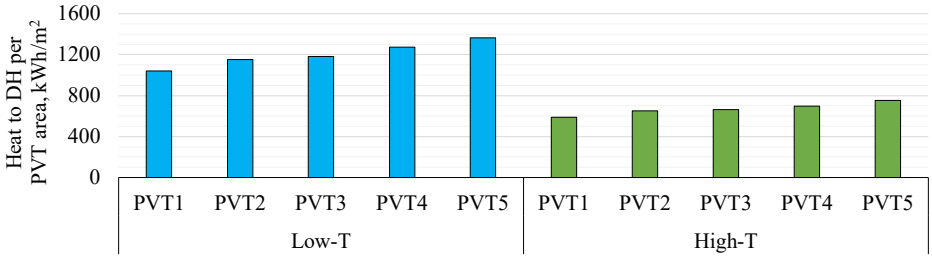

Fig. 3.14. Annual heat delivered to DH for different PVT types (Table 3.2) and two DH temperature regimes (Fig. 3.4).

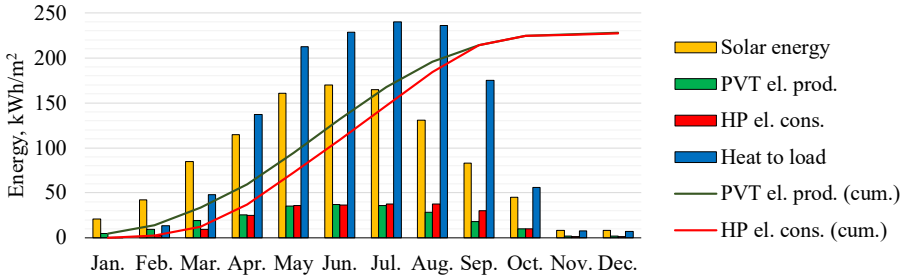

Fig. 3.15. Monthly solar energy irradiation, electricity production and consumption (HP and both circulation pumps) and heat delivered to DH by PVT5 + BWHP in low-T system.

In January – Mart the electricity produced by PVT is higher than electricity consumption by heat pump due to low heating energy production, so the surplus energy needs to be stored in the electrical grid, but the annual electricity consumption-production balance is achieved.

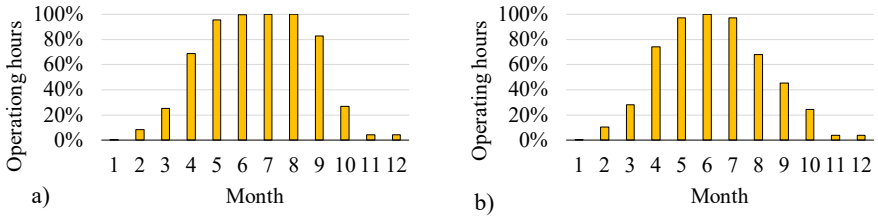

Fig. 3.16. Brine-to-water heat pump working time; a) PVT5 + low-T; b) PVT5 + high-T.

The controller activates the heat pump when the PVT outlet temperature exceeds the PVT inlet temperature by 2 K and deactivates the heat pump when the PVT outlet temperature falls below the PVT inlet temperature or drops below 0 °C, preventing energy losses. This explains why there are not too many operating hours during the winter period (Fig. 3.16). In the high-T case the operating hours decreases as well as the amount of produced useful heating energy.

Case 3 - PV

Air-to-water heat pump can work independently from solar energy since it gains energy from the air and can use electricity from the grid. But to fairly compare Case 3 with Case 1 and Case 2 in the context of solar energy usage, the limitation were introduced within two operating scenarios: "constant" and "solar" to make sure that annually heat pump consume no more energy than PV panels can produce. The operation strategy resulted in different useful heating energy delivered to DH system (Fig. 3.17).

Table 3.8.

Case 3 simulation results, low-T district heating temperature profile.

	"Constant" mode		"Solar" mode	
	PV1	PV2	PV1	PV5
Useful heating energy, kWh/m^2	774	977	918	1183
Thermal output ratio	74.9 %	94.6 %	88.9 %	112.3 %
Total operating hours	8760	8760	4272	4317
% of annual hours	100 %	100 %	48.8 %	49.3 %
PV electricity produced*, kWh/m^2	176	222	176	222
Circ. pump electricity cons., kWh/m^2	14.9	18.8	17.6	22.3
Heat pump COP (average)	4.41	4.41	5.23	5.23

* all produced electricity is used to power heat pump and circulation pump.

Table 3.9.

Case 3 simulation results, high-T district heating temperature profile.

	"Constant" mode		"Solar" mode	
	PV1	PV2	PV1	PV5
Useful heating energy, kWh/m^2	439	554	474	598
Thermal output ratio	42.5 %	53.7 %	45.9 %	57.9 %
Total operating hours	8760	8760	2613	2862
% of annual hours	100 %	100 %	29.8 %	32.7 %
PV electricity produced*, kWh/m^2	176	222	176	222
Circ. pump electricity cons., kWh/m^2	8.4	10.6	9.1	11.5
Heat pump COP (average)	2.50	2.50	2.70	2.70

* all produced electricity is used to power heat pump and circulation pump.

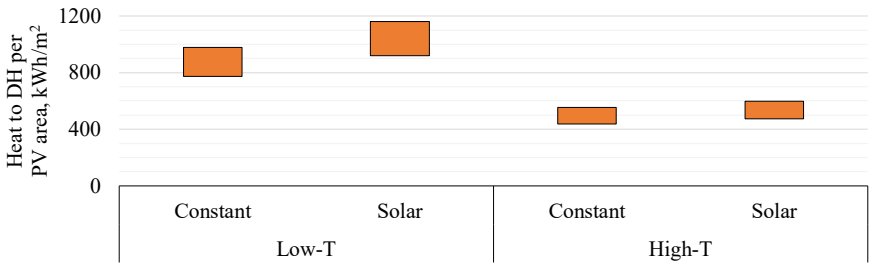

Fig. 3.17. Annual heat delivered to DH for different PV types (min – max) and two DH temperature regimes.; heat pump operation mode: "constant" and "solar".

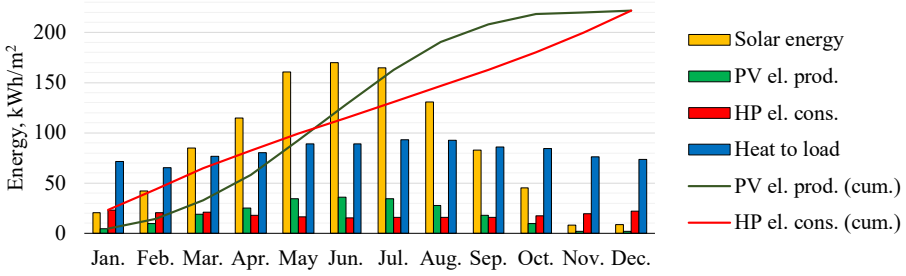

Fig. 3.18. Monthly solar energy irradiation, electricity prod. and cons. (HP and circulation pump) and heat delivered to DH by PV5 + AWHP in low-T system, "constant" mode.

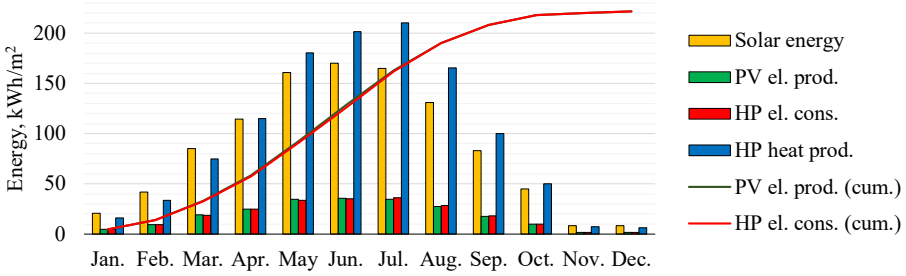

Fig. 3.19. Monthly solar energy irradiation, electricity prod. and cons. (HP and circulation pump) and heat delivered to DH by PV5 + AWHP in low-T system, "solar" mode.

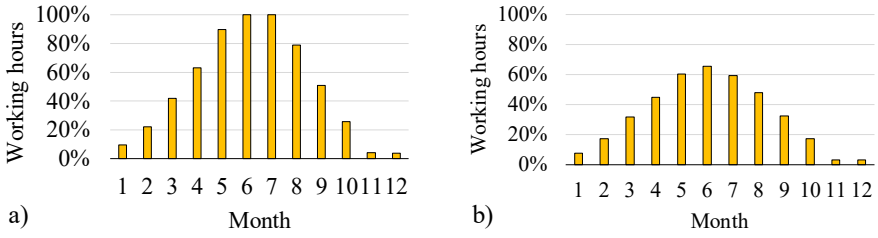

Fig. 3.20. Air-to-water heat pump working time in a "solar" mode;
a) PV5 + low-T; b) PV5 + high-T.

For the "constant" operation mode the heat pump works all the time but in "solar" mode it operates mainly in non-heating period since the produced electricity from PV panels is higher in this period. In spite of smaller operating hours, the COP of AWHP in "solar" mode is higher because the air temperature usually is higher when there are more solar energy.

Comparison

Since there are heat pumps in Case 2 and Case 3, their heat capacity is not directly related to the amount of available roof area and needs to be determined separately. Too low capacity leads to the situation when PVT or PV panels produce more energy when heat pumps can consume, but too big capacity leads to frequent ON/OFF cycles of heat pump operation and unnecessary high capital investments, so the optimal HP capacity for each case was determined and results shown on Fig. 3.21. Heat capacity for BWHP is presented at B0/W35 conditions, AWHP is presented at A7/W35 conditions. The AWHP operated in the "constant" mode requires the lowest heat pump capacity per installed PV area, while AWHP operated in the "solar" mode requires the highest capacity. Low temperature in DH system requires higher heat pump capacity since it works with higher COP meaning it can produce more heating energy with the same electrical power.

The BWHP (case 2) average COP for low-T: 5.74–6.09; for high-T: 3.27–3.34;

The AWHP (case 3) average COP for low-T: 3.27–3.34; for high-T: 2.50–2.70.

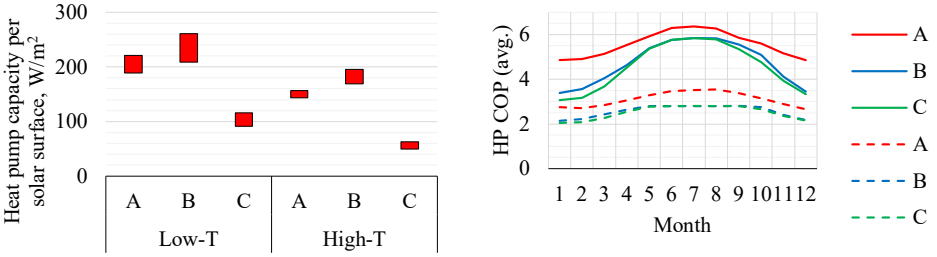

Fig. 3.21. Left: Comparison of optimum heat pump capacity at rated conditions (min – max).
Right: Heat pump monthly average COP for PVT5 (PV5).
A: PVT + BWHP; B: PV + AWHP "solar"; C: PV + AWHP "const".
Constant line: low-T; dashed line: high-T.

On Fig. 3.22 the results of useful energy production for all simulated cases are presented. It can be concluded that Case 2 (BWHP+PVT) has the higher potential for maximizing solar energy production from the limited area. Even in high-T case it shows more useful energy than Case 1 (ST collectors) in low-T case.

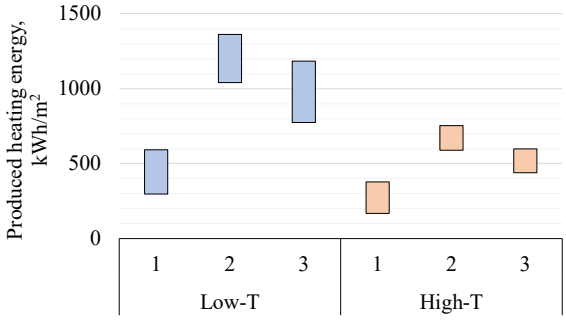

Fig. 3.22. Comparison of produced heating energy for each case; min/max.

3.3. Discussion and conclusions

There is a need and potential for greater solar energy integration into district heating (DH) systems. This can be achieved through large-scale centralized solar parks or small-scale decentralized solutions located near consumers, reducing transmission losses and utilizing unused rooftop space. As the roof area is limited, it must be optimized to maximize energy output. To achieve this, lowering DH temperatures is recommended, which requires significant capital investments but can be implemented gradually – through zoning strategies and in parallel with the building renovation process.

The study (Pakere & Blumberga, 2020) has presented a methodology for comparing different solar system designs for DH applications and energy management strategies. It analyzes three solar technologies (ST, PV + HP, and PVT + HP) under Latvian climatic conditions, considering the solar power-to-heat concept. The findings highlight that lowering DH network temperatures improves overall system performance and emphasize the critical role of heat tariffs, which serve as a key reference for economic evaluation and surplus power utilization strategies – whether converting excess electricity to heat or feeding it into the grid.

On the economic side, heat pump operation requires both heating energy and electricity, which come at different costs and have different climate impacts. It's important to understand who benefits from high and stable COP values and how this influences decision-making.

Two business models have been proposed in the literature (Vivian et al., 2018): (a) the "Business-as-Usual" (BaU) model, where the heat pump belongs to the end-user and he pays separately for electricity and district heat, while the DH utility manages only heat distribution; and (b) the "Investment-on-Utility" (IoU) model, where the DH utility invests in heat pumps, covers electricity costs, and users pay only for the heat delivered to their buildings.

In both business models, there is a desire to maximize the heat pump's COP to reduce electricity costs. In the BaU model, the end-user is interested in a high and stable DH grid temperature, while the DH operator wants lower temperatures to minimize heat losses and may not care about temperature fluctuations. In contrast, the IoU model aligns both the end-user and system operator around the goal of maximizing overall system performance by reducing energy losses and lowering tariffs. The IoU model is simpler and potentially more cost-effective, but it requires greater involvement from the DH operator side.

Energy performance calculations

When considering solar heating technologies, photovoltaic (PV) panels, solar thermal (ST) collectors, and photovoltaic-thermal (PVT) collectors compete. PV panels require a heat pump for heat production, whereas ST can operate independently. Since PVT generates both heat and electricity, it is most effective when combined with a heat pump. Simulation results show that using PVT as a heat and electricity source for a brine-to-water heat pump (BWHP) can maximize solar energy utilization, achieving 1040–1361 kWh/m^2 in a DH system with a supply temperature of 30 °C – 50 °C and a return temperature of 20 °C. This exceeds annual solar irradiation (1033 kWh/m²) on the PVT surface, because the heat carrier temperature in PVT is lower than ambient air temperature, allowing additional energy gains from the surrounding air.

This study assumes that the DH system has unlimited heating capacity, meaning it can absorb all produced heat without temperature changes. However, if the proposed system were installed on the roof of every building, total heat production could surpass consumption, leading to temperature increases and efficiency losses. To mitigate this, seasonal heat storage or restrictions on installed solar capacity per zone could be introduced.

Since peak solar heat production occurs in summer, when only domestic hot water (DHW) demand exists in residential areas, system feasibility must align with real consumption needs. Measurement data from multi-apartment buildings in Oslo, Norway (Walnum et al., 2021) shows that DHW heating energy demand ranges from 0.079 kWh/m^2 to 0.189 kWh/m^2 per day, averaging 0.127 kWh/m^2 per 24 hours or 46.2 kWh/m^2 per year. Assuming the DH system can store heat for a 24-hour period, it is possible to estimate the maximum ST, PV or PVT area.

Calculations show that in a low-T case, a BWHP + PVT system can produce 8.39 kWh/m² per day, meaning 1 m² of PVT can provide DHW heating for 66 m² of building area. In the study's case example, a 153.6 m² PVT system installed on a 530 m² roof could provide DHW for a 19-floor building or almost four five-story buildings. In such a way, it is possible to install both technologies – one building can produce heating energy in one of the ways discussed in this study and another building can produce electricity by using PV panels.

Limitations

This study focuses on the technical side of integrating solar energy and heat pumps into low-temperature district heating. A detailed economic analysis was not included, as it depends on multiple variable factors, like equipment prices, installation costs, energy tariffs, electricity prices, all of which vary by time and location. Technological advancements may lower equipment costs, while inflation can increase labor and material expenses. District heating tariffs and electricity prices also vary over time, significantly impacting the payback period and influencing system selection. The goal here was to build a solid technical base. The economic side can and should be addressed in future studies using these results as input.

4. Impact of temperature fluctuations on the brine-to-water heat pump performance

As demonstrated in Chapter 1, the heat carrier temperature in ST collectors can be unstable due to solar irradiation fluctuations and imperfect system control. Additional measurements taken by researchers from the Royal Institute of Technology (Francisco et al., 2024) confirm that the heat carrier temperature in photovoltaic-thermal (PVT) collectors also depends on solar irradiation intensity and its variations (Fig. 4.1). An analysis over an 8-hour period on a cloudy day showed that heat carrier temperature fluctuated within a 7.19 K range, with a mean value of 20.18 °C, standard deviation (SD) of 1.80 K and mean absolute deviation (MAD) of 1.51 K, while solar irradiation had a mean value of 623 W/m^2, with SD = 287 W/m^2, MAD = 259 W/m^2. The heat carrier temperature decreases with decreasing solar irradiation and increases as solar irradiation intensifies, showing a direct correlation between solar input and thermal response.

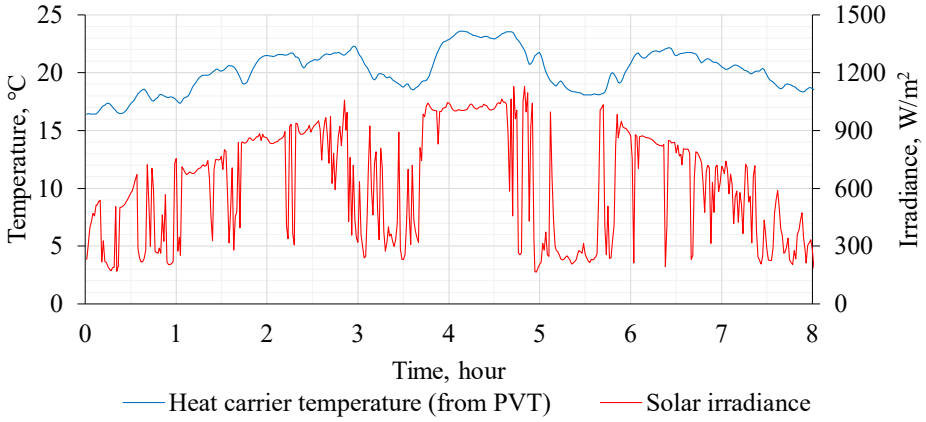

Fig. 4.1. Measurements from BC-AL-20 PVT collector (Francisco et al., 2024), data taken from KTH Royal Institute of Technology, time step: 1 minute.

During this study, the heat carrier temperature in an existing 3rd generation DH system was measured in a multi-apartment building over three summer weeks with 5-second time step. For one day with higher temperature fluctuations, the average supply temperature was 62.7 °C with a SD = 2.2 K, MAD = 2.0 K and a temperature range from 54.4 °C to 66.5 °C, but for the rest of the period, an average supply temperature of 65.0 °C with SD = 0.8 K and MAD = 0.6 K was recorded. Additionally, the district heating supply temperature was recorded in another building with a one-hour time step during a 2-year period. Measurements show that during the non-heating period, the average monthly supply temperature was 59.3–64.1 °C and monthly temperature SD varied from 1.2 K to 6.6 K, while MAD varied from 0.9 K to 3.3 K.

Considering a booster heat pump, the temperature in the district heating system needs to be lower, but this does not necessarily mean that temperature fluctuations become lower too, especially in the case of many small decentralized renewable heating sources with varying heating production load. Heating temperature lift is a key factor in heat pump system performance, but the impact of temperature fluctuations remains unexplored in the literature.

4.1. Heat pump test facility. COP measurements

As discussed in Chapter 3, the brine-to-water heat pump (BWHP) can be directly connected to photovoltaic-thermal (PVT) collectors as a heat source or linked to solar thermal (ST) collectors through the district heating (DH) system, connecting to the heat pump's sink side. In both configurations (see Fig. 4.2), PVT and ST collectors can cause heat carrier temperature fluctuations, as it was discussed before, which may impact the heat pump's operation and overall performance.

Usually, the heating energy source of brine-water or brine-to-water heat pump is geothermal heat, groundwater, lake or river with high inertia and low temperature fluctuations. Not all heat pumps are suitable for every source temperature range, and the standard conditions for HP manufacturing tests differ from those in ultra-low temperature district heating (ULTDH) systems (Reiners et al., 2021). Therefore, the compressor's operating range and required working conditions must be carefully evaluated, and reliable methods for simple estimation of HP COP beyond standard conditions need to be identified and tested (Pieper et al., 2021). Since the COP of the booster heat pump is highly sensitive to the evaporator outlet temperature (Zhu et al., 2023), the ULTDH system should aim for the highest possible return temperature. This requirement impacts the entire network design, as the low temperature difference between supply and return increases the necessary flow rate.

In Latvia, large-scale solar thermal collectors are already integrated in district heating systems (Lebedeva et al., 2023), but low scale decentralized solar collectors are under consideration and they might increase flow temperature fluctuations during cloudy days (Zajacs et al., 2022). In the case of connecting the booster heat pump to low or ultra-low temperature district heating system, the flow temperature fluctuations might be significant, especially if a lot of different heat sources are connected, so the performance of standard heat pump under these conditions might be different in comparison to the technical data provided by manufacturers.

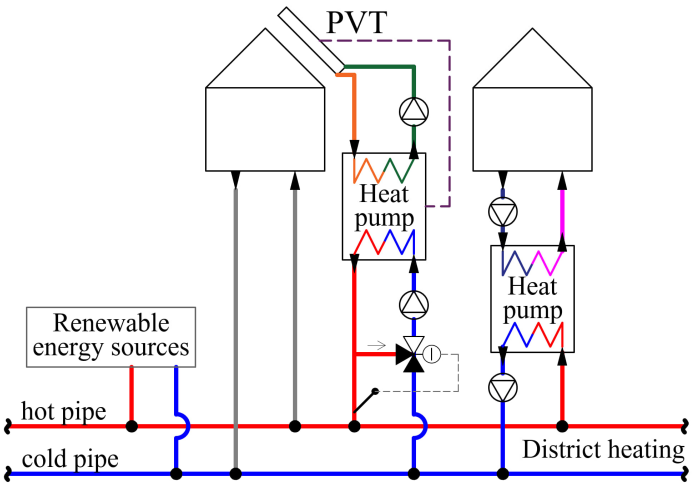

Fig. 4.2. Possible brine-to-water heat pump integration into district heating system.

The aim of this study is to evaluate how fluctuations in heat source and sink temperatures impact the coefficient of performance (COP) of a brine-to-water heat pump in laboratory conditions by comparing COP at stable and fluctuating heating carrier temperature conditions.

The main object of this study is a brine-to-water heat pump which operates under conditions shown on Fig. 4.3. Heat pump includes two circulation pumps which are taken into account when calculating the coefficient of performance. It is not connected to the district heating system, nor to the building heating and domestic hot water preparation system.

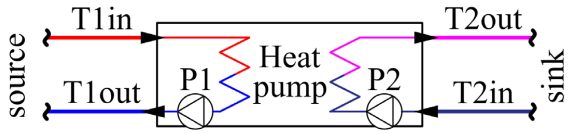

Fig. 4.3. Principal drawing of the studied system. P1, P2 – circulation pumps.

This study is based on laboratory measurements carried out at a heat pump test facility shown at Fig. 4.4. The test facility allows to simulate different set-ups and combinations, but for this study the configuration shown in Fig. 4.5 was used. It includes a 6-kW brine-to-water heat pump (R407C refrigerant), a 265 L storage tank (BT1), two 120 L storage tanks (BT2 and BT3), one heat exchanger (HE1), three three-way valves (M1, M2 and M3) for regulating heat carrier temperatures, four circulation pumps (P1 – P4), two flow meters (F1, F2), four manual balancing valves (B1 – B4), multiple temperature sensors, and a heating unit to release the excess heat. The specific heat of the heat carrier is 3.95 kJ/(kg·K) on the source side and 4.18 kJ/(kg·K) on the sink side, with corresponding densities of 1030 kg/m^3 and 990 kg/m^3. Flowrate at source side was 850–1050 m^3/h and at the sink side was 1150–1350 m^3/h. In general, flow rates during measurements remained almost constant within one case, but they might change slightly depending on the position of the M1 and M2 valves.

Fig. 4.4. Heat pump test facility.

Three-way valve M1 (Fig. 4.5) provides the desired flow temperature $T1_{in}$ for the heat pump source side, while three-way valve M2 provides the desired flow temperature $T2_{in}$ for the heat pump sink side, based on defined set points and measurements from the PT500 immersion temperature sensors. Control valves with high valve authority; actuators with fast response.

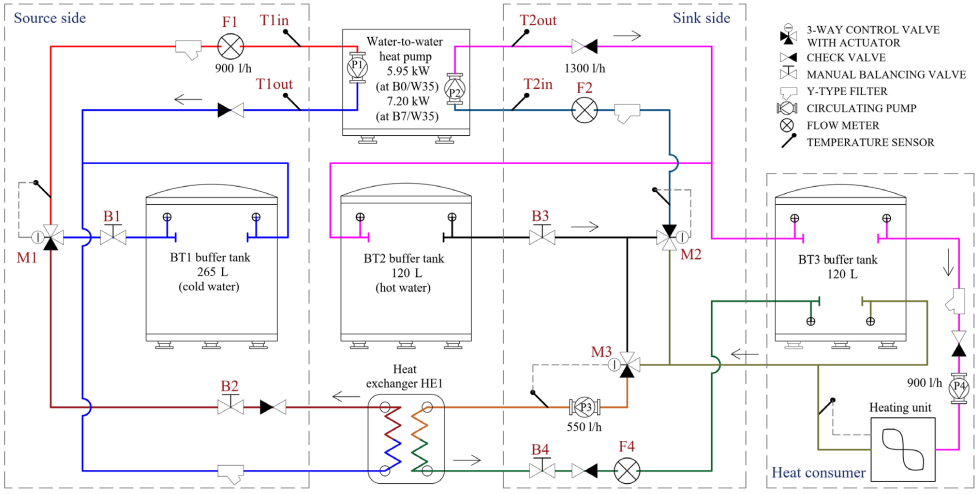

Fig. 4.5. Principal drawing of the studied system on the test facility.

During all measurements the heat pump works without interruptions at full load. It is isolated from both the building's heating system and any external heat source. To maintain stable conditions during measurements, the heat generated on the sink side is redirected to the source side via heat exchanger HE1. The three-way valve M3 regulates this process, ensuring that the flow temperature entering the heat exchanger does not exceed the $T2_{in}$ temperature. All circulation pumps operate at a constant speed. Due to the electricity input, the heat pump generates more thermal energy than it extracts from the source, so the excess heat is removed using a heating unit to maintain overall heat balance in the system.

Manual balancing valves B1, B2, and B3 are adjusted to minimize flow fluctuations during measurements. Ultrasonic flow meters F1 and F2 with nominal flow rate 1.5 m^3/h, accuracy class 2 (EN 1434-1), measurement interval: 120 seconds.

The temperatures $T1_{in}$, $T1_{out}$, $T2_{in}$, and $T2_{out}$ are measured using eight Class A surface temperature sensors (tolerance ± 0.15 + 0.002 t). These sensors are placed on opposite sides of the same cross-sectional area of the metal pipe (see Fig. 4.6*a*) as specified in EN 14511-3:2022, positioned as close to the heat pump as possible, and then insulated with closed cell flexible elastomeric foam insulation. The temperature at each point is calculated as the average of the two sensor readings. As shown in Fig. 4.6*b*, before the start of the measurements, when the heat pump was off, the temperature difference measured by different sensors was no more than 0.14 K. Temperature measurement interval: 5 seconds.

Additionally, the COP was calculated by using Class B surface temperature sensor (tolerance ± 0.3 + 0.005 t), which is commonly used in the heating systems. In total four temperature sensors were placed on the pipelines near Class A sensors (see Fig. 4.6*a*). The results gained using Class B sensors are used only in comparison with Class A sensors, but in all other analysis the COP calculated based on Class A sensors data was used.

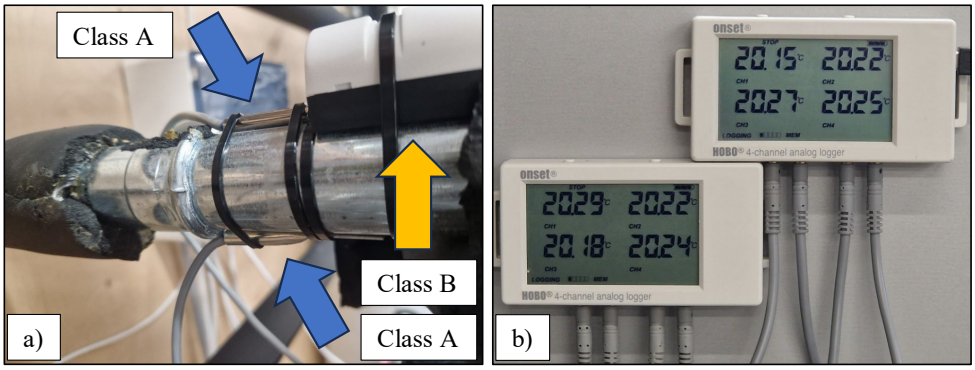

Fig. 4.6. a) two Class A and one Class B temperature sensors placed on a pipe;
b) temperature measurements when the system is off (in total 8 sensors on 4 pipes).

The system allows us to test the heat pump under different heat source and sink temperatures and calculate its coefficient of performance (COP) according to eq. (4.1).

$$\mathrm{COP_{HP}} = \frac{Q_h}{E}, \tag{4.1}$$

where $\mathrm{COP_{HP}}$ – heat pump coefficient of performance;
Q_h – heat pump produced heating energy, calculated according to eq. (4.2), kJ;
E – heat pump (E_{comp} + $E_{pumps\&ctrl}$) consumed electricity, kJ.

$$Q_h = \sum_{i=2}^{n} \left(c \cdot \rho \cdot \frac{V_i \cdot (T_{2out,i} - T_{2in,i}) + V_{i-1} \cdot (T_{2out,i-1} - T_{2in,i-1})}{2} \cdot \Delta t\right), \tag{4.2}$$

where Q_h – heat pump produced heating energy, kJ;
c – specific heat of the heat carrier, 4.18 kJ/(kg·K);
ρ – heat carrier density, 990 kg/m^3;
V – heat carrier flow rate, measured by F2 flow meter, m^3/s;
T_{2out}, T_{2in} – heat carrier outlet and inlet temperatures, K;
Δt – measurement time step, 5 sec.

Electricity power consumption is measured by three electricity meters with time interval 5 seconds and then converted from kWh to kJ (1 kWh = 3600 kJ):
E_{comp} – heat pump compressor power consumption, kJ;
$E_{pumps\&ctrl}$ – auxiliary electricity (both circulation pumps, control panel power cons.), kJ;
E_{P2pump} – heat pump sink side circulation pump P2 power consumption, kJ.

Additionally, the COP of the heat pump's compressor can be calculated using eq. (4.3). Since the circulation pump has a wet rotor, the electricity it consumes is converted into heat. Therefore, to determine the heat produced solely by the thermodynamic cycle, the heating energy added by the electricity consumption of the circulation pump must be subtracted from the total heating energy output of the heat pump, considering circulation pump efficiency.

$$\mathrm{COP_{comp}} = \frac{Q_h - E_{P2pump} \cdot \eta_{pump}}{E_{comp}}, \tag{4.3}$$

where $\mathrm{COP_{comp}}$ – heat pump's compressor coefficient of performance;
η_{pump} – circulation pump efficiency; assumed to be 0.5 for further calculations.

4.1.1. COP measurements under stable temperature conditions

Methods

According to the heat pump's technical documentation, the source temperature range should be maintained between -5 °C and +30 °C. To measure the COP at stable temperatures, the following procedure was applied. The sink-side inlet temperature $T2_{in}$ setpoint was initially set to 25 °C, while the source-side inlet temperature $T1_{in}$ setpoint was set to 0 °C. Every 25 minutes $T1_{in}$ was increased by 2 K until it reached 28 °C (Fig. 4.7*a*). The cycle was then repeated with $T2_{in}$ setpoints increased by 5 K, until it reached 55 °C (Fig. 4.7*b*). This resulted in a total of 105 measurement cycles, each taken at 25-minute intervals. To improve accuracy, this entire process was repeated twice as much, resulting in a total of 315 measurement cycles.

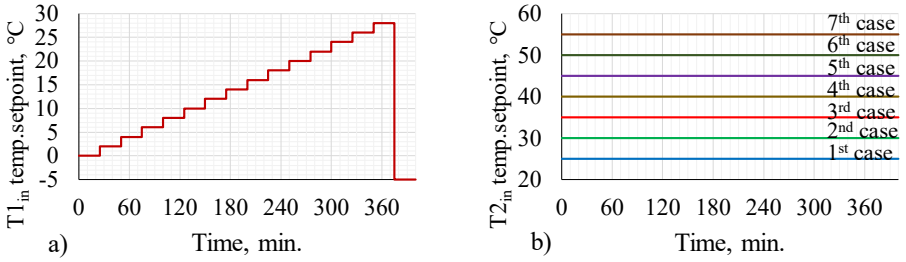

Fig. 4.7. a) $T1_{in}$ temperature setpoints in all cases and b) $T2_{in}$ temperature setpoint in different cases during stable temperature conditions measurements.

Since changes in the $T1_{in}$ temperature require time (valve movement speed, system inertia) and may cause fluctuations during the adjustments of the three-way valve, the initial 5 minutes of each measurement period were excluded from analysis to reduce possible errors. Only the stable 20-minute interval, from 5th to 25th minute, was used for the subsequent analysis.

Results

According to Fig. 4.8, the heat pump COP was between 2.35 and 4.82. The calculated COP values are displayed for one cycle at each constant $T2_{in}$ temperature. All measurements were repeated 3 times under identical conditions, labeled as “a”, “b” and “c”, showing almost identical results, meaning that the operation of the test facility was stable and there was no occasional influence on measurements from the outside. The maximum $T1_{in}$ temperature for $T2_{in} = 25$ °C was 18 °C and for $T2_{in} = 30$ °C was 22 °C because of test facility operation principle.

A simple linear regression analysis was performed to model the relationship between $T1_{in}$ and COP_{HP} and between $T1_{in}$ and COP_{comp} for different $T2_{in}$ values. The regression model is $f(x) = a \cdot x + b$, where a is the slope and b is the intercept. The estimated parameters were found by using the least squares regression method. The analysis shows that the relationship between $T1_{in}$ and COP is a piecewise function, which can be represented by two linear segments with regression coefficient $r > 0.99$. The regression functions are shown in Fig. 4.9. and the equations of each segment are presented in Table 4.1 and Table 4.2. The breakpoints occur at different $T1_{in}$ values for each $T2_{in}$ setpoint: at 7.6 °C for $T2_{in} = 25$ °C, 20.6 °C for $T2_{in} = 55$°C.

To quantify the uncertainty in these estimates, 99 % confidence intervals were computed for both the slope and intercept using the Student's *t*-distribution. The confidence interval is two-tailed, meaning it provides an upper and lower bound within which the true values of the slope and intercept are expected to lie with 99 % confidence.

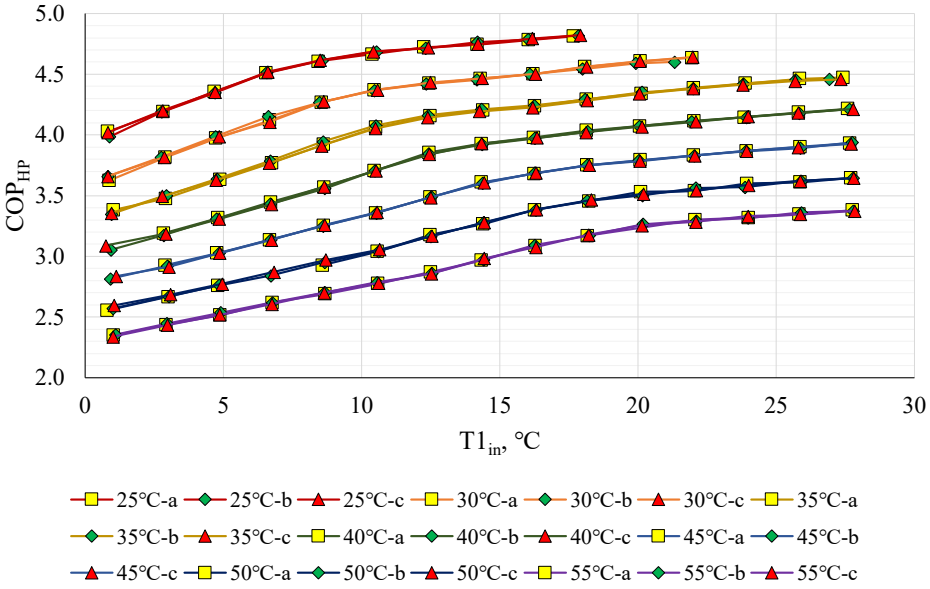

Fig. 4.8. Heat pump COP_{HP} dependence on $T1_{in}$ measured temperature at different $T2_{in}$ temperatures (25 °C – 55 °C). Each measurement cycle repeated 3 times (a, b, c).

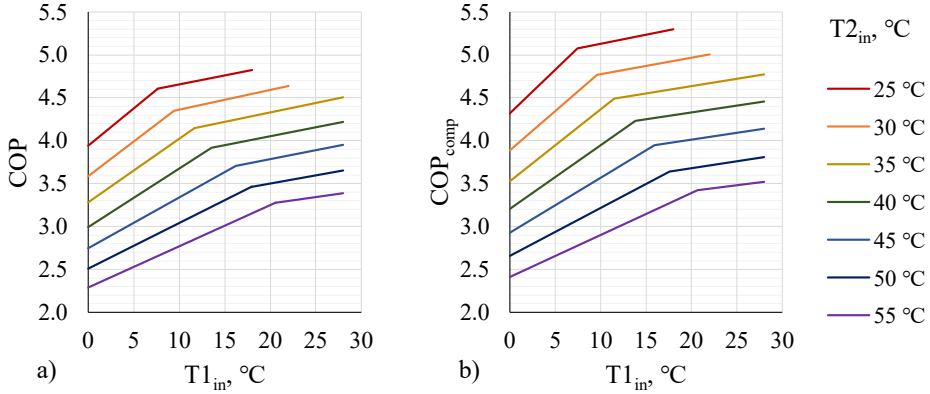

Fig. 4.9. a) COP of the heat pump; b) COP of the heat pump's compressor dependence on $T1_{in}$ measured temperature at different $T2_{in}$ temperature setpoints. The regression model.

Fig. 4.9 and Table 4.2 show the impact of heat source temperature on the heat pump's COP under different sink temperature conditions. The data clearly show that at lower heat source temperatures (before the breakpoint), the rate of COP increase per 1 K rise in source temperature is higher, with the slope ranging from 0.048 to 0.087. After the breakpoint, the impact of source temperature on COP decreases significantly, with the slope reduced by a factor of 2.8 to 4.1. Additionally, the data indicate that the slope also increases with decreasing sink temperature $T2_{in}$. This indicates that the heat pump's efficiency is more sensitive to heat source and sink temperatures when operating at lower temperatures.

The uncertainty analysis of the slope within the 99 % confidence interval shows a relative uncertainty of 1.6 % to 14.3 %. The uncertainty could be reduced by increasing the number of measurement cycles, though it remains dependent on the accuracy of temperature sensors and flow meter measurements.

As seen on (Fig. 4.10), the heat pump's coefficient of performance (COP_{HP}), calculated using eq. (4.1), is 3.9 % to 9.9 % lower than the COP of the heat pump's compressor (COP_{comp}), calculated using eq. (4.3). This difference is more strongly influenced by variation in $T2_{in}$ (sink temperature) than by $T1_{in}$ (source temperature). In absolute terms, the average difference decreases as $T2_{in}$ increases, ranging from 0.39 to 0.48 at $T2_{in}$ = 25 °C, and from 0.12 to 0.13 at $T2_{in}$ = 55 °C. By comparing Table 4.1 and Table 4.2, it is evident that the slope of COP_{comp} is steeper than the slope of COP_{HP}. This indicates that COP_{comp} is more sensitive to changes in heat source temperature than COP_{HP}. This difference can be attributed to the electricity consumption and heat gains of the two circulation pumps, which remain constant regardless of heat source and sink temperatures and does not scale with temperature variations.

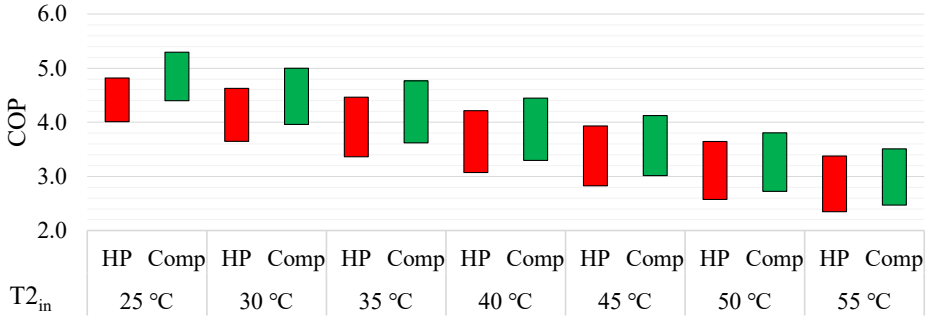

Fig. 4.10. COP of heat pump (HP) and COP of the heat pump's compressor (Comp.) – average values for three measurements. $T1_{in}$ temperature setpoint range: 0 °C – 28 °C (for $T2_{in}$ = 25 °C: $T1_{in}$ was 0 °C – 18 °C; for $T2_{in}$ = 30 °C: $T1_{in}$ was 0 °C – 22 °C).

Table 4.1

Linear regression function of COP_{HP} dependence on $T1_{in}$ temperature for different $T2_{in}$ temperature cases, expressed in the $f(x) = a \cdot x + b$ form as a piecewise function.

$T2_{in}$ setpoint	Before BP		Breakpoint (BP)	After BP	
	a	*b*		*a*	*b*
25 °C	0.087 ± 0.006	3.942 ± 0.024	7.64 °C	0.021 ± 0.003	4.446 ± 0.035
30 °C	0.081 ± 0.004	3.587 ± 0.024	9.40 °C	0.023 ± 0.001	4.132 ± 0.024
35 °C	0.074 ± 0.003	3.282 ± 0.017	11.69 °C	0.022 ± 0.001	3.890 ± 0.030
40 °C	0.068 ± 0.003	2.993 ± 0.021	13.57 °C	0.021 ± 0.001	3.631 ± 0.025
45 °C	0.059 ± 0.001	2.747 ± 0.012	16.24 °C	0.021 ± 0.002	3.364 ± 0.038
50 °C	0.053 ± 0.002	2.509 ± 0.017	18.00 °C	0.019 ± 0.003	3.121 ± 0.060
55 °C	0.048 ± 0.001	2.289 ± 0.014	20.58 °C	0.015 ± 0.003	2.968 ± 0.069

Table 4.2

Linear regression function of COP_{comp} dependence on $T1_{in}$ temperature for different $T2_{in}$ temperature cases, expressed in the $f(x) = a \cdot x + b$ form as a piecewise function.

$T2_{in}$ setpoint	Before BP		Breakpoint (BP)	After BP	
	a	*b*		*a*	*b*
25 °C	0.102 ± 0.007	4.320 ± 0.028	7.42 °C	0.021 ± 0.003	4.921 ± 0.037
30 °C	0.092 ± 0.004	3.888 ± 0.023	9.59 °C	0.019 ± 0.001	4.588 ± 0.023
35 °C	0.084 ± 0.003	3.528 ± 0.017	11.48 °C	0.017 ± 0.001	4.297 ± 0.019
40 °C	0.074 ± 0.003	3.206 ± 0.022	13.85 °C	0.016 ± 0.001	4.009 ± 0.021
45 °C	0.064 ± 0.001	2.928 ± 0.012	15.92 °C	0.016 ± 0.001	3.692 ± 0.026
50 °C	0.056 ± 0.001	2.658 ± 0.013	17.58 °C	0.016 ± 0.003	3.361 ± 0.058
55 °C	0.049 ± 0.001	2.412 ± 0.012	20.69 °C	0.013 ± 0.003	3.157 ± 0.072

For further analysis, the COP_{HP} of the heat pump, including circulation pumps, was examined. It is important to note that heat pump capacity and electrical power also depend on source and sink temperatures, as shown in Fig. 4.11. The heat pump's heat capacity ranged from 5.25 kW to 9.53 kW, while electrical power varied between 1.51 kW and 2.82 kW. The relationships presented in Fig. 4.11 were used to develop a heat pump performance dataset for use in the TRNSYS dynamic simulation program for further analysis and can be used in future research to simulate and analyze complex system behavior.

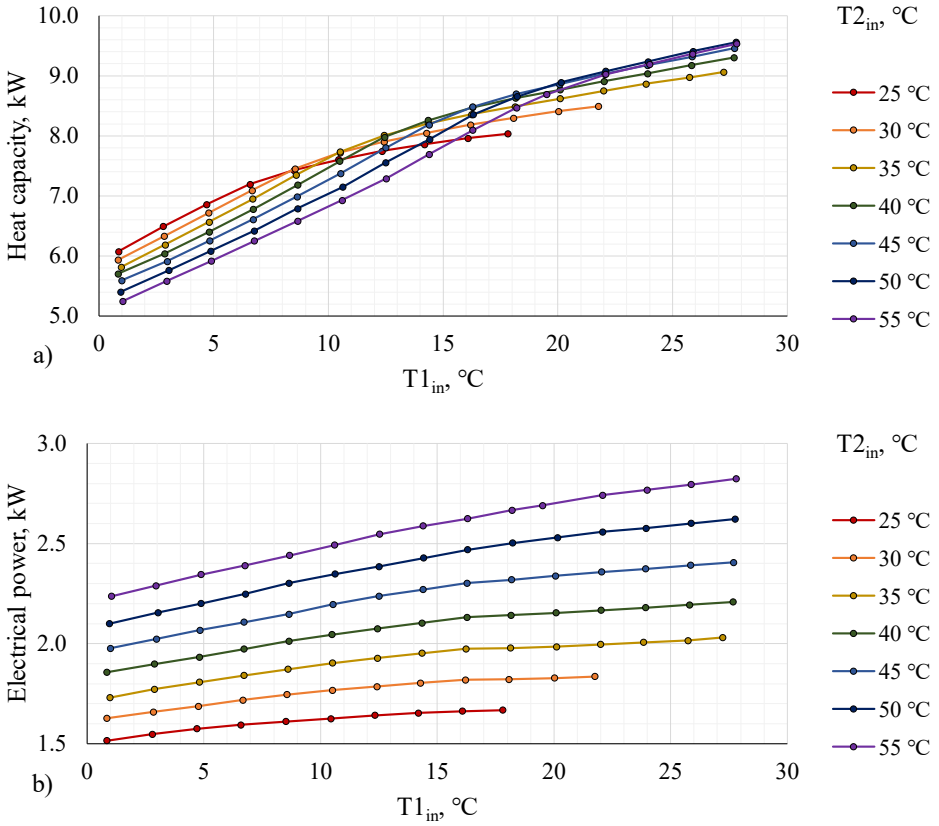

Fig. 4.11. Mean values from 3 measurements of a) heat pump heat capacity and b) electrical power dependence on $T1_{in}$ measured temperature at different $T2_{in}$ temperature setpoints.

4.1.2. COP measurements under fluctuating temperature conditions

Methods

To simulate fluctuating source temperatures, a setpoint pattern was created (Fig. 4.12). The $T1_{in}$ temperature setpoint was adjusted every 4 minutes, with each measurement cycle lasting 40 minutes, allowing for five complete oscillations per cycle. Between each cycle, a 4-minute interval with a -5 °C temperature setpoint was introduced. Six cycles were performed with different temperature fluctuations but equal average temperature setpoint.

The procedure described above was performed for two $T2_{in}$ setpoints: 30 °C and 55 °C, which remained constant during all measurements. With $T2_{in}$ = 30 °C the $T1_{in}$ was set to be (5 °C / 10 °C / 15 °C) but with $T2_{in}$ = 55 °C the $T1_{in}$ was set to be (5 °C / 15 °C / 25 °C).

To improve statistical robustness, this process was replicated three times with different temperature sequences: the second round followed the order 10 °C / 5 °C / 15 °C, and the third round used 15 °C / 10 °C / 5 °C. For each $T2_{in}$ setpoint, 54 measurement cycles were recorded, resulting in a total of 108 cycles analyzed across all setpoints.

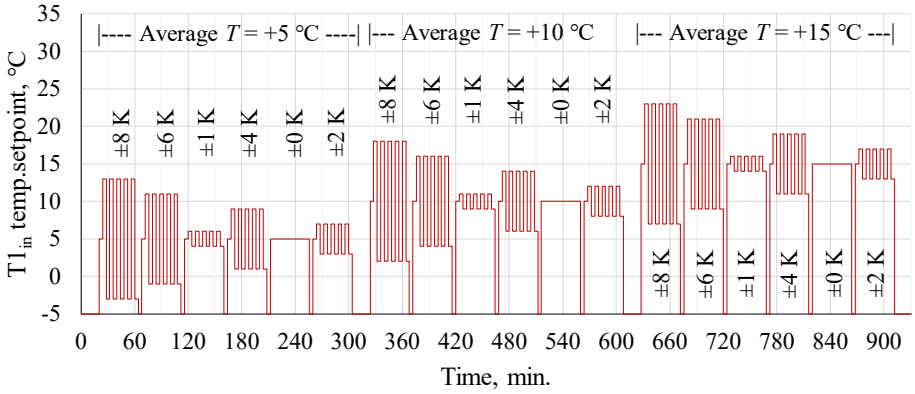

Fig. 4.12. $T1_{in}$ temperature setpoint during fluctuating temperature conditions measurements.

To study the sink temperature fluctuations, the similar approach was performed but, in this case, the $T1_{in}$ temperature was set to be constant 5 °C and the $T2_{in}$ temperature changes according to Fig. 4.13. pattern. $T2_{in}$ = (30 °C / 35 °C / 40 °C) and (45 °C / 50 °C / 55 °C) patterns were investigated, each 3 times, resulting in total of 108 cycles analyzed across all setpoints.

Measurements were performed following the $T1_{in}$ temperature setpoint pattern shown in Fig. 4.12 and Fig. 4.13. The actual measured $T1_{in}$ temperature for some cases displayed in Fig. 4.14. and summarized in Table 4.3 and Table 4.4 The measured mean temperatures were slightly different than the setpoints due to system inertia; however, the differences between cases were distinct and consistent, allowing for reliable use of these measurements in further analysis. The measured temperature data does not have the normal distribution. To analyze temperature fluctuations, the mean absolute deviation (MAD) of the measured values was calculated, with higher MAD indicating greater fluctuations. Mean absolute deviation shows the average distance between the values in a dataset and the mean of the dataset and has the same unit as measured values, which makes it clear and convenient way to describe fluctuations.

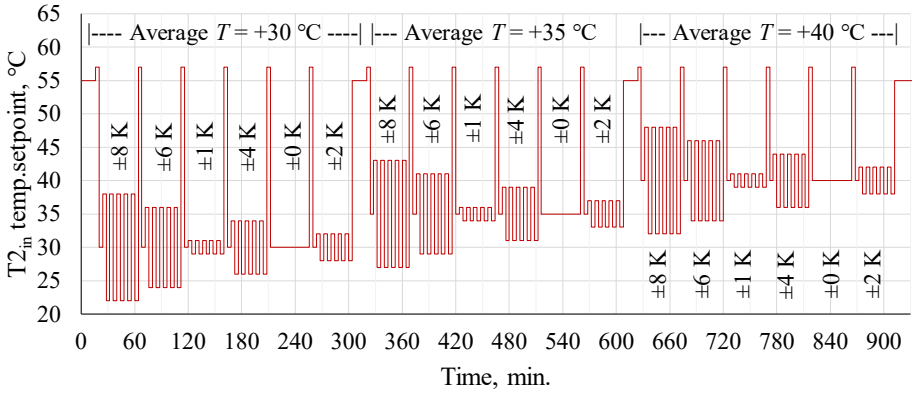

Fig. 4.13. $T2_{in}$ temperature setpoint during fluctuating temperature conditions measurements.

Table 4.3

Measured $T1_{in}$ temperature mean values and mean absolute deviations (MAD) for (a1, a2, a3, b1, b2, b3) cases in Fig. 4.14. at different temperature fluctuations.

Case:	a1		a2		a3		b1		b2		b3	
$T1_{in}$ average setpoint:	+5 °C		+10 °C		+15 °C		+5 °C		+15 °C		+25 °C	
$T2_{in}$ average setpoint:	+30 °C						+55 °C					
$T1_{in}$ setpoint fluctuat.	Mean	MAD	Mean	MAD	Mean	MAD	Mean	MAD	Mean	MAD	Mean	MAD
± 0 K	5.55	0.10	10.64	0.05	15.31	0.05	5.90	0.09	15.40	0.14	24.92	0.20
± 1 K	5.88	0.66	10.61	0.64	15.33	0.78	5.89	0.88	15.47	0.67	24.91	0.84
± 2 K	5.83	1.37	10.63	1.25	15.38	1.24	5.97	1.73	15.45	1.43	24.93	1.47
± 4 K	5.94	2.80	10.66	2.66	15.28	2.57	6.22	2.85	15.51	2.90	24.51	2.51
± 6 K	6.04	4.29	10.39	4.08	13.83	3.15	7.07	3.47	15.52	4.32	23.19	3.00
± 8 K	6.12	5.57	10.61	4.71	12.94	3.86	6.90	5.01	15.34	5.76	22.27	3.80

Table 4.4

Measured $T2_{in}$ temperature mean values and mean absolute deviations (MAD) for (c1, c2, c3, c4, c5, c6) cases in Fig. 4.14. at different temperature fluctuations.

Case:	c1		c2		c3		c4		c5		c6	
$T1_{in}$ average setpoint:	+5 °C											
$T2_{in}$ average setpoint:	+30 °C		+35 °C		+40 °C		+45 °C		+50 °C		+55 °C	
$T2_{in}$ setpoint fluctuat.	Mean	MAD	Mean	MAD	Mean	MAD	Mean	MAD	Mean	MAD	Mean	MAD
± 0 K	29.76	0.11	34.29	0.09	39.13	0.09	43.93	0.09	48.82	0.10	53.55	0.06
± 1 K	29.61	0.81	34.36	0.86	39.19	0.84	44.00	0.85	48.83	0.86	53.58	0.84
± 2 K	29.64	1.59	34.43	1.69	39.21	1.64	44.01	1.67	48.85	1.67	53.70	1.66
± 4 K	29.77	3.21	34.55	3.27	39.33	3.24	44.17	3.22	48.90	3.13	53.54	2.97
± 6 K	29.80	4.56	34.60	4.66	39.02	4.31	44.10	4.47	47.79	3.63	51.92	3.07
± 8 K	29.72	5.89	34.68	6.00	38.30	5.19	43.34	5.70	47.07	4.48	51.06	3.75

The data shown in Table 4.3 and Table 4.4 indicates that measured mean values of each cycle are very close to the setpoint average values as well as the increasing of setpoint fluctuations the MAD of measured values increased. It is normal that MAD is lower than setpoint fluctuations because fluctuations show the extreme temperature, but the real system has inertia and the control valve response time, so the heat carrier temperature does not change immediately as can be seen in Fig. 4.14. A shorter interval would reduce the temperature fluctuation range and reduce MAD, while a longer interval would introduce too many temperatures at both extremes.

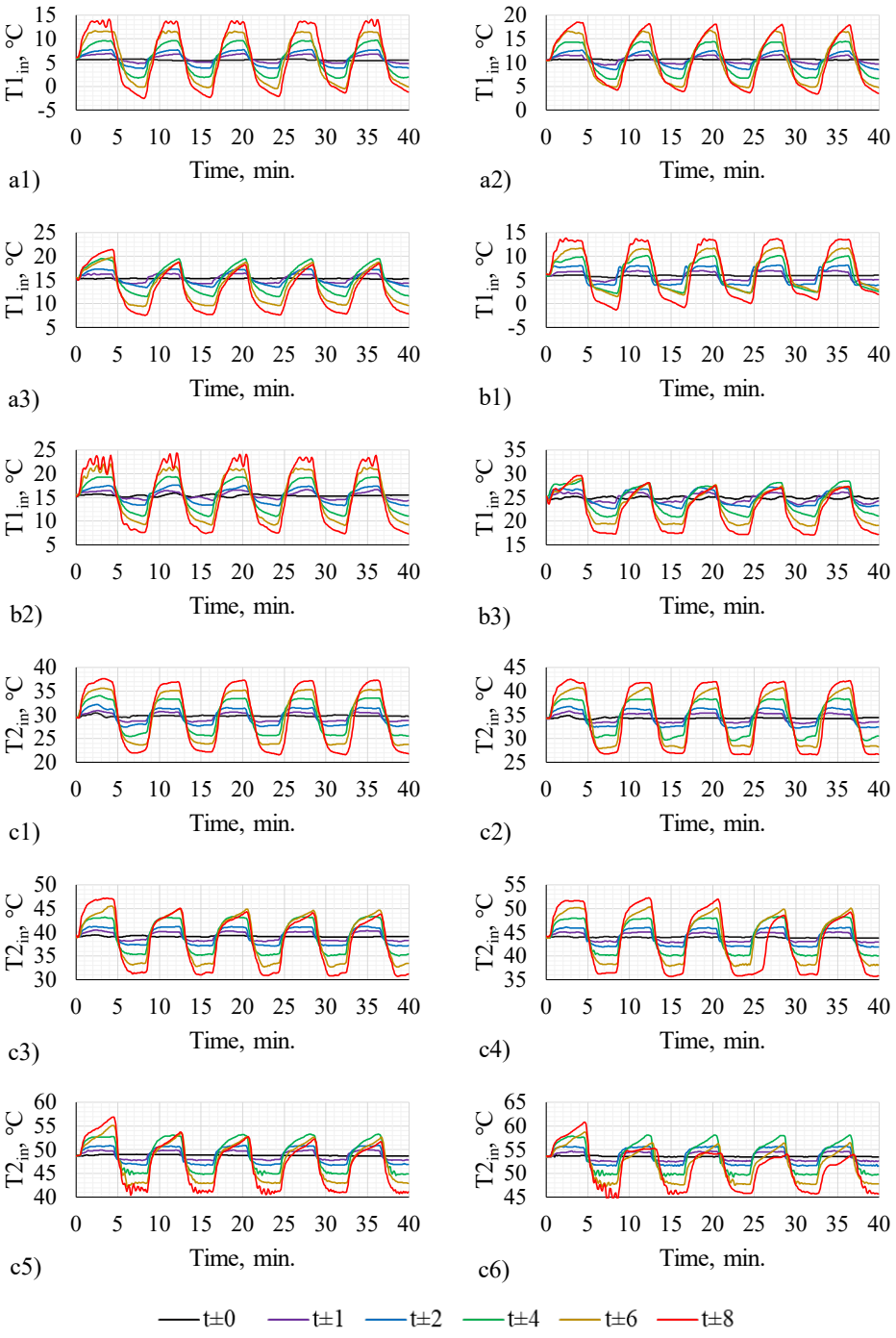

Fig. 4.14. Measured $T1_{in}$ and $T2_{in}$ temperatures during a 40-minute measurement interval for different cases: a1) t=5 °C; a2) t=10 °C; a3) t=15 °C; b1) t=5 °C; b2) t=15 °C; b3) t=25 °C; c1) t=30 °C; c2) t=35 °C; c3) t=40 °C; c4) t=45 °C; c5) t=50 °C; c6) t=55 °C.

Results

For each 40-minute measurement cycle, the heat pump's COP was calculated using eq. (4.1) and eq. (4.3) and is represented as a dot in Fig. 4.15 and Fig. 4.17. Since the mean $T1_{in}$ temperatures vary and are not constant, directly comparing COP values between measurement cycles would be misleading. Therefore, in this analysis, the COP for fluctuating cases is compared to a stable baseline case – representing the COP that would be expected at the same mean temperature without fluctuations, according to Fig. 4.9.

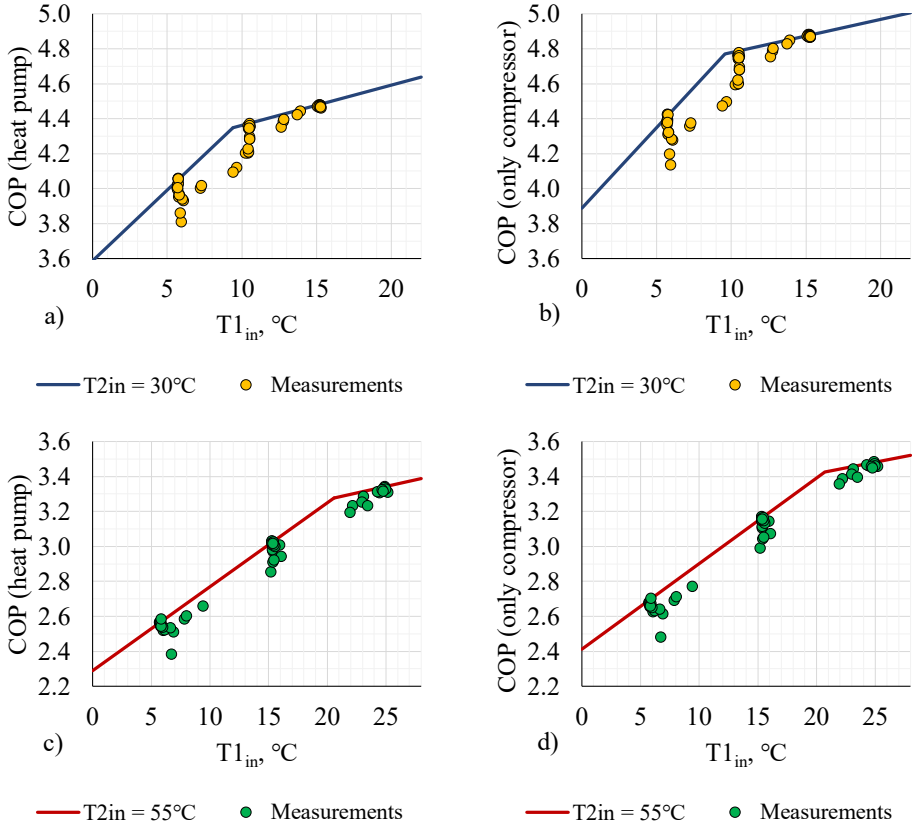

Fig. 4.15. COP dependence on $T1_{in}$ mean temperature. Dots – COP at various temperature fluctuations over a 40-minute interval; line – COP under stable temperature conditions. a) and c) COP based on eq.(4.1); b) and d) COP based on eq.(4.3).

From Fig. 4.15 it is clear that COP values under fluctuating conditions do not match the COP values expected at stable conditions. To evaluate the influence of fluctuations on this difference, Fig. 4.16 is provided. Each dot in Fig. 4.15 includes a corresponding mean absolute deviation (MAD) value, and for each dot, the difference (ΔCOP) between the calculated COP and the expected COP at the same mean temperature without fluctuations was determined. The relationships between these differences and the MAD values are shown in Fig. 4.16.

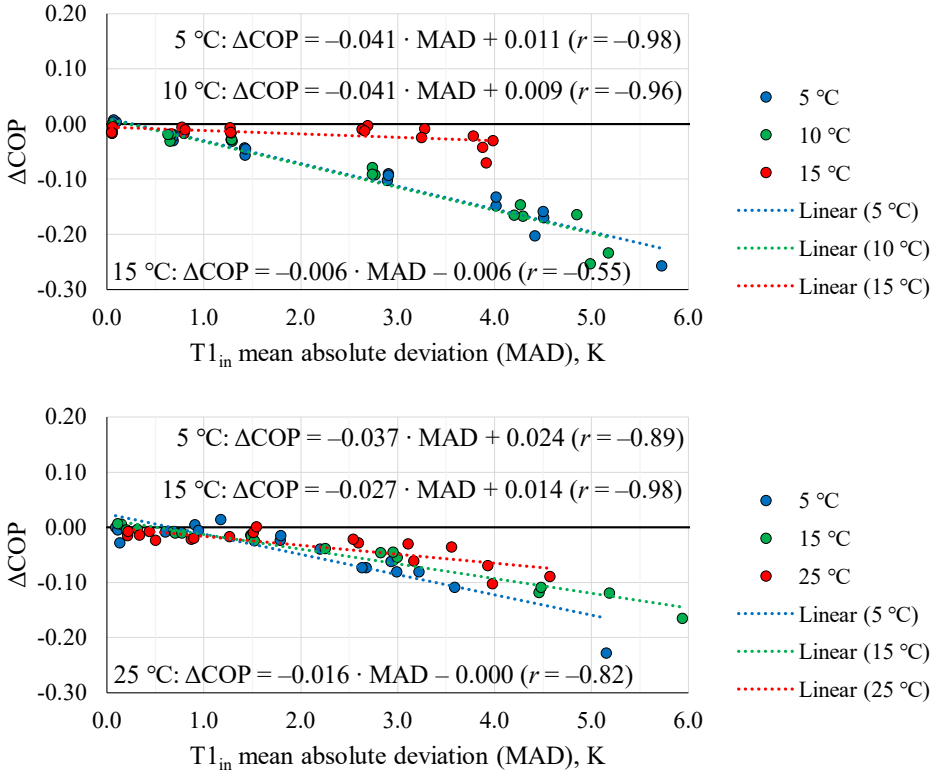

Fig. 4.16. Relationship between $T1_{in}$ MAD measured over 40-minute intervals and the difference between expected COP at the same mean temperature without fluctuations and calculated based on measured data. a) $T2_{in}$ = 30 °C; b) $T2_{in}$ = 55 °C.

For cases with $T2_{in}$ = 30 °C and $T2_{in}$ = 55 °C, there are statistically significant correlations ($p < 0.05$) between the mean absolute deviation (MAD) of $T1_{in}$ and the difference between the calculated and expected COP at the same mean temperature without fluctuations. The correlation coefficients (r) show strong relationships between MAD and ΔCOP at lower temperatures (5 °C and 10 °C for $T2_{in}$ = 30 °C and 5 °C and 15 °C for $T2_{in}$ = 55 °C). However, as the source temperature rises above the breakpoint temperature (Fig. 4.9 and Table 4.1), the correlation becomes weaker. The heat pump COP decreases by 0.027 to 0.041 for each 1 K increase in source temperature MAD, but at source temperatures above breakpoint temperature, fluctuations have low impact on COP.

To evaluate the impact of temperature fluctuations on COP, the uncertainty in COP under stable temperature conditions within a 99 % confidence interval were calculated. Since COP uncertainty depends on both regression coefficients (a and b, see Table 4.1), and their uncertainties are assumed to be independent, uncertainty propagation for a linear equation was applied to determine the COP uncertainty (σ_{COP}) for specific $T2_{in}$ and $T1_{in}$ values and results are presented in Table 4.5. This defines a range within which the true COP value is expected to lie, meaning the exact COP is not precisely known.

A linear regression model (Fig. 4.16) was used to describe the relationship between $T1_{in}$ MAD and ΔCOP. The interception values are very close to zero, which is logical, since with MAD equal to 0, meaning there are no fluctuations, the ΔCOP also needs to be 0, so for further analysis only the slope value of regression model is used. The uncertainty in the slope, as given by its 99 % confidence interval, was calculated and presented in Table 4.5.

To determine whether temperature fluctuations significantly impact COP value, ΔCOP must exceed the uncertainty of COP under stable conditions. The critical value of $T1_{in}$ MAD at which this occurs was calculated (Table 4.5). Because of uncertainties, it is impossible to determine the precise critical temperature MAD, so the interval in which it lies was provided.

Table 4.5

Heat pump COP and uncertainty (σ_{COP}) at stable temperature conditions, COP decrease slope with 99 % confidence interval and critical $T1_{in}$ MAD when ΔCOP exceeds COP uncertainty.

$T2_{in}$	$T1_{in}$	Based on Table 4.1		ΔCOP slope (Fig. 4.16)	$T1_{in}$ $MAD_{critical}$ when ΔCOP < σ_{COP}
		$COP = a \cdot T1_{in} + b$	σ_{COP}		
30 °C	5 °C	3.992	± 0.031	–0.041 ± 0.006	[0.66–0.89] K
30 °C	10 °C	4.362	± 0.026	–0.041 ± 0.008	[0.53–0.79] K
30 °C	15 °C	4.477	± 0.028	–0.006 ± 0.007	[2.15–28.0] K
55 °C	5 °C	2.529	± 0.015	–0.037 ± 0.013	[0.30–0.63] K
55 °C	15 °C	3.009	± 0.021	–0.027 ± 0.004	[0.68–0.91] K
55 °C	25 °C	3.343	± 0.102	–0.016 ± 0.008	[4.25–12.8] K

In summary, as source temperature $T1_{in}$ increases, the critical $T1_{in}$ MAD also increases, making it more difficult to distinguish whether ΔCOP is affected by temperature fluctuations or by COP measurement uncertainties. Overall, the results indicate that when the source temperature is low or near the breakpoint temperature (Table 4.1), temperature fluctuations influence ΔCOP if MAD exceeds 0.9 K. However, if MAD is below 0.9 K, this influence cannot be confirmed. For source temperatures above the breakpoint, it is not statistically determined that there is influence of MAD to ΔCOP.

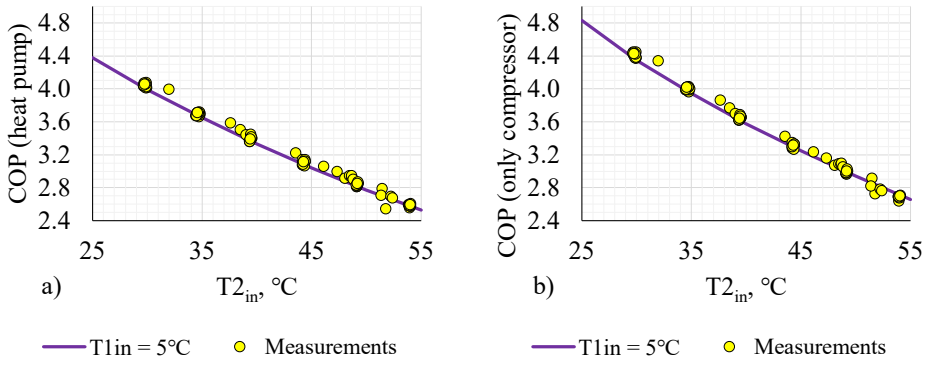

Fig. 4.17. COP dependence on $T2_{in}$ mean temperature. Dots – COP at various temperature fluctuations over a 40-minute interval; line – COP under stable temperature conditions. a) COP based on eq.(4.1); b) COP based on eq.(4.3).

By analyzing Fig. 4.17, where the results of measurements with constant source temperature $T1_{in}$ and fluctuated sink temperature $T2_{in}$ are presented, it can be seen that dots are close to the line, meaning that there is no noticeable difference between cases with and without sink temperature fluctuations. The detailed analysis (Fig. 4.18) shows that there are statistically significant ($p < 0.05$) moderate and strong correlations between the mean absolute deviation (MAD) of $T2_{in}$ and the difference between the calculated and expected COP at the same mean temperature without fluctuations for cases with $T2_{in}$ = 35 °C / 40 °C / 45 °C / 50 °C and no statistically significant correlation for cases with $T2_{in}$ = 30 °C / 55 °C.

Overall, the influence of sink temperature MAD on ΔCOP is weaker than that of source temperature MAD (Fig. 4.16). Moreover, the effect is opposite, with COP increasing by 0.009 to 0.016 for each 1 K increase in $T2_{in}$ MAD. However, since this slope is relatively small, it is difficult to determine whether this trend represents a real effect of temperature fluctuations or is simply due to COP measurement uncertainty.

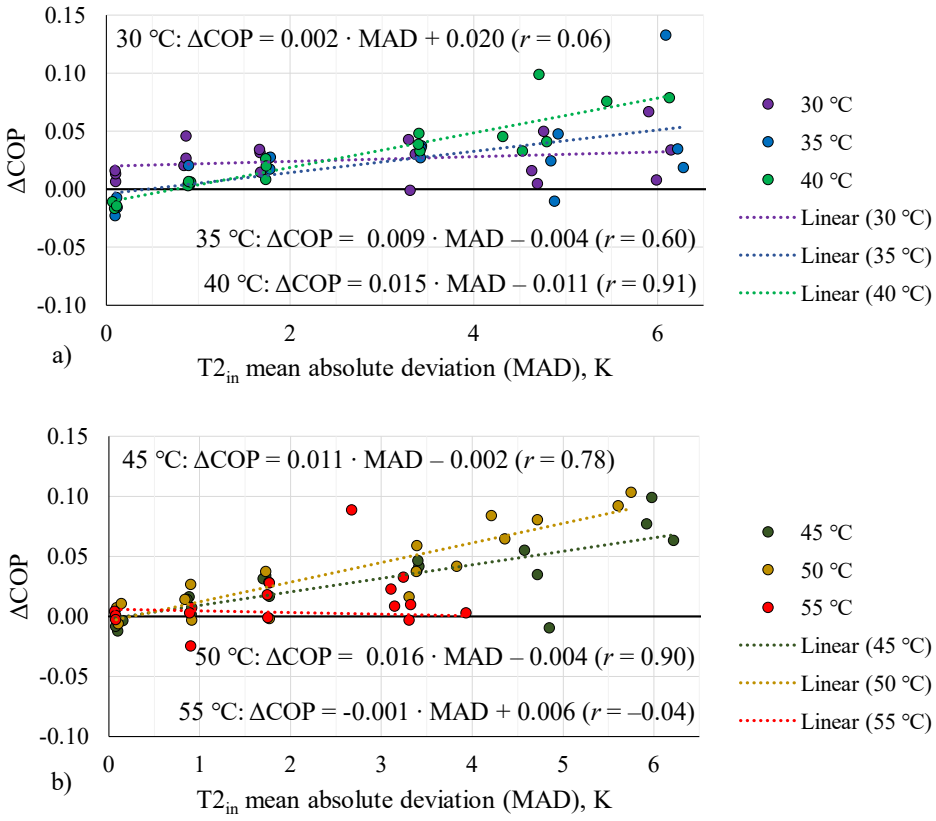

Fig. 4.18. Relationship between $T2_{in}$ MAD measured over 40-minute intervals and the difference between expected COP at the same temperature without fluctuations and calculated based on measured data. $T1_{in}$ = 5 °C. a) $T2_{in}$ = 30 / 35 /40 °C; b) $T2_{in}$ = 45 /50 /55 °C.

4.1.3. TRNSYS simulations of heat pump COP

Methods

The simple TRNSYS model was developed (Fig. 4.19) to simulate temperature fluctuations and compare results with the measured values.

Simulation time: 40 minutes with 0.1 second simulation time step.

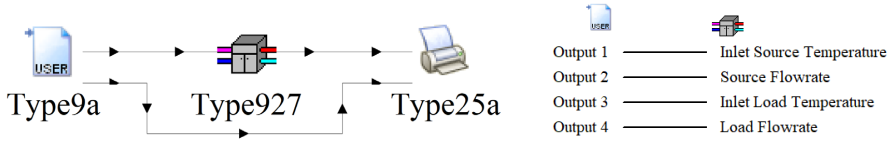

Fig. 4.19. Left: TRNSYS model; right: connection between Type9a and Type927.

Type927 – component models a single-stage brine-to-water heat pump. The performance dataset was stored in a text document prepared based on Fig. 4.11*a* and Table 4.1 data, so only the performance data gained under stable conditions were used.

Type9a – component serves the purpose of reading data at regular time intervals from a data file. The input values from measurements ($T1_{in}$, $T2_{in}$, Flow1, Flow2) were used with 5 second intervals, values were linearly interpolated. In total 216 cases were simulated by using all data generated in section 4.1.1.

Type25a – component was used to output selected system variables at specified intervals of time. The info for heat pump heat transfer to load and heat pump power, as well as $T1_{in}$ and $T2_{in}$ temperatures for control and compare with measured values was saved. The COP was calculated by dividing the sum of heating load to the sum of heat pump power.

Results

Results represent the comparison between measurements on the test facility, presented in Section 4.1.2 and TNRSYS 18 simulated data.

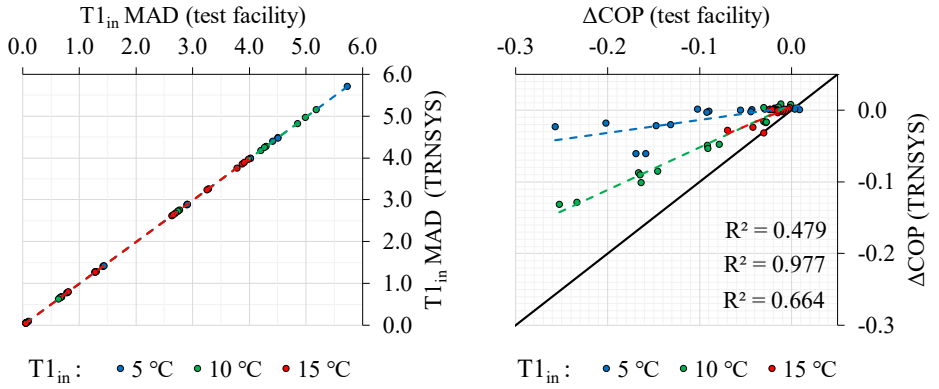

Fig. 4.20. Left: $T1_{in}$ MAD measured at test facility and simulated in TRNSYS software. Right: Difference between COP at stable and fluctuating conditions in real measurements at test facility and TRNSYS computer simulations. $T2_{in}$ = constant = 30 °C.

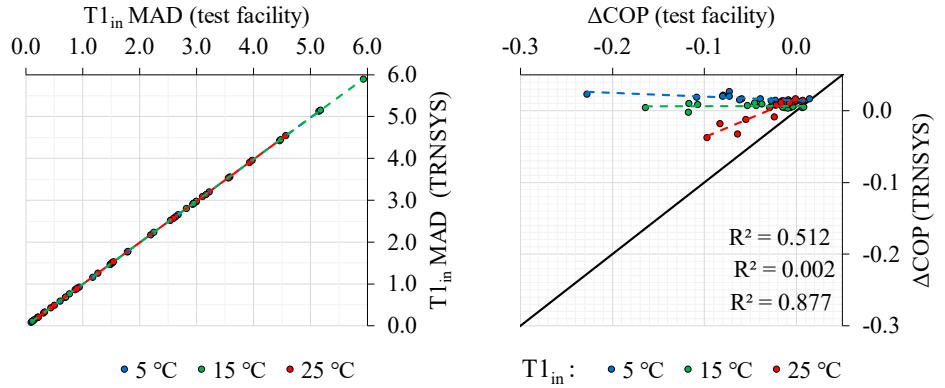

Fig. 4.21. Left: $T1_{in}$ MAD measured at test facility and simulated in TRNSYS software. Right: Difference between COP at stable and fluctuating conditions in real measurements at test facility and TRNSYS computer simulations. $T2_{in}$ = constant = 55 °C.

Results show (Fig. 4.20 and Fig. 4.21) that fluctuations occur not only in real measurement on the test facility but also in the computer model, which is based on heat pump measured data under stable temperature conditions. This means that fluctuations can be simulated on a computer, reducing the need for physical experiments and saving time and electricity.

The model shows that the difference (ΔCOP) between stable and fluctuating conditions increase with increasing the $T1_{in}$ MAD similarly as it was observed in experimental measurements. However, ΔCOP is greater in real measurements than in simulations. In real tests, ΔCOP reached up to –0.26, whereas in simulations, it was only up to –0.13. This discrepancy may be due to system inertia, which is not accounted for in the simulation, leading to a lower impact of temperature fluctuations on ΔCOP. Another possible explanation is that ΔCOP is influenced not only by heat pump's performance curves but also by the heat pump's compressor operating principles, which were not included in the model.

It can be concluded that, while the computer model is a useful tool for simulating heat pump performance, it does not account for all factors influencing COP under fluctuating temperature conditions. Therefore, experimental data remains more reliable for accurately assessing performance in real-world scenarios.

4.2. Measurements of solar-assisted heat pump

4.2.1. Impact of PVT collectors on the heat pump COP

In this section the situation showed on Fig. 4.2 when PVT collectors are connected to the heat pump source side is simulated and tested. The sink side temperature $T2_{in}$ = 50 °C. The profile (Fig. 4.22) of source side temperature $T1_{in}$ was taken from (Francisco et al., 2024) measurements from three PVT collectors under cloudy conditions during the summer. The calculations were performed in the developed TRNSYS model and experimental measurements were performed on the heat pump test facility. Results presented in Table 4.8.

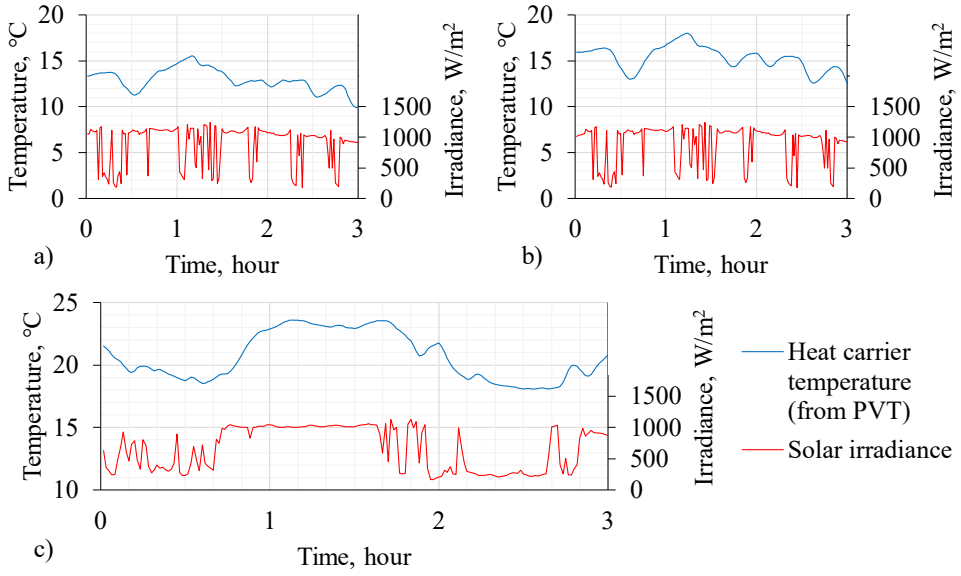

Fig. 4.22. Measurements from a) S&T; b) BC-PP; c) BC-AL-20 PVT collectors (Francisco et al., 2024), data taken from KTH Royal Institute of Technology, time step: 1 minute.

Table 4.6

Measured and simulated results of heat pump COP under stable and fluctuating conditions based on three heat source temperature profiles presented in Fig. 4.22.

	A		B			D	C			D
	Temperature, °C		Temperature, °C		COP_{HP}	COP_{HP}	Temperature, °C		COP_{HP}	COP_{HP}
	mean	MAD	mean	MAD			mean	MAD		
a)	12.95	0.97	12.96	0.96	3.19	3.20	13.36	0.89	3.23	3.22
	–	–	12.96	0.00	3.19	3.20	13.32	0.10	3.22	3.21
b)	15.31	1.09	15.32	1.08	3.31	3.32	15.63	1.01	3.35	3.34
	–	–	15.31	0.00	3.31	3.32	15.33	0.42	3.34	3.32
c)	20.63	1.71	20.63	1.71	3.51	3.51	20.16	2.21	3.49	3.50
	–	–	20.63	0.00	3.52	3.51	20.28	0.50	3.52	3.51

A – measured temperature profile (based on Fig. 4.22);
B – TRNSYS software (Fig. 4.19) simulation results;
C – heat pump test facility (Fig. 4.5) experimental results;
D – heat pump COP calculated based on Table 4.1 for given mean temperature (MAD = 0).

Results (Table 4.6) show that based on TRNSYS simulation results, the COP at stable and fluctuating conditions are the same for *a* and *b* profiles but for *c* profile, which has higher MAD, the ΔCOP = –0.01. Based on experimental measurements, the ΔCOP for *a* and *b* profiles are within measurement uncertainty, but for *c* profile the ΔCOP = –0.03.

4.2.2. Impact of solar thermal collectors on the heat pump COP

This study was done using laboratory measurements from the heat pump experimental test facility (described previously) and input data from the solar collector test facility (described in Chapter 1). The research evaluated the effectiveness of combining a heat pump (HP), solar thermal (ST) collectors and a district heating (DH) system under various operating conditions. In this setup, the ST collectors were connected to the HP's source side, enabling energy to be either utilized by the HP or stored within the low-temperature DH system (Fig. 4.23).

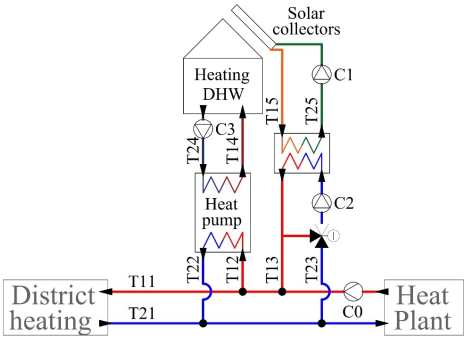

Fig. 4.23. Principal drawing of the studied system.

Methods

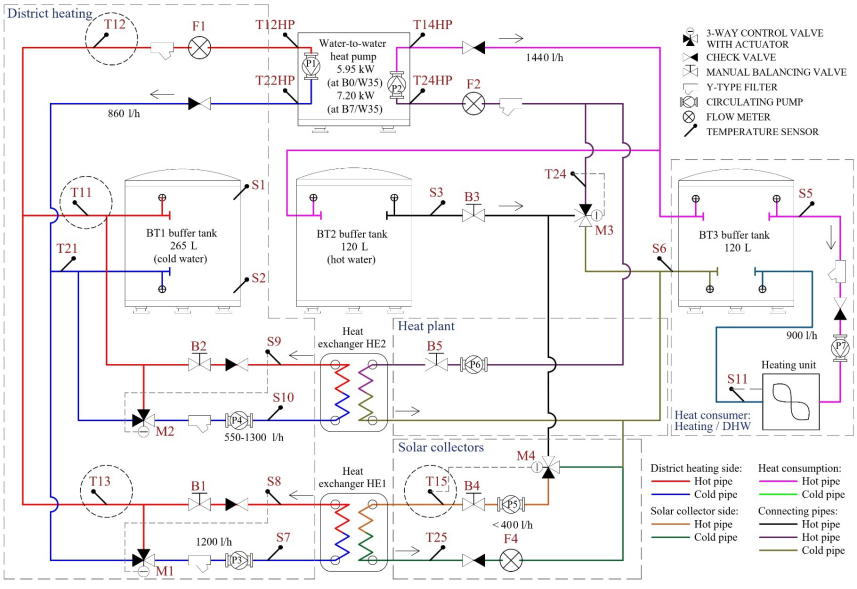

Fig. 4.24. Principal drawing of the studied system on the test facility.

HE2 functions as a “heat plant” (see Fig. 4.24), maintaining a constant temperature of 15.0 °C or 20.0 °C (two cases were simulated), with the M2 valve controlled by sensor S9. The electric heater in BT1 tank maintain the temperature of 15 °C ± 0.2 °C or 20 °C ± 0.2 °C in the middle of BT1 buffer tank. This setup ensures energy balance and stable temperatures on the “district heating side”. HE1 serves as a “heat exchanger for the solar collector”. The P5 pump, along with the M4 valve, simulates the flow and temperature from the solar thermal collectors based on five different profiles (Fig. 4.25). The M1 valve, controlled by sensor S8, maintains a temperature of 15 °C or 20.0 °C, while the M3 valve, controlled by T24, maintains a temperature of 50.0 °C.Inputs (see Fig. 4.25): The temperature T15 setpoint and the circulation pump P5 speed (controlled based on a PWM signal). The time interval for these inputs is set at 30 seconds. Measurements: 30-minutes cycle with a time step of 5 seconds.

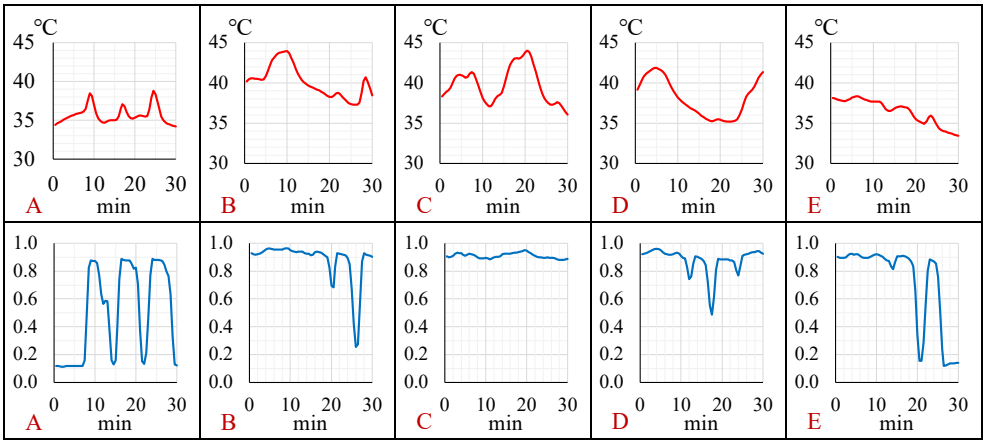

Fig. 4.25. Input data (setpoints) for solar collector simulation.
Based on measurements at solar collector test facility (described in Chapter 1).
Above: temperature T15. Below: pump P5 speed.

Table 4.7

Mean and mean absolute deviation (MAD) of input values from Fig. 4.25.

Case	T15 temperature		P5 circulation pump speed	
	Mean	MAD	Mean	MAD
A	35.7 °C	0.8 K	51 %	31 %
B	40.1 °C	1.6 K	88 %	9 %
C	39.8 °C	1.9 K	91 %	2 %
D	38.1 °C	2.1 K	88 %	6 %
E	36.5 °C	1.3 K	72 %	25 %

Each 30-minute cycle of measurements started when the heat pump was working on full load and heat carrier temperatures on both sides were stable. To increase reliability, each cycle with identical inputs was performed 3 times independently. There were at least 20-minute pauses between cycles to ensure that heat carrier temperature in the beginning of new cycle is stable and identical for all cycles.

Results

First, three 30-minute measurement cycles at constant "district heating" temperatures of 15 °C and 20 °C were measured without energy from "solar collectors". Results in Table 4.8.

Table 4.8

Heat pump COP and heat carrier temperature mean
and mean absolute deviation (MAD) values in two cases.

Case	COP_{HP}	$T1_{in}$	$T1_{in}$ MAD	$T2_{in}$	$T2_{in}$ MAD
15 °C	3.37	15.49 °C	0.16 K	49.14 °C	0.01 K
20 °C	3.53	19.03 °C	0.07 K	49.19 °C	0.06 K

According to Fig. 4.9, the heat pump COP in Case with 15 °C should be 3.32 and with 20 °C it should be 3.50. The difference for both cases is 0.03 which might be explained by different experimental setup configuration, which might influence the circulation pump electricity consumption which resulted in COP changes. For further analysis it is assumed that the heat pump COP at stable operation conditions is COP calculated based on Fig. 4.9 adding 0.03.

Next, simulations of Fig. 4.25 patterns were performed for 15 °C and 20 °C cases.

Heating energy received from "solar thermal side" was:

- Case A: 71 % – 90 %
- Case B: 108 % – 116 %
- Case C: 105 % – 110 %
- Case D: 89 % – 95 %
- Case E: 76 % – 78 %

As observed in Fig. 4.26, source temperatures for both cases (15 °C and 20 °C) are almost identical, except the beginning of measuring cycle. The temperature reaching the heat pump at the beginning of the measurement is low (in 15 °C case) and high (in 20 °C case) during the initial opening of the M1 valve. To minimize the impact of these initial conditions, only the 25-minute interval from 5 to 30 minutes was considered in the subsequent analysis. The temperature profiles are closely resembled to T15 temperature profiles (Fig. 4.25).

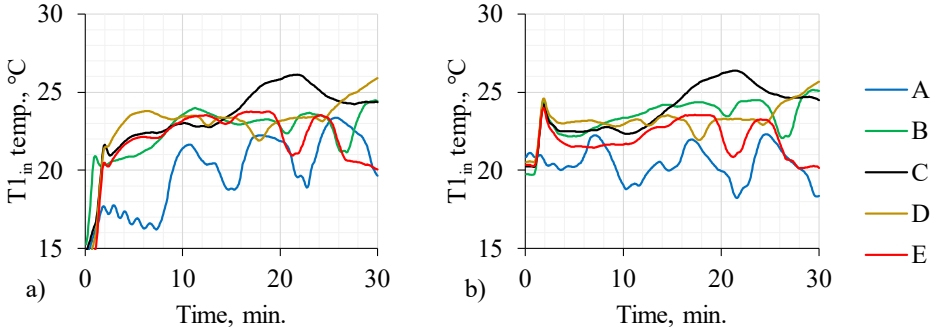

Fig. 4.26. Heat carrier temperatures entering heat pump in a) Case 15 °C; b) Case 20 °C.

As there are almost no differences between cases 15 °C and 20 °C cases, measurement results are combined in the further analysis. According to Fig. 4.27 – Fig. 4.30, measurements from the same pattern (A – E) are grouped together, indicating the stability of the experiment.

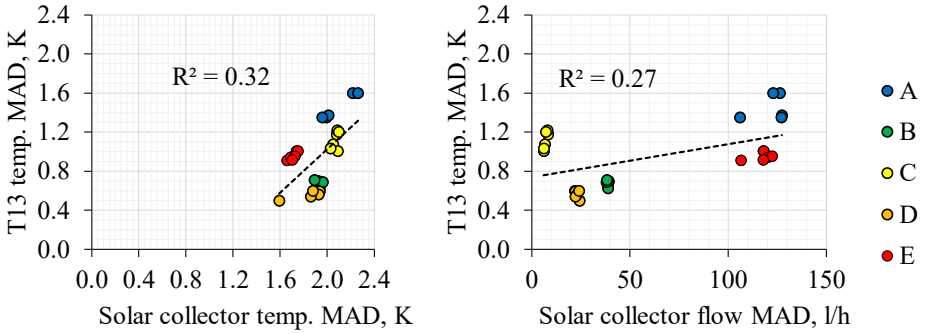

Fig. 4.27. T13 temperature MAD dependence on solar collector temperature MAD and flow MAD for different profiles (Fig. 4.25).

As shown on Fig. 4.27, there is a moderate positive correlation (r = 0.57) between T15 and T13 temperature MAD, but in general T13 temperature MAD are lower than T15 temperature MAD, statistically significant ($p < 0.05$) regression coefficient = 1.11. There is also a statistically significant ($p < 0.05$) moderate positive correlation (r = 0.52) between solar collector flow MAD (P5 pump flow) and T13 temperature MAD. T13 MAD is lower than T15 MAD by 0.60 K – 1.37 K, indicating that the heat exchanger with control valve reduces temperature fluctuations from solar collectors. Additional measurement with different M1 valve control speeds (Fig. 1.11) indicated that M1 valve control speed has no statistically significant effect on T13 temperature and its fluctuations but have minor effect on received amount of solar energy – decreasing the speed of valve decrease the amount of solar energy.

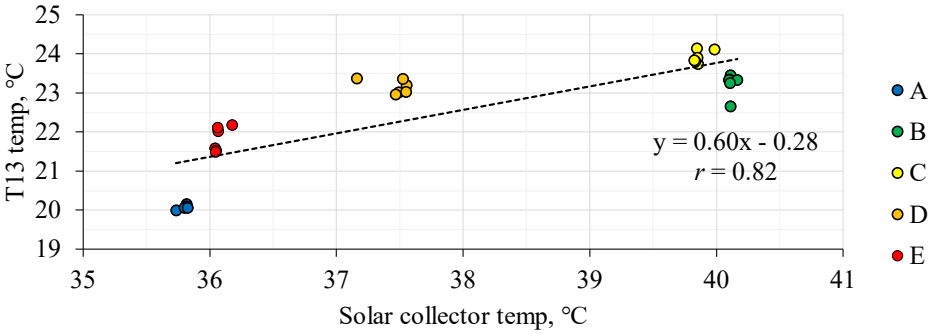

Fig. 4.28. T13 temperature dependence on solar collector temperature for different profiles (Fig. 4.25).

It was observed (Fig. 4.27 and Fig. 4.28) that the heat carrier temperature (T13) after the heat exchanger showed not only smaller fluctuations but also significantly lower absolute values (by 13.8 K – 17.5 K) compared to the temperature leaving the solar collectors. This

indicates that the heat exchanger with a three-way control valve helps reduce temperature fluctuations and supports more stable operating conditions. However, since solar collectors can heat up very quickly, the temperature on the "district heating side" can still rise. This must be taken into account, as the heat pump used in the experiment has a source temperature limit of 30 °C. When the source temperature exceeded this limit for more than 5 minutes, an error code was triggered – highlighting a clear upper boundary for acceptable heat carrier temperature.

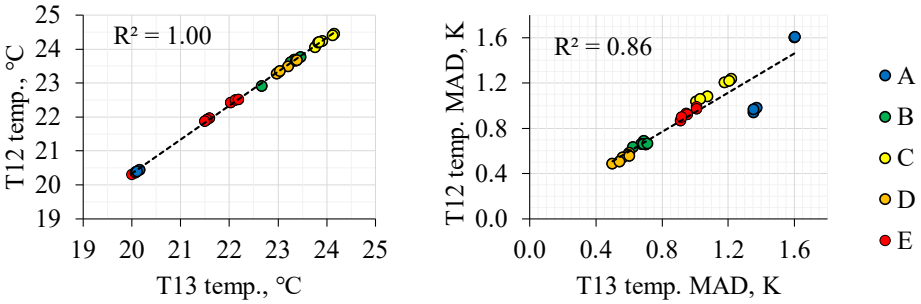

Fig. 4.29. T12 temperature mean values and temperature MAD dependence on T13 temperature mean values and MAD.

Fig. 4.29 shows a clear relationship between the temperature entering the heat pump (T12) and the temperature leaving the solar collector heat exchanger (T13). Fig. 4.30 illustrates the relationship between ΔCOP – the difference between COP under different profiles (Fig. 4.25) and under stable conditions – and the mean absolute deviation (MAD) of the heat pump inlet temperature (T12). Since T12 depends on T13, and T13 is influenced by the solar collector temperature, it can be concluded that ΔCOP is influenced by solar energy variation.

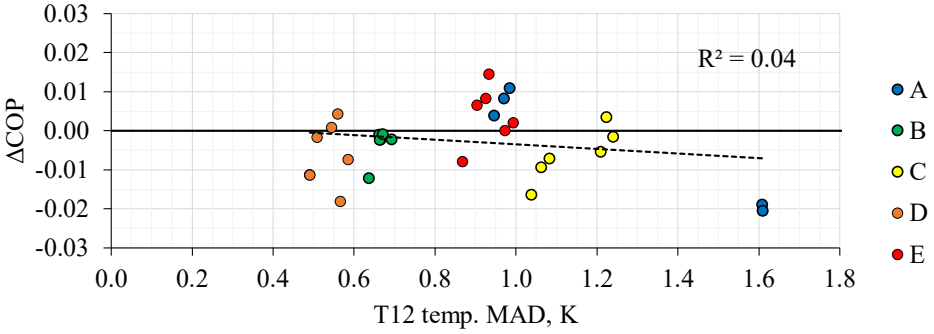

Fig. 4.30. Heat pump COP difference between COP for different profiles (Fig. 4.25) and COP under stable conditions dependence on heat pump entering temperature MAD.

In this experimental setup, $T2_{in}$ was fixed at 50 °C, meaning the breakpoint in the COP curve occurs at 18.0 °C (Table 4.1). However, the average source temperature entering the heat pump (T12) was above 20 °C (Fig. 4.29), implying that the impact of fluctuations on COP should be minimal. This was confirmed in Fig. 4.30, where no statistically significant correlation ($p > 0.05$) was found.

4.3. Discussion and conclusions

It is important to discuss the boundary conditions and potential practical implementation under which the findings from this research might be useful. Existing research on integrating heat pumps into DH systems primarily focuses on computer simulations, economic evaluations and system optimizations of various large-scale scenarios, sometimes using real system data, sometimes relying on assumptions and generalizations. There are limited real-world, short-step measurements of heat carrier temperature fluctuations and their impact on system performance.

Heat pump manufacturers provide standardized tests under a limited number of controlled conditions, which differ significantly from those in low and ultra-low-temperature DH systems. High source temperatures (> 20 °C) and temperature fluctuations are not taken into account. As a result, there is very little data on how these fluctuations affect the heat pump's COP.

The optimal heat temperature in DH depends on many factors, including network size and consumption profiles, so a universal solution seems to be impossible. However, this study identifies a range of acceptable temperature fluctuations in the grid that are not tied to any specific location, climate or system configuration. These findings can therefore be applied universally to guide better system design and control strategies.

The experimental process

This research tested a 6-kW brine-to-water heat pump with heat source temperature from 0 °C to 28 °C and heat sink inlet temperature 25 / 30 / 35 / 40 / 45 / 50 / 55 °C under full load conditions with potential application with PVT collectors connected to the source side or as a booster heat pump in ultra-low temperature district heating system.

To test the system, an experimental protocol was developed. As stated in previous sections, the measured mean absolute deviation (MAD) of heat carrier temperature from solar thermal collectors ranged from 0.47 K to 2.20 K at different temperature levels, control regimes, and weather conditions and the typical fluctuation period was measured to be from 8 to 15 minutes.

To measure the heat pump's COP at stable temperatures, a 25-minute interval was chosen, from which the initial 5 minutes of each measurement period were excluded from analysis to reduce possible errors during flow temperature adjustments. This shows good practice, since it allow for measuring a lot of different temperature combinations within a small time period, but provides good replication of measurements. Each measurement cycle was performed 3 times, and measurement uncertainty was calculated, which, for almost all measurements, were below 1 % (higher uncertainty was at high source temperatures and high sink temperatures).

For COP measurements under fluctuating conditions, a 4-minute interval of temperature setpoint changes was chosen, meaning that the fluctuation period was 8 minutes. One measurement cycle was 40 minutes. Six temperature ranges were used and arranged in non-regular order (±8 K, ±6 K, ±1 K, ±4 K, ±0 K, ±2 K) to avoid bias from a consistent increase or decrease in temperature fluctuations and ensuring that any observed effects on the heat pump's COP could not be attributed to a gradual trend in temperature changes. The MAD of the resulting fluctuations were in the range from 0.05 K (no fluctuations) to 6.00 K. To achieve this, a bot-driven setpoint control computer program was written, which changed the setpoint every 4 minutes and allowed to perform the experiment without interruption during the day and night.

Main findings

The results show that the heat pump's (including both circulation pumps) COP is 3.9 % to 9.9 % lower than the COP of the heat pump's compressor (only). This difference is strongly influenced by the customer-side temperature change rather than by the source-side temperature.

Regression analysis showed that the relationship between source-side inlet temperature and heat pump COP can be described as a piecewise linear function: a 1 K change in source temperature has a greater impact on COP at lower temperatures than at higher ones. The breakpoint temperature depends on the customer-side temperature (Table 4.1). For source temperatures below the breakpoint, a 1 K increase in the mean absolute deviation (MAD) of source temperature fluctuations results in a COP decrease of 0.027–0.041 (approximately 1 %). Above the breakpoint, the impact of fluctuations is minimal. Sink-side temperature fluctuations had a minimal influence on COP and remained within the measurement uncertainty.

When the MAD of temperature fluctuations on a source-side stays below 0.9 °C, its impact on COP is within the measurement uncertainty. Taking into account that low-temperature solar collector experiments showed MAD values below 1 K, it can be concluded that solar energy variability under such conditions does not significantly affect heat pump performance.

TRNSYS simulations were performed using COP curves measured under stable conditions and temperature data from fluctuating conditions as an input. While the simulations also indicated a drop in COP with increased temperature fluctuation, the influence was weaker. This suggests that computer models do not fully capture all real-world impact on COP under dynamic conditions. Therefore, experimental data is more reliable for performance assessments.

Additional measurements using temperature and flow data from both solar thermal (ST) and photovoltaic-thermal (PVT) test facilities confirmed that when MAD values remain below or close to the critical MAD value (Table 4.5), the observed ΔCOP falls within measurement uncertainty. When MAD exceeds this threshold, a noticeable COP decrease occurs.

Measured data from PVT and ST collectors showed that the heat carrier temperature typically stays near or above the COP curve breakpoint temperature, and temperature MAD remains low. Under these conditions, no significant impact on heat pump COP was observed. However, in the case of widespread installation across a DH grid or poorly configured control algorithms, the COP of booster heat pumps potentially could be negatively affected.

Limitations

This research focused on a single brine-to-water heat pump using R407C refrigerant, with operation limited to source temperatures up to 30 °C. While this approach provided consistency and control, different heat pump models, refrigerants or compressor types may show varied performance, offering a path for future comparative studies. Load fluctuations were not part of this study but will be explored in future work using the experimental methods developed here. Additionally, variations in pressure difference and fluctuations in DH networks could affect circulation pump energy use and system COP because of higher electricity consumption with the pressure increase. To move closer to real-world operation, further testing under variable customer-side temperatures, flow profiles and partial load conditions is recommended using the developed methodology. These next steps will support practical, large-scale implementation.

CONCLUSIONS AND FUTURE STUDIES

The aim of this study was achieved by comparing the performance of different system configurations and operating conditions, showing the significant potential of the development of photovoltaic-thermal systems combined with brine-to-water heat pumps in low-temperature district heating networks. The results not only demonstrate the benefits of this integrated approach but also identify a clear pathway for future research and practical implementation.

The developed research methodology combines experimental measurements, simulations and statistical analysis, offering a flexible framework for future studies focused on evaluating heat carrier temperature fluctuations, calculating system thermal output and testing heat pump performance under varying conditions. This methodology serves as a foundation for further research, including the testing of different heat pump models, exploring additional system layouts and implementing alternative control algorithms.

The main conclusions:

1. There is significant potential to expand the use of solar thermal (ST) collectors in Latvia. The key challenges are the seasonal mismatch, with around 75 % of useful ST energy absorbed between April and September, and low performance in traditional applications. This study recommends integrating ST collectors into low- or ultra-low-temperature district heating (DH) networks to utilize more solar energy and reduce overheating risk by utilizing the storage capacity of the network and enable energy sharing between buildings.
2. Heat carrier temperature fluctuations in ST systems are primarily influenced by solar irradiance variations, chosen operating temperature level and control strategy. These fluctuations can be effectively characterized by using the mean absolute deviation (MAD) parameter. Measurements showed that MAD values ranged from 0.47 K to 0.96 K at low temperatures (50/30 °C), 1.03 K to 1.61 K at medium temperatures (65/42 °C), and 1.02 K to 2.20 K at high temperatures (80/50 °C).
3. Large-scale solar collector plants have been successfully implemented in countries like Denmark, Sweden, Germany and Latvia. However, household-scale integration, where consumers also act as prosumers, remains rare. The limited availability of case studies and operational data from real-world applications slows down the development and practical implementation of the concept of decentralized solar integration in DH networks.
4. TRNSYS 18 simulations confirm that small-scale DH systems can effectively act as thermal storage for decentralized ST collectors, reducing reliance on local electric boilers during the non-heating period – a practice commonly observed in small towns in Latvia. Compared to “local” solutions, the “district” configuration showed 13–22 % higher solar energy utilization due to lower operating temperatures and larger storage volume.
5. The study confirms the energy viability of combining solar energy with heat pumps in DH systems. In particular, photovoltaic-thermal (PVT) collectors paired with brine-to-water heat pumps (BWHP) show strong potential to maximize solar heat output from limited areas. This combination enables high solar heat utilization, efficient use of space and improved overall system performance in low-temperature DH networks.

6. TRNSYS 18 simulations showed that PVT + BWHP systems produced the highest annual heat output: 1040–1361 kWh/m² in a low-temperature DH system. This is 1.8 to 4.6 times more than the calculated output from solar thermal collectors directly connected to the DH grid and up to 7.6 times more than the measured output of a traditional solution with local storage in a single-family house. However, to avoid overproduction and efficiency losses, seasonal heat storage or capacity limits must be considered when scaling up the system.
7. The relationship between source-side inlet temperature and BWHP COP is a piecewise linear function. Below the breakpoint (BP), a 1 K increase in MAD reduces COP by up to 1 %; above the BP, the effect is minimal, indicating higher sensitivity to temperature fluctuations at lower source temperatures. When MAD is below 0.9 K, this impact falls within the 99 % confidence interval and cannot be statistically confirmed. Fluctuations on the sink side had minimal influence and remained within the measurement uncertainty.
8. Temperature and flow fluctuations from ST and PVT collectors had little effect on the heat pump's COP, as measured MAD values stayed near or below critical thresholds. However, large-scale implementation or poor control strategies could cause higher variability and reduce heat pump efficiency, highlighting the importance of monitoring and system design.

The hypothesis was confirmed through experimental measurements, showing that heat source temperature fluctuations caused by solar energy variations can reduce the coefficient of performance of a brine-to-water heat pump when the source temperature is low (8–21 °C, depending on sink temperature), as is typical in ultra-low-temperature district heating systems. Under low-temperature DH conditions (≥ 20 °C), temperature fluctuations had no significant impact on COP. It should be noted that these tests were performed on a specific heat pump model, so results may vary with other models. However, the general testing principles and the developed methodology are applicable for evaluating other heat pumps in future studies.

The results of this study have been published in scientific journals and presented at international conferences, with at least two more journal articles planned based on the findings.

These results can aid decision-making in district heating system development, optimizing solar energy integration and heat pump utilization to improve overall efficiency. However, a detailed economic analysis considering real prices and energy tariffs is necessary to determine payback periods, which remains a future research direction. Additionally, the low- and ultra-low-temperature DH concept offers the potential for district cooling development using heat pumps, making this an important area for future research and system optimization.

ACKNOWLEDGEMENTS

This work has been supported by:

- Riga Technical University's Doctoral Grant programme;
- the European Social Fund within the Project No. 8.2.2.0/20/I/008, “Strengthening of PhD students and academic personnel of Riga Technical University and BA School of Business and Finance in the strategic fields of specialization”, of the Specific Objective 8.2.2 “To Strengthen Academic Staff of Higher Education Institutions in Strategic Specialization Areas” of the Operational Programme “Growth and Employment”;
- the EU Recovery and Resilience Facility within the Project No. 5.2.1.1.i.0/2/24/I/CFLA/003 “Implementation of consolidation and management changes at Riga Technical University, Liepāja University, Rēzekne Academy of Technology, Latvian Maritime Academy and Liepāja Maritime College for the progress towards excellence in higher education, science and innovation” academic career doctoral grant (ID 1071).

DECLARATION OF GENERATIVE AI

During the preparation of this work, the OpenAI “ChatGPT” was used in order to improve readability and language. After using this tool, the content was reviewed and edited as needed.

REFERENCES

Angelidis, O., Ioannou, A., Friedrich, D., Thomson, A., & Falcone, G. (2023). District heating and cooling networks with decentralised energy substations: Opportunities and barriers for holistic energy system decarbonisation. In *Energy* (Vol. 269). https://doi.org/10.1016/j.energy.2023.126740

Antoniadis, C. N., & Martinopoulos, G. (2019). Optimization of a building integrated solar thermal system with seasonal storage using TRNSYS. *Renewable Energy*, *137*, 56–66. https://doi.org/10.1016/j.renene.2018.03.074

Arabzadeh, V., Pilpola, S., & Lund, P. D. (2019). Coupling variable renewable electricity production to the heating sector through curtailment and power-to-heat strategies for accelerated emission reduction. *Future Cities and Environment*, *5*(1). https://doi.org/10.5334/FCE.58

Averfalk, H., Benakopoulos, T., Best, I., Dammel, F., Engel, C., Geyer, R., Gudmundsson, O., Lygnerud, K., Nord, N., Oltmanns, J., Ponweiser, K., Schmidt, D., Schrammel, H., Østergaard, D. S., Svendsen, S., Tunzi, M., & Werner, S. (2021). *Low-temperature district heating implementation guidebook. IEA DHC Report* (Issue September).

Barco-Burgos, J., Bruno, J. C., Eicker, U., Saldaña-Robles, A. L., & Alcántar-Camarena, V. (2022). Review on the integration of high-temperature heat pumps in district heating and cooling networks. *Energy*, *239*. https://doi.org/10.1016/j.energy.2021.122378

Bertelsen, N. ;, Mathiesen, B. V, Djørup, S. R., Schneider, N. C. A., Paardekooper, S. ;, Sánchez García, L. ;, Thellufsen, J. Z., Kapetanakis, J. ;, Angelino, L. ;, & Kiruja, J. (2021). *Integrating low-temperature renewables in district energy systems - Guidelines for policy makers*.

Bogdanovičs, R. (2021). *Decentralizēto saules kolektoru integrēšana pilsētas centralizētajā siltumapgādes sistēmā* [Master's thesis]. Riga Technical University.

Bogdanovičs, R., Borodinecs, A., Zajacs, A., & Šteinerte, K. (2018). Review of Heat Pumps Application Potential in Cold Climate. In *Advances in Intelligent Systems and Computing* (Vol. 692). https://doi.org/10.1007/978-3-319-70987-1_58

Bogdanovics, R., Zeiza-Seleznova, A., Zemitis, J., & Zajacs, A. (2022). TRNSYS model with 3-way valve for heat carrier temperature control of solar thermal collectors integrated into district heating system. *BuildSim Nordic 2022 Technical Papers*.

Bogdanovics, R., Zemitis, J., Zajacs, A., & Borodinecs, A. (2024). Small-scale district heating system as heat storage for decentralized solar thermal collectors during non-heating period. *Energy*, *298*. https://doi.org/10.1016/j.energy.2024.131260

Brand, L., Calvén, A., Englund, J., Landersjö, H., & Lauenburg, P. (2014). Smart district heating networks - A simulation study of prosumers' impact on technical parameters in distribution networks. *Applied Energy*, *129*, 39–48. https://doi.org/10.1016/j.apenergy.2014.04.079

Brange, L., Englund, J., & Lauenburg, P. (2016). Prosumers in district heating networks - A Swedish case study. *Applied Energy*, *164*. https://doi.org/10.1016/j.apenergy.2015.12.020

Brange, L., Lauenburg, P., Sernhed, K., & Thern, M. (2017). Bottlenecks in district heating networks and how to eliminate them – A simulation and cost study. *Energy*, *137*. https://doi.org/10.1016/j.energy.2017.04.097

Brange, L., Sernhed, K., & Thern, M. (2019). Decision-making process for addressing bottleneck problems in district heating networks. *International Journal of Sustainable Energy Planning and Management*, *20*. https://doi.org/10.5278/ijsepm.2019.20.4

Brozovsky, J., Gustavsen, A., & Gaitani, N. (2021). Zero emission neighbourhoods and positive energy districts – A state-of-the-art review. In *Sustainable Cities and Society*. https://doi.org/10.1016/j.scs.2021.103013

Buffa, S., Cozzini, M., D'Antoni, M., Baratieri, M., & Fedrizzi, R. (2019). 5th generation district heating and cooling systems: A review of existing cases in Europe. *Renewable and Sustainable Energy Reviews*, *104*, 504–522. https://doi.org/10.1016/j.rser.2018.12.059

Cabinet of Ministers. (2010). Republic of Latvia Cabinet Regulation No. 906. Regulations Regarding the Sanitary Maintenance of a Residential House. In *Latvijas Vēstnesis* (906). https://likumi.lv/ta/en/en/id/218830-regulations-regarding-the-sanitary-maintenance-of-a-residential-house.

Cabinet of Ministers Republic of Latvia. (2019). Regulations Regarding the Latvian Construction Standard LBN 002-19, Thermotechnics of Building Envelopes. In *Latvijas Vēstnesis, 135* (280).

Cabinet of Ministers Republic of Latvia. (2021). Ēku energoefektivitātes aprēķina metodes un ēku energosertifikācijas noteikumi. In *Latvijas Vēstnesis, 72* (222).

Cabinet of Ministers Republic of Latvia. (2022). *Latvia's Report to the United Nations on the Implementation of the Sustainable Development Goals*.

Cabinet of Ministers Republic of Latvia. (2024). *Aktualizētais Nacionālais enerģētikas un klimata plāns 2021.–2030. gadam* (573).

Çakir, U., Çomakli, K., Çomakli, Ö., & Karsli, S. (2013). An experimental exergetic comparison of four different heat pump systems working at same conditions: As air to air, air to water, water to water and water to air. *Energy*, *58*. https://doi.org/10.1016/j.energy.2013.06.014

Calise, F., Cappiello, F. L., Dentice d'Accadia, M., Petrakopoulou, F., & Vicidomini, M. (2022). A solar-driven 5th generation district heating and cooling network with ground-source heat pumps: a thermo-economic analysis. *Sustainable Cities and Society*. https://doi.org/10.1016/j.scs.2021.103438

Cao, Y., Dhahad, H. A., Togun, H., El-Shafay, A. S., Alamri, S., Rajhi, A. A., Anqi, A. E., & Ibrahim, B. F. (2022). Development and transient performance analysis of a decentralized grid-connected smart energy system based on hybrid solar-geothermal resources; Techno-economic evaluation. *Sustainable Cities and Society*. https://doi.org/10.1016/j.scs.2021.103425

Capone, M., Guelpa, E., Mancò, G., & Verda, V. (2021). Integration of storage and thermal demand response to unlock flexibility in district multi-energy systems. *Energy*, *237*. https://doi.org/10.1016/j.energy.2021.121601

Central Statistical Bureau of Latvia. (n.d.). *Official Statistics Portal*. Retrieved February 27, 2025, from https://stat.gov.lv/

Chen, J., Chen, K., Zhang, W., Su, J. M., Zhao, B., Hu, M., & Pei, G. (2025). Numerical study of a solar district heating system with photovoltaic-thermal collectors and pit thermal energy storage. *Energy*, *317*, 134705. https://doi.org/10.1016/j.energy.2025.134705

Chhugani, B., Pärisch, P., Helmling, S., & Giovannetti, F. (2023). *Comparison of PVT - heat pump systems with reference systems for the energy supply of a single-family house*. *3*(December 2022).

Chhugani, B., Pärisch, P., Kirchner, M., Littwin, M., Lampe, C., & Giovannetti, F. (2020). Model Validation and Performance Assessment of Unglazed Photovoltaic-Thermal Collectors with Heat Pump Systems. *EuroSun 2020 ISES Conference Proceedings*. https://doi.org/10.18086/eurosun.2020.05.13

Chicherin, S., & Anvari-Moghaddam, A. (2021). Adjusting heat demands using the operational data of district heating systems. *Energy*, *235*. https://doi.org/10.1016/j.energy.2021.121368

Cholewa, T., Siuta-Olcha, A., Smolarz, A., Muryjas, P., Wolszczak, P., Guz, Ł., Bocian, M., & Balaras, C. A. (2022). An easy and widely applicable forecast control for heating systems in existing and new buildings: First field experiences. *Journal of Cleaner Production*, *352*. https://doi.org/10.1016/j.jclepro.2022.131605

Dalla Rosa, A., Li, H., Svendsen, S., Werner, S., Persson, U., Ruehling, K., Felsmann, C., Crane, M., Burzynski, R., & Bevilacqua, C. (2014). Annex X Final report Toward 4 th Generation District Heating : Experience and Potential of Low-Temperature District Heating. *IEA Annex X*, 205.

David, A. (2016). Large heat pumps in European district heating systems. *En+Eff - 22nd International Trade Fair and Congress*, *79*(April), 1275–1284.

Debbarma, J., & Choi, Y. (2022). A taxonomy of green governance: A qualitative and quantitative analysis towards sustainable development. *Sustainable Cities and Society*, *79*(January), 103693. https://doi.org/10.1016/j.scs.2022.103693

Degelin, A., Tassenoy, R., Vieren, E., Demeester, T., T'Jollyn, I., & De Paepe, M. (2024). Influence of supply temperature and booster technology on the energetic performance and levelized cost of heat of a district heating network with central heat pump. *Energy*, *312*. https://doi.org/10.1016/j.energy.2024.133589

Delfi.lv news portal. (2024, December 27). *"Sadales tīkla" vadītājs: ar saules ģenerācijas attīstību esam nonākuši "no viena grāvja otrā."* https://www.delfi.lv/bizness/37264250/biznesa_vide/120055520/sadales-tikla-vaditajs-ar-saules-generacijas-attistibu-esam-nonakusi-no-viena-gravja-otra

Dienas Bizness. (2023). Rīgas siltuma mērķis ir kļūt par enerģijas apmaiņas platformu. In *https://www.db.lv/zinas/rigas-siltuma-merkis-ir-klut-par-energijas-apmainas-platformu-512377*.

Dino, G. E., Catrini, P., Buscemi, A., Piacentino, A., Palomba, V., & Frazzica, A. (2023). Modeling of a bidirectional substation in a district heating network: Validation, dynamic analysis, and application to a solar prosumer. *Energy*, *284*. https://doi.org/10.1016/j.energy.2023.128621

Directorate-General for Communication. (2024). *Latvia - Final updated NECP 2021-2030*. Https://Commission.Europa.Eu/Publications/Latvia-Final-Updated-Necp-2021-2030-Submitted-2024_en.

EUR-Lex - 52016DC0051 - EN - EUR-Lex. (n.d.). Retrieved January 28, 2025, from https://eur-lex.europa.eu/legal-content/EN/TXT/?qid=1575551754568&uri=CELEX:52016DC0051

European Commission. (2020). *2050 long-term strategy*. Https://Climate.Ec.Europa.Eu/Eu-Action/Climate-Strategies-Targets/2050-Long-Term-Strategy_en.

European Commission. (2023). *Heat pumps – action plan to accelerate roll-out across the EU*. Https://Ec.Europa.Eu/Info/Law/Better-Regulation/Have-Your-Say/Initiatives/13771-Heat-Pumps-Action-Plan-to-Accelerate-Roll-out-across-the-EU_en.

European Commission. (2024a). *Heating and cooling. Heating and cooling constitute around half of the EU energy consumption.* Https://Energy.Ec.Europa.Eu/Topics/Energy-Efficiency/Heating-and-Cooling_en.

European Commission. (2024b). *Photovoltaic Geographical Information System (PVGIS). Version 5.3.* https://re.jrc.ec.europa.eu/pvg_tools/en/tools.html

Figaj, R., & Żołądek, M. (2021). Experimental and numerical analysis of hybrid solar heating and cooling system for a residential user. *Renewable Energy*, *172*, 955–967. https://doi.org/10.1016/j.renene.2021.03.091

Francisco, B., Nelson, S., Jaakko, E., & Hatef, M. (2024). Empirical investigation of solar photovoltaic-thermal collectors for heat pump integration. *Applied Thermal Engineering*, *248*. https://doi.org/10.1016/j.applthermaleng.2024.123175

Frank, E., Mauthner, F., & Fischer, S. (2015). Overheating prevention and stagnation handling in solar process heat applications. In *IEA SHC Task 49 Solar process heat for production and advanced applications*. https://doi.org/10.1016/j.rser.2009.07.014

Fuentes, E., Arce, L., & Salom, J. (2018). A review of domestic hot water consumption pro fi les for application in systems and buildings energy performance analysis. *Renewable and Sustainable Energy Reviews*, *81*, 1530–1547. https://doi.org/10.1016/j.rser.2017.05.229

Gaigalis, V., Skema, R., Marcinauskas, K., & Korsakiene, I. (2016). A review on Heat Pumps implementation in Lithuania in compliance with the National Energy Strategy and EU policy. In *Renewable and Sustainable Energy Reviews* (Vol. 53). https://doi.org/10.1016/j.rser.2015.09.029

Gasser, L., Flück, S., Kleingries, M., Meier, C., Bätschmann, M., & Wellig, B. (2017). High efficiency heat pumps for low temperature lift applications. *12th IEA Heat Pump Conference*. http://hpc2017.org/wp-content/uploads/2017/05/O.1.4.5-High-efficiency-heat-pumps-for-low-temperature-lift-applications.pdf

Gendelis, S., & Mikelsons, M. (2022). *Experimental performance of solar thermal collector systems in real operation conditions in Latvia*. 81–88. https://doi.org/10.5593/sgem2022/4.1/s17.11

Grzegórska, A., Rybarczyk, P., Lukoševičius, V., Sobczak, J., & Rogala, A. (2021). Smart asset management for district heating systems in the baltic sea region. In *Energies* (Vol. 14, Issue 2). https://doi.org/10.3390/en14020314

Guzzini, A., Pellegrini, M., Pelliconi, E., & Saccani, C. (2020). Low temperature district heating: An expert opinion survey. In *Energies* (Vol. 13, Issue 4). https://doi.org/10.3390/en13040810

Hamburg, A., Kuusk, K., Mikola, A., & Kalamees, T. (2020). Realisation of energy performance targets of an old apartment building renovated to nZEB. *Energy*, *194*. https://doi.org/10.1016/j.energy.2019.116874

Harrabi, I., Hamdi, M., Bessifi, A., & Hazami, M. (2021). Dynamic modeling of solar thermal collectors for domestic hot water production using TRNSYS. *Euro-Mediterranean Journal for Environmental Integration*, *6*(1). https://doi.org/10.1007/s41207-020-00223-6

Harrison, S., & Cruickshank, C. A. (2012). A review of strategies for the control of high temperature stagnation in solar collectors and systems. *Energy Procedia*, *30*, 793–804. https://doi.org/10.1016/j.egypro.2012.11.090

He, K. L., Zhao, T., Ma, H., & Chen, Q. (2023). Optimal operation of integrated power and thermal systems for flexibility improvement based on evaluation and utilization of heat storage in district heating systems. *Energy*, *274*. https://doi.org/10.1016/j.energy.2023.127421

Heating and cooling. (n.d.). Retrieved January 28, 2025, from https://energy.ec.europa.eu/topics/energy-efficiency/heating-and-cooling_en

Hengel, F., Heschl, C., Inschlag, F., & Klanatsky, P. (2020). System efficiency of pvt collector-driven heat pumps. *International Journal of Thermofluids*, *6*.

Heymann, M., Rosemann, T., Rühling, K., Tietze, T., & Hafner, B. (2018). Concept and Measurement Results of Two Decentralized Solar Thermal Feed-in Substations. *Energy Procedia*, *149*, 363–372. https://doi.org/10.1016/j.egypro.2018.08.200

Heymann, M., Rühling, K., & Felsmann, C. (2017). Integration of Solar Thermal Systems into District Heating - DH System Simulation. *Energy Procedia*, *116*, 394–402. https://doi.org/10.1016/j.egypro.2017.05.086

Hiris, D. P., Pop, O. G., & Balan, M. C. (2022). Preliminary sizing of solar district heating systems with seasonal water thermal storage. *Heliyon*, *8*(2), e08932. https://doi.org/10.1016/j.heliyon.2022.e08932

Huang, P., Copertaro, B., Zhang, X., Shen, J., Löfgren, I., Rönnelid, M., Fahlen, J., Andersson, D., & Svanfeldt, M. (2020). A review of data centers as prosumers in district energy systems: Renewable energy integration and waste heat reuse for district heating. In *Applied Energy* (Vol. 258). https://doi.org/10.1016/j.apenergy.2019.114109

IEA. (2020). *Total operating district heat pipelines in Europe, 2005-2019*. https://www.iea.org/data-and-statistics/charts/total-operating-district-heat-pipelines-in-europe-2005-2019

International Energy Agency. (2024). *Latvia 2024 Energy Policy Review. Executive summary*. Https://Www.Iea.Org/Reports/Latvia-2024/Executive-Summary.

Järvelä, M., Lappalainen, K., & Valkealahti, S. (2020). Characteristics of the cloud enhancement phenomenon and PV power plants. *Solar Energy*, *196*. https://doi.org/10.1016/j.solener.2019.11.090

Jebamalai, J. M., Marlein, K., & Laverge, J. (2022). Design and cost comparison of district heating and cooling (DHC) network configurations using ring topology – A case study. *Energy*, *258*. https://doi.org/10.1016/j.energy.2022.124777

Ji, P., Rhoads, W. J., Edwards, M. A., & Pruden, A. (2017). Impact of water heater temperature setting and water use frequency on the building plumbing microbiome. *ISME Journal*, *11*(6). https://doi.org/10.1038/ismej.2017.14

Jiang, M., Rindt, C., & Smeulders, D. M. J. (2022). Optimal Planning of Future District Heating Systems—A Review. *Energies*, *15*(19), 7160. https://doi.org/10.3390/en15197160

Jodeiri, A. M., Goldsworthy, M. J., Buffa, S., & Cozzini, M. (2022). Role of sustainable heat sources in transition towards fourth generation district heating – A review. *Renewable and Sustainable Energy Reviews*, *158*, 112156. https://doi.org/10.1016/j.rser.2022.112156

Johansen, K., & Werner, S. (2022). Something is sustainable in the state of Denmark: A review of the Danish district heating sector. In *Renewable and Sustainable Energy Reviews* (Vol. 158). https://doi.org/10.1016/j.rser.2022.112117

Kaldellis, J. K., Kapsali, M., & Kavadias, K. A. (2014). Temperature and wind speed impact on the efficiency of PV installations. Experience obtained from outdoor measurements in Greece. *Renewable Energy*, *66*. https://doi.org/10.1016/j.renene.2013.12.041

Kang, A., Korolija, I., & Rovas, D. (2022). Photovoltaic Thermal District Heating: A review of the current status, opportunities and prospects. In *Applied Thermal Engineering* (Vol. 217). https://doi.org/10.1016/j.applthermaleng.2022.119051

Kolsi, L., Abbasi, A., Alqsair, U. F., Farooq, W., Omri, M., & Khan, S. U. (2021). Thermal enhancement of ethylene glycol base material with hybrid nanofluid for oblique stagnation point slip flow. *Case Studies in Thermal Engineering*. https://doi.org/10.1016/j.csite.2021.101468

Krumins, A., Lebedeva, K., Tamane, A., & Millers, R. (2022). Possibilities of Balancing Buildings Energy Demand for Increasing Energy Efficiency in Latvia. *Environmental and Climate Technologies*, *26*(1). https://doi.org/10.2478/rtuect-2022-0009

Kuosa, M., Kiviranta, P., Sarvelainen, H., Tuliniemi, E., Korpela, T., Tallinen, K., & Koponen, H. K. (2022). Optimisation of district heating production by utilising the storage capacity of a district heating network on the basis of weather forecasts. *Results in Engineering*, *13*, 100318. https://doi.org/10.1016/j.rineng.2021.100318

Lake, A., Rezaie, B., & Beyerlein, S. (2017). Review of district heating and cooling systems for a sustainable future. *Renewable and Sustainable Energy Reviews*, *67*, 417–425. https://doi.org/10.1016/j.rser.2016.09.061

Larsen, M. A. D., Petrović, S., Radoszynski, A. M., McKenna, R., & Balyk, O. (2020). Climate change impacts on trends and extremes in future heating and cooling demands over Europe. *Energy and Buildings*, *226*. https://doi.org/10.1016/j.enbuild.2020.110397

Latvian Environment Geology and Meteorology Centre. (n.d.). *Environmental data archive. Meteorology*. Retrieved February 28, 2025, from https://videscentrs.lvgmc.lv/noverojumu-arhivs/meteo

Lauka, D., Gusca, J., & Blumberga, D. (2015). Heat pumps integration trends in district heating networks of the Baltic States. *Procedia Computer Science*, *52*(1), 835–842. https://doi.org/10.1016/j.procs.2015.05.140

Lebedeva, K., Migla, L., & Odineca, T. (2023). Solar district heating system in Latvia: A case study. *Journal of King Saud University - Science*, *35*(10). https://doi.org/10.1016/j.jksus.2023.102965

Lee, M., Han, C., Kwon, S., & Kim, Y. (2023). Energy and cost savings through heat trading between two massive prosumers using solar and ground energy systems connected to district heating networks. *Energy*, *284*(December). https://doi.org/10.1016/j.energy.2023.129347

Lennermo, G. (2020). *Solvärmeteknik – en handbok*. Svensk Byggtjänst.

Lennermo, G., Lauenburg, P., & Werner, S. (2019). Control of decentralised solar district heating. *Solar Energy*, *179*(December 2018), 307–315. https://doi.org/10.1016/j.solener.2018.12.080

Lepiksaar, K., Kajandi, G. M., Sukumaran, S., Krupenski, I., Kirs, T., & Volkova, A. (2025). Optimizing solar energy integration in Tallinn's district heating and cooling systems. *Smart Energy*, *17*. https://doi.org/10.1016/J.SEGY.2024.100166

Li, H., Hou, J., Tian, Z., Hong, T., Nord, N., & Rohde, D. (2022). Optimize heat prosumers' economic performance under current heating price models by using water tank thermal energy storage. *Energy*, *239*. https://doi.org/10.1016/j.energy.2021.122103

Lichtenegger, K., Wöss, D., Halmdienst, C., Höftberger, E., Schmidl, C., & Pröll, T. (2017). Sustainable Energy , Grids and Networks Intelligent heat networks : First results of an energy-information-cost-model. *Sustainable Energy, Grids and Networks*, *11*, 1–12. https://doi.org/10.1016/j.segan.2017.05.001

Liu, Y., Tang, H., Chen, Y., Wang, D., & Song, C. (2022). Optimization of layout and diameter for distributed solar heating network with multi-source and multi-sink. *Energy*, *258*. https://doi.org/10.1016/j.energy.2022.124788

LowTEMP project. (2020). *Project aims*. Https://Www.Lowtemp.Eu/About_en/.

Lu, M., Zhang, C., Zhang, D., Wang, R., Zhou, Z., Zhan, C., Zai, X., & Jing, Q. (2021). Operational optimization of district heating system based on an integrated model in TRNSYS. *Journal of Energy Storage*, *230*. https://doi.org/10.1016/j.enbuild.2020.110538

Lund, H., Østergaard, P. A., Chang, M., Werner, S., Svendsen, S., Sorknæs, P., Thorsen, J. E., Hvelplund, F., Mortensen, B. O. G., Mathiesen, B. V., Bojesen, C., Duic, N., Zhang, X., & Möller, B. (2018a). The status of 4th generation district heating: Research and results. In *Energy* (Vol. 164). https://doi.org/10.1016/j.energy.2018.08.206

Lund, H., Østergaard, P. A., Chang, M., Werner, S., Svendsen, S., Sorknæs, P., Thorsen, J. E., Hvelplund, F., Mortensen, B. O. G., Mathiesen, B. V., Bojesen, C., Duic, N., Zhang, X., & Möller, B. (2018b). The status of 4th generation district heating: Research and results. In *Energy* (Vol. 164). https://doi.org/10.1016/j.energy.2018.08.206

Lund, H., Østergaard, P. A., Nielsen, T. B., Werner, S., Thorsen, J. E., Gudmundsson, O., Arabkoohsar, A., & Mathiesen, B. V. (2021). Perspectives on fourth and fifth generation district heating. *Energy*, *227*, 120520. https://doi.org/10.1016/j.energy.2021.120520

Lund, H., Vad Mathiesen, B., Connolly, D., & Østergaarda, P. A. (2014). Renewable energy systems - A smart energy systems approach to the choice and modelling of 100 % renewable solutions. *Chemical Engineering Transactions*, *39*(Special Issue), 1–6. https://doi.org/10.3303/CET1439001

Lund, H., Werner, S., Wiltshire, R., Svendsen, S., Thorsen, J. E., Hvelplund, F., & Mathiesen, B. V. (2014). 4th Generation District Heating (4GDH). Integrating smart thermal grids into future sustainable energy systems. *Energy*, *68*, 1–11. https://doi.org/10.1016/j.energy.2014.02.089

Lund, R., Østergaard, D. S., Yang, X., & Mathiesen, B. V. (2017). Comparison of low-temperature district heating concepts in a long-term energy system perspective. *International Journal of Sustainable Energy Planning and Management*, *12*. https://doi.org/10.5278/ijsepm.2017.12.2

Lygnerud, K., Popovic, T., Schultze, S., & Støchkel, H. K. (2023). District heating in the future - thoughts on the business model. *Energy*, *278*. https://doi.org/10.1016/j.energy.2023.127714

Martin, N., Zinck Thellufsen, J., Chang, M., Talens-Peiró, L., & Madrid-López, C. (2024). *The many faces of heating transitions. Deeper understandings of future systems in Sweden and beyond*. *290*(March). https://doi.org/10.1016/j.energy.2024.130264

Martin-Du Pan, O., Woods, P., & Hanson-Graville, R. (2019). Optimising pipe sizing and operating temperatures for district heating networks to minimise operational energy consumption. *Building Services Engineering Research and Technology*, *40*(2). https://doi.org/10.1177/0143624418802590

Meggers, F., & Leibundgut, H. (2011). The potential of wastewater heat and exergy: Decentralized high-temperature recovery with a heat pump. *Energy and Buildings*, *43*(4), 879–886. https://doi.org/10.1016/j.enbuild.2010.12.008

Meggers, F., Mast, M., & Leibundgut, H. (2010). The missing link for low exergy buildings: low temperature-lift, ultra-high COP heat pumps. *Clima 2010: Sustainable Energy Use in Buildings*, *December 2013*.

Mertz, T., Serra, S., Henon, A., & Reneaume, J. M. (2016). A MINLP optimization of the configuration and the design of a district heating network: Academic study cases. *Energy*, *117*. https://doi.org/10.1016/j.energy.2016.07.106

Migla, L., Snegirjovs, A., & Shutenkova, O. (2020). Performance analysis of solar assisted ground coupled heat pump system in Latvia. *E3S Web of Conferences*, *172*, 22011. https://doi.org/10.1051/e3sconf/202017222011

Miglioli, A., Aste, N., Del Pero, C., & Leonforte, F. (2021). Photovoltaic-thermal solar-assisted heat pump systems for building applications: Integration and design methods. *Energy and Built Environment*. https://doi.org/10.1016/j.enbenv.2021.07.002

Millar, M. A., Yu, Z., Burnside, N., Jones, G., & Elrick, B. (2021a). Identification of key performance indicators and complimentary load profiles for 5th generation district energy networks. *Applied Energy*, *291*(September 2020), 116672. https://doi.org/10.1016/j.apenergy.2021.116672

Millar, M. A., Yu, Z., Burnside, N., Jones, G., & Elrick, B. (2021b). Identification of key performance indicators and complimentary load profiles for 5th generation district energy networks. *Applied Energy*, *291*, 116672. https://doi.org/10.1016/j.apenergy.2021.116672

Monsalvete Álvarez de Uribarri, P., Eicker, U., & Robinson, D. (2017). Energy performance of decentralized solar thermal feed-in to district heating networks. *Energy Procedia*, *116*, 285–296. https://doi.org/10.1016/j.egypro.2017.05.075

Morvaj, B., Evins, R., & Carmeliet, J. (2016). Optimising urban energy systems: Simultaneous system sizing, operation and district heating network layout. *Energy*, *116*. https://doi.org/10.1016/j.energy.2016.09.139

Nannou, T., Jadwiszczak, P., Sayegh, M. A., Danielewicz, J., Jouhara, H., Miniewicz, M., & Piekarska, K. (2016). Trends of European research and development in district heating technologies. *Renewable and Sustainable Energy Reviews*, *68*, 1183–1192. https://doi.org/10.1016/j.rser.2016.02.023

Nielsen, S., & Möller, B. (2012). Excess heat production of future net zero energy buildings within district heating areas in Denmark. *Energy*, *48*(1), 23–31. https://doi.org/10.1016/j.energy.2012.04.012

Østergaard, D. S., Smith, K. M., Tunzi, M., & Svendsen, S. (2022). Low-temperature operation of heating systems to enable 4th generation district heating: A review. *Energy*, *248*, 123529. https://doi.org/10.1016/j.energy.2022.123529

Østergaard, P. A., & Andersen, A. N. (2016). Booster heat pumps and central heat pumps in district heating. *Applied Energy*, *184*. https://doi.org/10.1016/j.apenergy.2016.02.144

Pakere, I., & Blumberga, D. (2020). Solar power or solar heat: What will upraise the efficiency of district heating? Multi-criteria analyses approach. *Energy*, *198*. https://doi.org/10.1016/j.energy.2020.117291

Pakere, I., Lauka, D., & Blumberga, D. (2018). Solar power and heat production via photovoltaic thermal panels for district heating and industrial plant. *Energy*, *154*. https://doi.org/10.1016/j.energy.2018.04.138

Pardo García, N., Zubi, G., Pasaoglu, G., & Dufo-López, R. (2017). Photovoltaic thermal hybrid solar collector and district heating configurations for a Central European multi-family house. *Energy Conversion and Management*, *148*. https://doi.org/10.1016/j.enconman.2017.05.065

Park, B. R., Chung, M. H., & Moon, J. W. (2022). Becoming a building suitable for participation in peer-to-peer energy trading. *Sustainable Cities and Society*, *76*. https://doi.org/10.1016/j.scs.2021.103436

Paulick, S., Schroth, C., Guddusch, S., & Rühling, K. (2018). Resulting Effects on Decentralized Feed-In into District Heating Networks - A Simulation Study. *Energy Procedia*, *149*, 49–58. https://doi.org/10.1016/j.egypro.2018.08.168

Perez-Mora, N., Bava, F., Andersen, M., Bales, C., Lennermo, G., Nielsen, C., Furbo, S., & Martínez-Moll, V. (2018). Solar district heating and cooling: A review. In *International Journal of Energy Research* (Vol. 42, Issue 4). https://doi.org/10.1002/er.3888

Pieper, H., Krupenski, I., Brix Markussen, W., Ommen, T., Siirde, A., & Volkova, A. (2021). Method of linear approximation of COP for heat pumps and chillers based on thermodynamic modelling and off-design operation. *Energy*, *230*. https://doi.org/10.1016/j.energy.2021.120743

Pipiciello, M., Caldera, M., Cozzini, M., Ancona, M. A., Melino, F., & Di Pietra, B. (2021). Experimental characterization of a prototype of bidirectional substation for district heating with thermal prosumers. *Energy*, *223*. https://doi.org/10.1016/j.energy.2021.120036

Quirosa, G., Torres, M., Soltero, V. M., & Chacartegui, R. (2022). Analysis of an ultra-low temperature district heating and cooling as a storage system for renewable integration. *Applied Thermal Engineering*, *216*. https://doi.org/10.1016/j.applthermaleng.2022.119052

Rämä, M., & Mohammadi, S. (2017). Comparison of distributed and centralised integration of solar heat in a district heating system. *Energy*. https://doi.org/10.1016/j.energy.2017.03.115

Reiners, T., Gross, M., Altieri, L., Wagner, H. J., & Bertsch, V. (2021). Heat pump efficiency in fifth generation ultra-low temperature district heating networks using a wastewater heat source. *Energy*, *236*, 121318. https://doi.org/10.1016/j.energy.2021.121318

Revesz, A., Jones, P., Dunham, C., Davies, G., Marques, C., Matabuena, R., Scott, J., & Maidment, G. (2020). Developing novel 5th generation district energy networks. *Energy*, *201*, 117389. https://doi.org/10.1016/j.energy.2020.117389

Rīgas Siltums JSC. (2013, January). Aktuālais siltumtīklos. Rīgas pilsētas siltumtīkli. *AS "Rīgas Siltums" Avīze*. https://www.rs.lv/sites/default/files/page_file/rs_avize_1.pdf

Rīgas Siltums JSC. (2024). *Apraksts*. Https://Www.Rs.Lv/Saturs/Rigas-Siltums#:~:Text=R%C4%ABgas%20pils%C4%93tas%20kop%C4%93jais%20siltumt%C4%ABklu%20garums%20ir%20aptuveni%20800,SILTUMS%20ir%20publisku%20personu%20kontrol%C4%93%20eso%C5%A1a%20priv%C4%81ta%20kapit%C4%81lsabiedr%C4%ABba.

Sadeghi, H., Ijaz, A., & Singh, R. M. (2022). Current status of heat pumps in Norway and analysis of their performance and payback time. *Sustainable Energy Technologies and Assessments*, *54*. https://doi.org/10.1016/J.SETA.2022.102829

Samuel, O., Javaid, N., Alghamdi, T. A., & Kumar, N. (2022). Towards sustainable smart cities: A secure and scalable trading system for residential homes using blockchain and artificial intelligence. *Sustainable Cities and Society*, *76*. https://doi.org/10.1016/j.scs.2021.103371

Sayegh, M. A., Jadwiszczak, P., Axcell, B. P., Niemierka, E., Bryś, K., & Jouhara, H. (2018). Heat pump placement, connection and operational modes in European district heating. In *Energy and Buildings*. https://doi.org/10.1016/j.enbuild.2018.02.006

Schäfer, K., & Thomas, S. (2018). Experimental Plant for Analyzing the Technical Feasibility of Decentralized Solar Heat Feed-In. *EuroSun 2018*, 1–9. https://doi.org/10.18086/eurosun2018.05.04

Schmidt, D. (2018). Low Temperature District Heating for Future Energy Systems. *Energy Procedia*, *149*, 595–604. https://doi.org/10.1016/j.egypro.2018.08.224

Schmidt, T., Pauschinger, T., Sørensen, P. A., Snijders, A., Djebbar, R., Boulter, R., & Thornton, J. (2018). Design Aspects for Large-scale Pit and Aquifer Thermal Energy Storage for District Heating and Cooling. *Energy Procedia*, *149*, 585–594. https://doi.org/10.1016/j.egypro.2018.08.223

Selvakkumaran, S., Axelsson, L., & Svensson, I.-L. (2021). Drivers and barriers for prosumer integration in the Swedish district heating sector. *Energy Reports*, *7*(September), 193–202. https://doi.org/10.1016/j.egyr.2021.08.155

Selvakkumaran, S., Eriksson, L., & Svensson, I.-L. (2021). How do business models for prosumers in the district energy sector capture flexibility? *Energy Reports*, *7*(September), 203–212. https://doi.org/10.1016/j.egyr.2021.08.154

Sernhed, K., Lygnerud, K., & Werner, S. (2018). Synthesis of recent Swedish district heating research. *Energy*, *151*, 126–132. https://doi.org/10.1016/j.energy.2018.03.028

Solar Energy Laboratory University of Wisconsin-Madison, & Thermal Energy Systems Specialists LLC. (2023). *TRNSYS 18 Volume 4 Mathematical Reference*.

Sørensen, P. A., Nielsen, J. E., Battisti, R., Schmidt, T., & Trier, D. (2012). Solar district heating guidelines: Collection of fact sheets. WP3 – D3.1 & D3.2. *Solar Distric Heating*, *August*, 152.

SPF Institute for Solar Technology. (n.d.). *Collectors*. Retrieved January 2, 2025, from https://www.spftesting.info/data/1.collectors/

Sporleder, M., Rath, M., & Ragwitz, M. (2022). Design optimization of district heating systems: A review. In *Frontiers in Energy Research* (Vol. 10). https://doi.org/10.3389/fenrg.2022.971912

Statistics overview, country by country, 2015 Survey. (2015). https://www.euroheat.org/wp-content/uploads/2016/03/2015-Country-by-country-Statistics-Overview.pdf

Stegmann, M., Bertram, E., Rockendorf, G., & Janßen, S. (2011). Model of an unglazed photovoltaic thermal collector based on standard test procedures. *30th ISES Biennial Solar World Congress 2011, SWC 2011*, *4*. https://doi.org/10.18086/swc.2011.19.30

Stock, J., Schmidt, T., Xhonneux, A., & Müller, D. (2024). Optimisation of district heating transformation for the efficient integration of a low-temperature heat source. *Energy*, *308*. https://doi.org/10.1016/j.energy.2024.132461

Sun, F., Zhao, X., & Hao, B. (2023). Novel solar-driven low temperature district heating and cooling system based on distributed half-effect absorption heat pumps with lithium bromide. *Energy*, *270*. https://doi.org/10.1016/j.energy.2023.126884

SunCalc.org. (n.d.). *Computation path of the sun for Paula Valdena iela 1-1, Riga, 1048, LVA 01.05.2021 12:00*.

Tamasauskas, R., Monstvilas, E., Bliūdžius, R., Banionis, K., & Miškinis, K. (2015). Comparison of Calculation Methods of Renewable Energy Generated by Electric Heat Pumps. *Journal of Sustainable Architecture and Civil Engineering*, *11*(2), 11. https://doi.org/10.5755/j01.sace.11.2.9986

Taşcıkaraoğlu, A. (2018). Economic and operational benefits of energy storage sharing for a neighborhood of prosumers in a dynamic pricing environment. *Sustainable Cities and Society*. https://doi.org/10.1016/j.scs.2018.01.002

TESS. (2012). *TESSLibs 17 - Hydronics Library Mathematical Reference*.

Tian, Z., Zhang, S., Deng, J., Fan, J., Huang, J., Kong, W., Perers, B., & Furbo, S. (2019). Large-scale solar district heating plants in Danish smart thermal grid: Developments and recent trends. *Energy Conversion and Management*, *189*, 67–80. https://doi.org/10.1016/j.enconman.2019.03.071

Tonita, E. M., Russell, A. C. J., Valdivia, C. E., & Hinzer, K. (2023). Optimal ground coverage ratios for tracked, fixed-tilt, and vertical photovoltaic systems for latitudes up to 75°N. *Solar Energy*, *258*. https://doi.org/10.1016/j.solener.2023.04.038

Topal, H. I., & Arabkoohsar, A. (2024). Enhancing ultra low temperature district heating systems with neighborhood-scale heat pump and triple-pipe distribution: A techno-economic analysis. *Journal of Building Engineering*, *95*. https://doi.org/10.1016/j.jobe.2024.110316

Vesterlund, M., Toffolo, A., & Dahl, J. (2017). Optimization of multi-source complex district heating network, a case study. *Energy*, *126*. https://doi.org/10.1016/j.energy.2017.03.018

Veyron, M., Voirand, A., Mion, N., Maragna, C., Mugnier, D., & Clausse, M. (2022). Dynamic exergy and economic assessment of the implementation of seasonal underground thermal energy storage in existing solar district heating. *Energy*, *261*. https://doi.org/10.1016/j.energy.2022.124917

Vivian, J., Emmi, G., Zarrella, A., Jobard, X., Pietruschka, D., & De Carli, M. (2018). Evaluating the cost of heat for end users in ultra low temperature district heating networks with booster heat pumps. *Energy*, *153*. https://doi.org/10.1016/j.energy.2018.04.081

Volkova, A., Pakere, I., Murauskaite, L., Huang, P., Lepiksaar, K., & Zhang, X. (2022). 5th generation district heating and cooling (5GDHC) implementation potential in urban areas

with existing district heating systems. *Energy Reports*, *8*. https://doi.org/10.1016/j.egyr.2022.07.162

Volkova, A., Pieper, H., Koduvere, H., Lepiskar, K., & Siirde, A. (2021). *Heat pump potential in the Baltic states*. Nordic Energy Research. https://doi.org/10.6027/NER2021-02

Walnum, H. T., Sørensen, Å. L., & Stråby, K. (2021). Measurement data on domestic hot water consumption and related energy use in hotels, nursing homes and apartment buildings in Norway. *Data in Brief*, *37*. https://doi.org/10.1016/j.dib.2021.107228

Wang, D., Carmeliet, J., & Orehounig, K. (2021). Design and assessment of district heating systems with solar thermal prosumers and thermal storage. *Energies*, *14*(4). https://doi.org/10.3390/en14041184

Wang, J., Huo, S., Yan, R., & Cui, Z. (2022). Leveraging heat accumulation of district heating network to improve performances of integrated energy system under source-load uncertainties. *Energy*, *252*. https://doi.org/10.1016/j.energy.2022.124002

wedistrict.eu. (2020). *Interactive map: Share of District Heating and Cooling across Europe*.

Weiss, W., & Spörk-Dür, M. (2024). *Solar Heat Worldwide. Edition 2024. Global market development and trends in 2023. Detailed market figures 2022.* 96.

Werner, S. (2017). International review of district heating and cooling. *Energy*, *137*, 617–631. https://doi.org/10.1016/j.energy.2017.04.045

Winterscheid, C., Dalenback, J.-O., & Holler, S. (2017). Integration of solar thermal systems in existing district heating systems. *Energy*, *137*, 579–585.

Wittenburg, R., Gierow, C., Pötke, R., Müller, K., & Holtz, D. (2023). Transition of district heating from fossil to renewable energies – Pathways analysed by dynamic simulation. *Renewable Energy Focus* , *45*. https://doi.org/10.1016/j.ref.2023.04.008

Wyssen, I., Gasser, L., Wellig, B., & Meier, M. (2010). Chiller with small temperature lift for efficient building cooling. *Proceedings of Clima2010*, *March*.

Xu, Y., Zhan, C., Jensen, A. R., Gao, M., Kong, W., & Fan, J. (2024). Thermo-economic analysis of a solar district heating plant with an air-to-water heat pump. *Renewable Energy*, *237*, 121490. https://doi.org/10.1016/j.renene.2024.121490

Yang, L., Entchev, E., Rosato, A., & Sibilio, S. (2017). Smart thermal grid with integration of distributed and centralized solar energy systems. *Energy*, *122*. https://doi.org/10.1016/j.energy.2017.01.114

Yang, X., Li, H., & Svendsen, S. (2016). Evaluations of different domestic hot water preparing methods with ultra-low-temperature district heating. *Energy*, *109*. https://doi.org/10.1016/j.energy.2016.04.109

You, T., Wu, W., Shi, W., Wang, B., & Li, X. (2016). An overview of the problems and solutions of soil thermal imbalance of ground-coupled heat pumps in cold regions. In *Applied Energy* (Vol. 177). https://doi.org/10.1016/j.apenergy.2016.05.115

You, T., Wu, W., Yang, H., Liu, J., & Li, X. (2021). Hybrid photovoltaic/thermal and ground source heat pump: Review and perspective. In *Renewable and Sustainable Energy Reviews* (Vol. 151). https://doi.org/10.1016/j.rser.2021.111569

Zajacs, A., Bogdanovics, R., Zeiza-Seleznova, A., Valancius, R., & Zemitis, J. (2022). Integration of decentralized solar collectors into a district heating system. *Sustainable Cities and Society*, *83*, 103920. https://doi.org/10.1016/j.scs.2022.103920

Zajacs, A., & Borodiņecs, A. (2019). Assessment of development scenarios of district heating systems. *Sustainable Cities and Society*, *48*, 101540. https://doi.org/10.1016/j.scs.2019.101540

Zajacs, A., Borodinecs, A., & Vatin, N. (2021). Environmental impact of district heating system retrofitting. *Atmosphere*, *12*, 1110. https://doi.org/10.3390/atmos12091110

Zajacs, A., Shogenova, A., Shogenov, K., Volkova, A., Sliaupa, S., Sliaupiene, R., & Jõeleht, A. (2025). Utilization of geothermal energy: New possibilities for district heating networks in the Baltic states. *Renewable Energy*, *242*. https://doi.org/10.1016/J.RENENE.2025.122375

Zemīte, M., Pūle, D., Kiriļina-Gūtmane, O., Ķimse, L., Strods, M., Zemītis, J., Mežule, L., Valciņa, O., & Juhna, T. (2023). Effect of microbially available phosphorous removal on Legionella spp. in multi-storey residential dwellings in Latvia. *Environmental Science: Water Research and Technology*, *10*(1). https://doi.org/10.1039/d3ew00588g

Zhu, T., Du, Y., Liang, J., Rohlfs, W., Eric Thorsen, J., & Elmegaard, B. (2023). Integration of booster heat pumps in ultra-low temperature district heating network: Prototype demonstration and refrigerant charge investigation. *Energy and Buildings*, *298*. https://doi.org/10.1016/j.enbuild.2023.113516

Ziemele, J., Talcis, N., Osis, U., & Dace, E. (2021). A methodology for selecting a sustainable development strategy for connecting low heat density consumers to a district heating system by cascading of heat carriers. *Energy*, *230*. https://doi.org/10.1016/j.energy.2021.120776

Zirngibl, J. (2020). Heat pump standard EN 15316-4-2 – From compliance to real consumption. *REHVA Journal*, *57*(6), 5–9.

Raimonds Bogdanovičs was born in 1996 in Daugavpils, Latvia. He received a Bachelor's degree and an engineer's qualification (2020) and a Master's degree (2021) in Heat, Gas and Water Engineering Systems from Riga Technical University (RTU). Since 2019, he has been working at RTU, initially as a research assistant and, since 2022, as a lecturer and researcher at the Institute of Sustainable Building Materials and Engineering Systems. Since 2022, he has been a certified building specialist in the design of heating, ventilation, and air conditioning systems. He has a strong scientific interest in developing efficient building engineering systems that integrate renewable energy – especially solar and heat pumps – while addressing decarbonization, climate challenges, and energy costs in Latvia and the Baltic region. He aims for results that are both scientifically grounded and practically applicable, improving system performance and reducing environmental impact.